

Old Dominion University

ODU Digital Commons

---

Civil & Environmental Engineering Theses &  
Dissertations

Civil & Environmental Engineering

---

Winter 2003

## Boussinesq Model and the Relative Trough Froude Number (RTFN) for Wave Breaking

Takashi Okamoto  
*Old Dominion University*

Follow this and additional works at: [https://digitalcommons.odu.edu/cee\\_etds](https://digitalcommons.odu.edu/cee_etds)



Part of the [Civil Engineering Commons](#)

---

### Recommended Citation

Okamoto, Takashi. "Boussinesq Model and the Relative Trough Froude Number (RTFN) for Wave Breaking" (2003). Doctor of Philosophy (PhD), Dissertation, Civil & Environmental Engineering, Old Dominion University, DOI: 10.25777/5ezr-fd63  
[https://digitalcommons.odu.edu/cee\\_etds/39](https://digitalcommons.odu.edu/cee_etds/39)

This Dissertation is brought to you for free and open access by the Civil & Environmental Engineering at ODU Digital Commons. It has been accepted for inclusion in Civil & Environmental Engineering Theses & Dissertations by an authorized administrator of ODU Digital Commons. For more information, please contact [digitalcommons@odu.edu](mailto:digitalcommons@odu.edu).

**BOUSSINESQ MODEL AND THE RELATIVE TROUGH FROUDE  
NUMBER (RTFN) FOR WAVE BREAKING**

by

Takashi Okamoto

B.S. March 1995, Kyoto University, Japan

M.S. March 1997, Kyoto University, Japan

A Dissertation Submitted to the Faculty of  
Old Dominion University in Partial Fulfillment of  
the Requirement for the Degree of

DOCTOR OF PHILOSOPHY

CIVIL ENGINEERING

OLD DOMINION UNIVERSITY

December 2003

Approved by:

---

David R. Basco (Chairman)

---

Jaewan Yoon (Member)

---

John M. Klinck (Member)

## ABSTRACT

### BOUSSINESQ MODEL AND THE RELATIVE TROUGH FROUDE NUMBER (RTFN) FOR WAVE BREAKING

Takashi Okamoto  
Old Dominion University, 2003  
Director: Dr. David R. Basco

The relative trough Froude number (RTFN) theory is a new phase-resolving type, wave breaking trigger model introduced by Utku (1999) and Utku and Basco (2002). Based on the moving hydraulic jump concept, this model provides a better implementation of wave breaking in terms of hydrodynamics. Development of computer resources permits the use of the phase-resolving type, Boussinesq wave models in nearshore areas. The Boussinesq equation, however, does not include the physics of wave breaking, so that an additional mechanism is required to initiate wave breaking in the model. The main objective of this study is to develop a new wave breaking trigger model for the Boussinesq equation model by using the RTFN theory.

A theoretical analysis is performed to determine the analytical expression of the RTFN theory and the critical condition for wave breaking (CTFN). The RTFN theory is redefined for this purpose. Coupling with wave theories (both linear and nonlinear), the analytical form of the RTFN is obtained. The Miche (1944) formula provides a wave breaking condition. All results agree with  $RTFN=1.45$  as the theoretical CTFN.

A wave tank experiment is performed to obtain data for model confirmation. Wave breaking locations are measured with the assistance of a digital video recording. Wave gauge records are used to adjust input wave heights in the numerical model.

Wave celerity calculation methods for the RTFN calculation are investigated inten-

sively because 90% of the RTFN calculation is the contribution due to the celerity (Utku and Basco, 2002). To satisfy both applicability and robustness, a hybrid method is introduced.

Extensive numerical experiments are executed for the confirmation, calibration, and verification of the model. Qualitative studies confirm that the RTFN evolution along with the nonlinear wave transformation correctly behave for a wave breaking trigger. The model calibration performed with data obtained from the wave tank experiment determines the  $CTFN=1.47$  for the numerical model, which is very close to the theoretical value. Verification tests with calibrated  $CTFN$  reveal that the momentum sink term locating mechanism associated with the RTFN theory is also needed for completing the RTFN wave breaking model. This aspect of the work is left for the future.

To my parents.



## ACKNOWLEDGMENTS

The author wishes to express his sincere gratitude to his advisor, Dr. David R. Basco, for his constant guidance, encouragement and thoughtfulness. He originated the idea of the subject study, and I am grateful that I could participate in it. His valuable advice and support made it possible to complete this dissertation.

The author also would like to acknowledge committee members, Dr. Jaewan Yoon and Dr. John M. Klinck, for their generous advice and support. In addition, the author also wishes to acknowledge Dr. James T. Kirby at the University of Delaware for providing the source code of FUNWAVE and for his comments at the International Conference on Coastal Engineering in Cardiff, Wales, U.K., and to Dr. Qin Chen at the University of South Alabama for his advice on FUNWAVE.

Special thanks are due to the faculty and staff of the Civil and Environmental Engineering Department, especially the graduate program director, Dr. Isao Ishibashi for his support.

Lastly, the author would like to express his appreciation to his family and friends for their support, especially to his friend, Mr. Leo King who saved the dissertation data from a crashed hard drive on the author's personal computer.

## NOMENCLATURE

$a$	=	Wave amplitude in solitary wave
$a_0$	=	Typical amplitude
$a_1$	=	Characteristic coefficient in the governing equation of FUNWAVE
$a_2$	=	Characteristic coefficient in the governing equation of FUNWAVE
$b_1$	=	Characteristic coefficient in the governing equation of FUNWAVE
$b_2$	=	Characteristic coefficient in the governing equation of FUNWAVE
$C$	=	Wave celerity
$C_{crest}$	=	Wave celerity at the crest of the wave
$C_{trough}$	=	Wave celerity at the trough of the wave
$CTFN$	=	The critical relative trough Froude number for wave breaking
$d$	=	Water depth
$d_b$	=	Breaking water depth
$D$	=	Relative length scale
$F_b$	=	Additional momentum term due to the bottom friction
$F_{br}$	=	Additional momentum term due to the wave breaking
$F_{bs}$	=	Additional momentum term due to the absorption dumping
$Fr_t$	=	Relative trough Froude number (RTFN)
$Fr_{tc}$	=	Critical relative trough Froude number for wave breaking (CTFN)
$g$	=	The acceleration of gravity
$h$	=	Still water depth
$h_0$	=	Characteristic water depth
$H$	=	Wave height
$H_0$	=	Deep water wave height

$H_b$	=	Breaking wave height
$i$	=	Crest node
$j$	=	Trough node
$k$	=	Wave number = $2\pi/L$
$L$	=	Wave length
$L_0$	=	Deep water wave length
$m$	=	Bottom slope angle
$n$	=	Multiplication factor
$P$	=	Depth-integrated volume flux per unit time in $x$ -direction
$Q$	=	Depth-integrated volume flux per unit time in $y$ -direction
$RTFN$	=	Relative trough Froude number
$t_b$	=	Time when the wave breaking is initiated
$t^*$	=	Time scale for the development of surface roller
$T$	=	Wave period
$T^*$	=	Transition time (Duration)
$u$	=	Particle velocity
$u_{trough}$	=	Particle velocity at the trough of the wave
$u_\alpha$	=	Horizontal velocity component at $z = z_\alpha$
$Ur$	=	Ursell number = $aL^2/h^3$
$W$	=	Window size
$x_{i,k}$	=	Wave crest/trough location of $k$ th wave in the domain at time $i$
$X_b$	=	Wave breaking location from the toe of the beach slope
$z_\alpha$	=	Arbitrary depth
$\alpha$	=	Coefficient in Miche formula (0.142)

$\beta$	=	Turbulent mixing coefficient
$\gamma$	=	Characteristic coefficient in the governing equation of FUNWAVE
$\delta$	=	Total water depth = $h + \eta$
$\Delta t$	=	Time increment
$\Delta x$	=	Grid spacing
$\varepsilon$	=	Relative amplitude = $a_0/h_0$
$\varepsilon(\xi)$	=	Least square error
$\zeta$	=	Dimensionless reference water depth = $z_\alpha/h$
$\eta$	=	Free surface displacement from the equilibrium position
$\eta_{trough}$	=	Free surface displacement at the trough of the wave
$\eta_t^*$	=	Critical vertical acceleration of the free surface for FUNWAVE wave breaking trigger
$\eta_t^{(F)}$	=	Termination condition for FUNWAVE wave breaking trigger
$\eta_t^{(I)}$	=	Initiation condition for FUNWAVE wave breaking trigger
$\mu$	=	Relative depth = $h_0/L$
$\xi$	=	Location in subgrid system
$\xi_{min}$	=	Location where the least square error becomes minimum
$\phi$	=	Critical front face slope angle
$\phi_0$	=	Initiation slope angle
$\phi_B$	=	Termination slope angle

## TABLE OF CONTENTS

	Page
ABSTRACT .....	ii
COPYRIGHT .....	iv
DEDICATION .....	v
ACKNOWLEDGMENTS .....	vi
NOMENCLATURE .....	vii
TABLE OF CONTENTS .....	x
LIST OF FIGURES .....	xii
LIST OF TABLES .....	xiv
 Chapter	
I. INTRODUCTION .....	1
1.1 Background .....	1
1.2 Objectives .....	3
1.3 Scope of Study and Outline .....	4
II. LITERATURE REVIEW .....	6
2.1 Extension of the Boussinesq Equation .....	6
2.2 FUNWAVE .....	10
2.3 Wave Breaking Triggers .....	12
2.3.1 Phase-Averaged Type Wave Breaking Trigger .....	13
2.3.2 Phase-Resolving Type Wave Breaking Trigger .....	14
2.4 Relative Trough Froude Number Theory .....	18
2.5 Properly-Posed Boundary Value Problem .....	19
III. THEORETICAL ANALYSIS .....	21
3.1 Overview .....	21
3.2 Redefinition of the RTFN .....	21
3.3 The RTFN with Linear Wave Theory .....	22
3.4 The RTFN with Stokes Second Order Wave Theory .....	23
3.5 The RTFN with Solitary Wave Theory .....	25
3.6 The CTFN and Wave Breaking Indexes in Shallow Water on Sloping Bottom .....	27
3.7 Summary for Theoretical Analysis .....	30

Chapter	Page
IV. WAVE TANK EXPERIMENT .....	31
4.1 Introduction .....	31
4.2 Experimental Setting .....	31
4.3 Results .....	33
V. CALCULATION METHODS .....	37
5.1 Introduction .....	37
5.2 The Calculation Procedure of the RTFN .....	37
5.3 Implementation into FUNWAVE .....	38
5.4 Wave Celerity Calculation .....	39
5.4.1 Analytical Formula .....	39
5.4.2 Using Pure Advection Equation .....	40
5.4.3 Tracking Crest and Trough Position .....	42
5.4.4 Least Square Estimation .....	44
5.4.5 Summary for Wave Celerity Calculation .....	49
VI. NUMERICAL EXPERIMENTS .....	50
6.1 Introduction .....	50
6.2 Qualitative Study .....	50
6.2.1 Plane Slope Beach .....	51
6.2.2 Bar-Trough Beach .....	56
6.2.3 Real Bathymetry .....	58
6.2.4 Summary of Qualitative Studies .....	61
6.3 Calibration of the CTFN .....	62
6.4 Slope Effect .....	77
6.5 Duration of the Wave Breaking .....	83
VII. CONCLUSIONS AND RECOMMENDATIONS .....	88
7.1 Overview .....	88
7.2 Summary for the Entire Work .....	88
7.3 Conclusions and Recommendations .....	92
REFERENCES .....	94
APPENDIXES	
A. SOURCE CODE (SUBROUTINES ADDED) .....	98
B. RESULT (SLOPE EFFECT) .....	110
VITA .....	118

## LIST OF FIGURES

Figure	Page
2.1 Definition sketch of surface angle method (From Schäffer et al., 1993) .....	15
2.2 Definition sketch of the RTFN (From Utku and Basco, 2002) .....	19
3.1 The CTFN with Stokes second order wave theory .....	25
3.2 Definition sketch of solitary wave case .....	26
3.3 Definition sketch for sloped bottom .....	28
4.1 Wave tank setting .....	32
4.2 Wave gauge record .....	34
4.3 Wave breaking location analysis on digital video record .....	34
5.1 Wave celerity calculated by analytical formulas .....	41
5.2 Wave celerity calculated from pure advection equation .....	42
5.3 Wave celerity calculated by tracking method .....	43
5.4 Wave celerity calculated by least square estimation .....	46
5.5 Wave celerity calculated by least square method and analytical formula .....	48
6.1 The RTFN evolution on a plane slope .....	53
6.2 Wave profile envelopes on plane beach	
(a) The RTFN trigger	
(b) FUNWAVE original trigger .....	54
6.3 Eddy viscosity generated by wave breaking : plane slope	
(a) The RTFN trigger	
(b) FUNWAVE original trigger .....	55
6.4 Bathymetry setting and water surface profile : bar-trough beach .....	57
6.5 The RTFN evolution on a bar-trough beach .....	58

Figure	Page
6.6 Eddy viscosity generated by wave breaking : bar-trough beach	
(a) The RTFN trigger	
(b) FUNWAVE original trigger .....	59
6.7 Bathymetry setting and water surface profile : real bathymetry .....	60
6.8 The RTFN evolution on a real bathymetry .....	61
6.9 Wave breaking location comparison (CTFN=1.36 & FUNWAVE) .....	66
6.10 Wave breaking location comparison (CTFN=1.68) .....	69
6.11 Wave breaking location comparison (CTFN=1.47) .....	73
6.12 Wave breaking location comparison (Least square estimation method) .....	76
6.13 Slope effect on breaking depth (T=0.75sec) .....	78
6.14 Slope effect on breaking depth (T=1.0sec) .....	78
6.15 Slope effect on breaking depth (T=1.5sec) .....	79
6.16 Slope effect on breaking depth (T=2.0sec) .....	79
6.17 Determination of wave breaking height .....	81
6.18 Slope effect : comparison with Goda(1970) .....	82
6.19 Example wave profile over the bar .....	84
6.20 Wave profile evolution over a wide bar (RTFN) .....	87
6.21 RTFN evolution over a wide bar .....	87

## LIST OF TABLES

Table	Page
4.1 Wave breaking location(m), d=30cm .....	36
4.2 Wave breaking location(m), d=40cm .....	36
4.3 Wave breaking location(m), d=50cm .....	36
6.1 Wave breaking location(m), d=30cm (RTFN) .....	64
6.2 Wave breaking location(m), d=30cm (RTFN) .....	64
6.3 Wave breaking location(m), d=50cm (RTFN) .....	64
6.4 Wave breaking location(m), d=30cm (FUNWAVE) .....	65
6.5 Wave breaking location(m), d=40cm (FUNWAVE) .....	65
6.6 Wave breaking location(m), d=50cm (FUNWAVE) .....	65
6.7 RTFN value at the wave breaking location in physical experiment (30cm) .....	67
6.8 RTFN value at the wave breaking location in physical experiment (40cm) .....	67
6.9 RTFN value at the wave breaking location in physical experiment (50cm) .....	67
6.10 Wave breaking location(m), d=30cm (CTFN=1.68) .....	68
6.11 Wave breaking location(m), d=40cm (CTFN=1.68) .....	68
6.12 Wave breaking location(m), d=50cm (CTFN=1.68) .....	68
6.13 Wave breaking location(m), d=30cm (CTFN=1.47) .....	72
6.14 Wave breaking location(m), d=40cm (CTFN=1.47) .....	72
6.15 Wave breaking location(m), d=50cm (CTFN=1.47) .....	72
6.16 Wave breaking location(m), d=30cm (Least square estimation) .....	75
6.17 Wave breaking location(m), d=40cm (Least square estimation) .....	75
6.18 Wave breaking location(m), d=50cm (Least square estimation) .....	75

Table	Page
B.1 T=0.75sec, H=0.016m (RTFN) .....	110
B.2 T=0.75sec, H=0.016m (FUNWAVE) .....	110
B.3 T=0.75sec, H=0.052m (RTFN) .....	111
B.4 T=0.75sec, H=0.052m (FUNWAVE) .....	111
B.5 T=1.0sec, H=0.016m (RTFN) .....	112
B.6 T=1.0sec, H=0.016m (FUNWAVE) .....	112
B.7 T=1.0sec, H=0.052m (RTFN) .....	113
B.8 T=1.0sec, H=0.052m (FUNWAVE) .....	113
B.9 T=1.5sec, H=0.016m (RTFN) .....	114
B.10 T=1.5sec, H=0.016m (FUNWAVE) .....	114
B.11 T=1.5sec, H=0.052m (RTFN) .....	115
B.12 T=1.5sec, H=0.052m (FUNWAVE) .....	115
B.13 T=2.0sec, H=0.016m (RTFN) .....	116
B.14 T=2.0sec, H=0.016m (FUNWAVE) .....	116
B.15 T=2.0sec, H=0.052m (RTFN) .....	117
B.16 T=2.0sec, H=0.052m (FUNWAVE) .....	117

## CHAPTER I

### INTRODUCTION

#### 1.1 Background

It is very important for coastal engineers to know where and when waves break in the nearshore zone.<sup>1</sup> Coastal engineers build various structures in the coastal region. Here the term “structure” does not only mean classical concrete or rock structures, such as a sea wall, jetty, or groin, but also includes sandy beaches by beach nourishment. Whatever is constructed in the nearshore zone, the location of wave breaking is a major factor of design. Because the energy stored in the wave is exerted during wave breaking, the wave breaking causes two things that are of concern for design: (1) the wave forces acting on the coastal structures are maximized at the location of wave breaking, and (2) the energy exerted from the wave breaking is the main driving force of various nearshore hydrodynamic phenomena such as wave set-up/down, wave run-up, longshore current, rip current, and nearshore circulation. The first effect is directly related to the location and the stability of the structure. If where the wave breaking occurs is known, the designer can choose the structure location away from the breaking location, or if the structure location is predetermined, the structure design has to be made strong enough against the waves. The second effect dictates the hydraulics inside of the surfzone, which is very important to sediment transportation. Therefore, wave breaking gives great influence on the stability and efficiency of the coastal “structures” so that coastal engineers must consider the wave breaking location for designing any kind of coastal project.

Numerous studies about wave breaking have been undertaken for over a century. The earliest study were in the late nineteenth century (Stokes, 1890; Mitchell, 1893; McCowen,

---

<sup>1</sup>The journal model for this dissertation is Coastal Engineering.

1894). Since wave breaking is a highly non-linear and turbulent process, it is difficult to analyze the physics inside of a breaking wave. Results from early studies include the empirical relation of wave characteristics, such as wave height and wave length in the deep water, and the location of wave breaking, or geometrical limit in the wave shape at the breaking location. Most are determined from field observations and laboratory experiments (LeMéhanté and Koh, 1967; Goda, 1970; Weggel, 1972; Kaminsky and Kraus, 1993; among others).

Many efforts during the last decade have been made to extend the Boussinesq (1872) equation (Madsen et al., 1991; Nwogu, 1993; Wei et al., 1995) to shorter wave periods. In addition, the development of computer resources permits the use of phase resolving Boussinesq equation model as a nearshore wave model. The Boussinesq equation model can solve non-hydrostatic pressure conditions in the wave so that it can compute nonlinear finite amplitude wave transformation. But the Boussinesq equation does not include the physics of wave breaking. Without a breaking mechanism, the Boussinesq model will collapse in the nearshore zone because the wave shape goes beyond the geometrical limit as a result of wave transformation. It is, therefore, necessary to develop a new wave breaking mechanism including a wave breaking trigger as well as energy dissipation or momentum sink during the breaking suitable for phase resolving numerical models.

Utku (1999) introduced an entirely new concept for wave breaking trigger criteria, the relative trough Froude number (RTFN). This concept is based on the physics of the moving hydraulic jump. Therefore, it satisfies properly posed boundary value problem (Abbott, 1966) explicitly so that this model achieves a hydraulically more appropriate trigger than empirically obtained breaking trigger mechanism. Utku (1999) calculated its critical value as 1.36 from the analogy to the undular hydraulic jump in the open flume

and confirmed it from experiments at the laboratory scale.

Phase resolving wave models compute the water surface elevation and the velocity at each grid point at each time step. Thus, by specifying trough and crest location in the wave profile, the RTFN can be calculated for each wave at each time step. This study focuses on implementing the new wave breaking trigger model based on the RTFN theory into the phase resolving Boussinesq equation wave model, and performing numerical experiments in order to determine the model parameters.

## 1.2 Objectives

The primary purpose of this study is to implement the new wave breaking trigger mechanism based on the RTFN theory into an existing, phase resolving Boussinesq equation wave model (FUNWAVE, Kirby et al., 1998). The wave celerity calculation is the most important part for the numerical modeling of the RTFN theory because the RTFN mainly depends on the contribution due to the wave celerity. For this reason, extensive studies are performed for determination of the wave celerity. The other important feature concerned with the wave breaking in numerical modeling is the dissipation of energy or extraction of momentum from the wave after the initiation of wave breaking. However, this aspect is not considered here and is left for future research.

Numerical experiments have two phases: qualitative study and quantitative study. In addition, a wave tank experiment is performed to measure the exact location of initiation of wave breaking, and the result is used for model parameter calibration.

Though the experimental study by Utku (1999) proved that the RTFN theory can be used as a wave breaking trigger, it is unknown why the RTFN theory gives one universal threshold value as a wave breaking trigger. Therefore, a theoretical analysis is also carried out to determine the analytical expression of the RTFN model and the critical condition for

wave breaking. Coupled with various wave theories, the theory displays the effectiveness of the RTFN theory as a wave breaking trigger mechanism for the complete wave range from deep to shallow water.

### 1.3 Scope of Study and Outline

This work contains the following chapters.

Chapter II summarizes the current literature related to this subject. A brief history of the expansion of the Boussinesq equation and the technical specification of the model called FUNWAVE are reviewed in order to get a better understanding of the model for this study. Existing wave breaking trigger models are classified and summarized by parameters that are used in the model and how they control the wave breaking event. Finally, the foundation of the relative trough Froude number (RTFN) theory and the experimental work performed by Utku (1999) is summarized for this study.

Chapter III presents a theoretical analysis for the RTFN theory. In this research, the main object of the theoretical analysis is to define the critical condition theoretically. Utku (1999) introduced the theoretical framework of the RTFN theory, but none of the theoretical work for the critical condition was performed. Without the critical condition, the theory does not have any meaning for the wave breaking trigger. Therefore, the critical conditions of the RTFN theory under different wave theories are derived from substituting related equations and expressions into the RTFN framework. A theoretical explanation of the wave breaking indexes in shallow water is also developed in this chapter.

Wave tank experiments were performed to obtain data for calibration of the model. Chapter IV explains the experimental setting, including wave tank dimensions, input wave conditions, and data recording methods, then results are summarized for later use.

Chapter V shows numerical modeling techniques used. The calculation procedure is

explained in detail but most of this chapter is devoted to explaining how to calculate the wave celerity at the wave crest and the trough position. The most important and the most difficult part of the RTFN calculation is to find the correct wave celerity at both locations, crest and trough. Four alternatives are selected and are closely examined to find the right solution.

Chapter VI is the main focus of this study – the numerical model computation. Numbers of numerical experiments are tested in different situations and methodologies. First, models with the CTFN given by Utku (1999) are examined qualitatively to confirm the RTFN theory works “properly” as a wave breaking trigger in the numerical model. Then the model parameter calibration is accomplished with data obtained from the wave tank experiment performed in Chapter IV. After the CTFN is calibrated, the model is tested with different beach slopes to see the bottom slope effect against the wave breaking location. Results are compared with another wave breaking trigger for a phase-resolving wave model and the theory by Goda (1970). Lastly, the model is examined on bar-trough shaped beach for wave decay after the wave breaking. The result identifies what is missing in the present formulation of the RTFN theory for wave breaking.

Lastly, Chapter VII summarizes all the results obtained in this study and makes some recommendations for future studies.

## CHAPTER II

### LITERATURE REVIEW

#### 2.1 Extension of the Boussinesq Equation

There are many mathematical equations to express water motion and waves. Among them, the three dimensional, fully nonlinear Navier-Stokes equations gives the most accurate mathematical expression for the water movement. Therefore, the solution of the Navier-Stokes equations gives us the most accurate wave model as a result. But it is difficult to solve the three dimensional fully nonlinear Navier-Stokes equations because of the non-linearity and complex boundary conditions in the mathematical sense and the lack of computer resources for numerical modeling. Therefore, some approximated models have been used under certain assumptions, in other words, within some restrictions.

The Boussinesq equation is a depth-integrated model so that the vertical structures of the velocity distribution and the pressure distribution are estimated and integrated under some assumption. This equation was first derived by Boussinesq (1872) for describing the solitary wave motion in an open canal. The main difference from the more simplified shallow water equation is that the pressure distribution under the free surface includes an effect from the dynamical motion of the wave. In the Boussinesq equation, the ratio of the water depth to the wave length is assumed to be a finite number. On the other hand, this ratio in shallow water equation is assumed to be an infinitesimally small number. As a result, the streamline has curvature in the Boussinesq equation and the pressure distribution under the free surface is not hydrostatic. There are many variants of the Boussinesq equation depending upon how to take account the depending variables. Here

is one of the classical forms of the Boussinesq equation. Continuity equation is given as;

$$\frac{\partial \eta}{\partial t} + \frac{\partial P}{\partial x} + \frac{\partial Q}{\partial y} = 0 \quad (2.1)$$

And momentum equations are;

$$\frac{\partial P}{\partial t} + \frac{\partial}{\partial x} \left( \frac{P^2}{\delta} \right) + \frac{\partial}{\partial y} \left( \frac{PQ}{\delta} \right) + g\delta \frac{\partial \eta}{\partial x} - \frac{1}{3}h^2 \left( \frac{\partial^3 P}{\partial x^2 \partial t} + \frac{\partial^3 Q}{\partial x \partial y \partial t} \right) = 0 \quad (2.2)$$

$$\frac{\partial Q}{\partial t} + \frac{\partial}{\partial y} \left( \frac{Q^2}{\delta} \right) + \frac{\partial}{\partial x} \left( \frac{PQ}{\delta} \right) + g\delta \frac{\partial \eta}{\partial y} - \frac{1}{3}h^2 \left( \frac{\partial^3 Q}{\partial y^2 \partial t} + \frac{\partial^3 P}{\partial x \partial y \partial t} \right) = 0 \quad (2.3)$$

where  $\eta$  = free surface displacement from the equilibrium position,  $P, Q$  = the depth integrated mass flux per unit time (or may be called depth integrated velocity component ( $m^2/s$ ) as stated in Madsen et al., 1991) in  $x$  and  $y$  respectively,  $h$  = the still water depth,  $\delta$  = the total water depth(=  $h + \eta$ ), and  $g$  = the acceleration of gravity.

The Boussinesq equation can solve finite amplitude irregular waves because of the non-hydrostatic pressure assumption mentioned above. And the Boussinesq equation also has the capability of reproducing various nearshore wave phenomena such as shoaling, refraction, and diffraction. But the classical type of the Boussinesq equation is only accurate in very shallow water.

Madsen et al. (1991) made a comparison of the dispersion relations from various forms of the classical Boussinesq equation. In the comparison of the phase celerity of the wave, these classical forms of the Boussinesq equations are only accurate in depths less than 12 to 22% of the equivalent deep water wave lengths, depending on the form of the equation, with 5% error against the Stokes wave celerity. This restriction is fatal for application of the Boussinesq equation to the nearshore wave model, because the applicable area is constrained within a very narrow strip from the coastline. In many cases, the wave climate at the offshore boundary of the numerical model is estimated from the hindcast data measured at the far offshore location. If the model can be applied far enough from

the coastline so that the wave train would stay in the deep water wave at the boundary of the model, the wave data measured at the offshore site can be used as an incident wave condition without any problem of transformation as the wave feels the bottom. But the wave train could be transformed by the time it reaches the offshore boundary with this depth restriction if the applicable area of the model is restricted to very shallow water. Therefore, numerous efforts have been made for expanding the applicable limit of the Boussinesq equation towards deep water.

Madsen et al. (1991) introduced additional, third order differential terms into the momentum equations, Eqns 2.2 and 2.3. These terms vanish in very shallow water so that they do not disturb the dispersion properties of the original Boussinesq equation in that area. These additional terms improve the dispersion relation in relatively deeper water. With appropriate selection of the parameter, the phase celerity error is less than 3% for the depth of shallower than 55% of the equivalent deep water wave length, and the group velocity error is less than 6% within the range of 0 to 55% of deep water wave length.

As mentioned above, the Boussinesq equation is a depth-integrated model, therefore, the dependent variables  $P$  and  $Q$  in the above equations are the integrated values over the water depth. Usage of the mass flux in the conservation form of the Boussinesq equation guarantees the momentum conservation across the control section, thus a numerical model based on this form of the Boussinesq equation has a capability to handle shock phenomena such as hydraulic jump. However, an additional calculation or estimation for the determination of the velocity at a specified depth is needed (For details, see Madsen et al. (1996), for example). Specially in the deeper water, a simple  $P/\delta$  calculation, in Eqn 2.2 for example, may not correctly represent the velocity at the given location. The integration process averages out the velocity distribution, and unlike the open channel flow

which has fairly uniform velocity distribution in most of the water column, the averaged velocity and the velocity at a certain depth could have a significant difference.

Nwogu (1993) derived another form of the Boussinesq Equation from the integration of the Euler's equation of the motion using a vertical distribution expression referenced to the horizontal velocity component  $\mathbf{u}_\alpha$  at the arbitrary depth,  $z_\alpha$ . The resulting form of the Boussinesq equation is shown as follows;

$$\eta_t + \nabla \cdot [(h + \varepsilon\eta)\mathbf{u}_\alpha] + \mu^2 \nabla \cdot \left\{ \left( \frac{z_\alpha^2}{2} - \frac{h^2}{6} \right) h \nabla (\nabla \cdot \mathbf{u}_\alpha) + \left( z_\alpha + \frac{h}{2} \right) h \nabla [\nabla \cdot (h\mathbf{u}_\alpha)] \right\} = 0 \quad (2.4)$$

$$\mathbf{u}_{\alpha t} + \nabla \eta + \varepsilon (\mathbf{u}_\alpha \cdot \nabla) \mathbf{u}_\alpha + \mu^2 \left\{ \frac{z_\alpha^2}{2} \nabla (\nabla \cdot \mathbf{u}_{\alpha t}) + z_\alpha \nabla [\nabla \cdot (h\mathbf{u}_{\alpha t})] \right\} = 0 \quad (2.5)$$

where subscript  $t$  denotes the time derivative, and  $h$  = still water depth,  $\varepsilon = a_0/h_0$ ,  $\mu = h_0/L$ ,  $a_0$  = typical amplitude,  $h_0$  = characteristic depth, and  $L$  = wave length. Compared to the classical form of the Boussinesq equation, this equation contains additional terms in the continuity equation for the conservation of mass (Eqn. 2.4). The accuracy of the dispersion relationship in this equation is calculated that the maximum error in phase celerity is 2% for  $0 < h/L_0 < 0.5$  and 12% in the group velocity. This equation can be used as an alternative governing equation in FUNWAVE, which will be discussed fully below.

The above mentioned equations achieved significant improvement in the dispersion relationship so that the Boussinesq equation can be applied further offshore than before. But these equations are restricted in the situation with weakly non-linear interactions. Because these equations neglect higher order terms in the vertical velocity distribution, which is higher than  $O(\varepsilon, \varepsilon\mu^2)$ ; the nonlinearity of the equation is weak. Wei et al. (1995a) argues that this weak nonlinear perturbation assumption is critical for waves just about

to break, because the wave has strong nonlinearity as a result of shoaling. Therefore, they derived “fully” nonlinear Boussinesq equations with truncated error of  $O(\varepsilon\mu^2, \mu^4)$ . Even though the derivation method is different, the resulting equation has similar structure to the Nwogu’s equation. In fact, neglecting the higher order term recovers Nwogu’s equation, Eqn 2.4 and 2.5. The continuity equation has following form,

$$\eta_t + \nabla \cdot \left[ (h + \varepsilon\eta) \left[ \mathbf{u}_\alpha + \mu^2 \left\{ \left( \frac{z_\alpha^2}{2} - \frac{1}{6} (h^2 - h\varepsilon\eta + (\varepsilon\eta)^2) \right) \nabla (\nabla \cdot \mathbf{u}_\alpha) + \left( z_\alpha + \frac{1}{2} (h - \varepsilon\eta) \right) \nabla [\nabla \cdot (h\mathbf{u}_\alpha)] \right\} \right] \right] = 0 \quad (2.6)$$

and the momentum equation is;

$$\mathbf{u}_{\alpha t} + \varepsilon(\mathbf{u}_\alpha \cdot \nabla)\mathbf{u}_\alpha + \nabla\eta + \mu^2\mathbf{V}_1 + \varepsilon\mu^2\mathbf{V}_2 = 0 \quad (2.7)$$

where

$$\mathbf{V}_1 = \frac{1}{2}z_\alpha^2\nabla(\nabla \cdot \mathbf{u}_{\alpha t} + z_\alpha\nabla(\nabla \cdot (h\mathbf{u}_{\alpha t}))) - \nabla \left[ \frac{1}{2}(\varepsilon\eta)^2\nabla \cdot \mathbf{u}_{\alpha t} + \varepsilon\eta\nabla \cdot (h\mathbf{u}_{\alpha t}) \right] \quad (2.8)$$

$$\mathbf{V}_2 = \nabla \left[ (z_\alpha - \varepsilon\eta)(\mathbf{u}_\alpha \cdot \nabla)(\nabla \cdot (h\mathbf{u}_\alpha)) + \frac{1}{2}(z_\alpha^2 - (\varepsilon\eta)^2)(\mathbf{u}_\alpha \cdot \nabla)(\nabla \cdot (h\mathbf{u}_\alpha)) \right] + \frac{1}{2}\nabla \left[ (\nabla \cdot (h\mathbf{u}_\alpha) + \varepsilon\eta\nabla \cdot \mathbf{u}_\alpha)^2 \right] \quad (2.9)$$

Wei et al. (1995a) compared the numerical result of fully nonlinear Boussinesq model (FNBM), Nwogu’s model (BM) and fully nonlinear potential flow model (FNPF, Grilli et al., 1994). The result of the FNBM showed good agreement with the result of the FNPF, while the wave shape of the BM is not realistic as a result of shoaling (See Figure 4 through Figure 10 in Wei et al., 1995a). This model is the default governing equation of FUNWAVE, which will be mentioned in the following section.

## 2.2 FUNWAVE

FUNWAVE (Kirby et al., 1998) is the acronym for “Fully Nonlinear Boussinesq Wave model”. This model is developed and maintained by the University of Delaware. Many

studies which employ FUNWAVE as a numerical modeling scheme have been reported (Chen et al., 1999; Chen et al., 2000a; Chen et al., 2000b; Kennedy et al., 2000). The governing equation of the model is based on the Boussinesq equation incorporated with frictional damping, wave breaking, and a slot scheme for a moving shoreline. The type of the Boussinesq equation can be chosen either classical Boussinesq equation, nonlinear shallow water equation, Nwogu's equation or Wei's equation. And Wei's fully nonlinear Boussinesq equation is chosen in this study.

The main purpose of this study is to implement and examine the validation of the RTFN theory so that the one dimensional Boussinesq equation model is used in this study. The governing equations can be reduced to

$$\eta_t = E(\eta, u) + \gamma E_2(\eta, u) + f(x, t) \quad (2.10)$$

$$[U(u)]_t = F(\eta, u) + \gamma [F_2(\eta, u) + F^t(\eta, u_t)] + F_{br} + F_b + F_{sp} \quad (2.11)$$

The quantities  $U$ ,  $E$ ,  $E_2$ ,  $F$ ,  $F_2$ , and  $F^t$  have following definitions:

$$U = u + h [b_1 h u_{xx} + b_2 (hu)_{xx}] \quad (2.12)$$

$$E = -\frac{1}{\kappa} (\Lambda u)_x - \left\{ a_1 h^3 u_{xx} + a_2 h^2 (hu)_{xx} \right\}_x \quad (2.13)$$

$$F = -g\eta_x - uu_x \quad (2.14)$$

$$E_2 = - \left\{ \left[ a_1 h^2 \eta + \frac{1}{6} \eta (h^2 - \eta^2) \right] u_{xx} \right\}_x - \left\{ \left[ a_2 h \eta - \frac{1}{2} \eta (h + \eta) \right] (hu)_{xx} \right\}_x \quad (2.15)$$

$$F_2 = - \left\{ \frac{1}{2} (z_\alpha^2 - \eta^2) uu_{xx} \right\}_x - \{ z_\alpha - \eta \} u (hu)_{xx} \}_x - \frac{1}{2} \left\{ [(hu)_x + \eta(u_x)]^2 \right\}_x \quad (2.16)$$

$$F^t = \left\{ \frac{1}{2} \eta^2 u_{xt} + \eta (hu_t)_x \right\}_x \quad (2.17)$$

The parameters  $a_1$ ,  $a_2$ ,  $b_1$ ,  $b_2$ , and  $\gamma$  determine the characteristics of the Boussinesq equation. For fully nonlinear Boussinesq equation,

$$a_1 = \frac{1}{2} \zeta^2, \quad a_2 = \zeta + \frac{1}{2}, \quad b_1 = \frac{1}{2} \zeta^2, \quad b_2 = \zeta, \quad \gamma = 1 \quad (2.18)$$

and,  $\zeta$  is the dimensionless reference water depth, which is  $\zeta = z_\alpha/h = -0.531$ . The quantities  $F_{br}$ ,  $F_{bs}$ , and  $F_b$  are additional momentum sink terms which allows the model to be applied to realistic situations, and they correspond to the wave breaking component, the absorption damping component at the boundary, and the bottom friction component, respectively. The detail of the wave breaking model will be explained in the following section. And finally, the quantity  $f$  is the source function term which generates waves in the field.

Discretization of the Boussinesq equation must be performed very carefully because the truncation error introduced by the finite differencing can corrupt the nonlinear effect led by the higher order terms. Therefore, FUNWAVE employs a complicated combined scheme. For the first order spatial differential terms, the five point finite difference scheme is used so that the truncation error from this formation is as low as order of  $(\Delta x)^4$ , while, the centered three point finite difference is used for the second order derivatives. The Adams-Bashforth-Moulton scheme is a predictor and corrector scheme for the time derivatives. The combination of third order Adams-Bashforth scheme for the predictor step and the fourth order Adams-Moulton scheme for the corrector step reduces the truncation error to the order of  $(\Delta t)^4$ .

### 2.3 Wave Breaking Triggers

The most fundamental principle for the wave breaking condition in terms of hydrodynamics is that the waves become unstable when the particle velocity at the crest exceeds the celerity of the wave. This principle explains why or how the wave breaking would occur but does not tell us where or when it would happen in the field. Therefore, many wave breaking criteria have been proposed for over a century. Wave breaking criteria can be divided into the two categories, traditional phase-averaged type and the new phase-

resolving type mainly utilized for the Boussinesq equation based numerical model.

### 2.3.1 Phase-averaged Type Wave Breaking Trigger

First, phase-averaged type wave breaking triggers are reviewed in this subsection. They are called “phase-averaged” type because these formulas are composed with wave characteristics, i.e. the wave height and the length/period, and these wave characteristics are representative values of one full phase of the wave. Phase-averaged type wave breaking criteria can be furthermore classified into two types. The first type describes the geometrical limit of the wave at the breaking location, and the second type explains the breaking height ratio against the incoming deep water wave height accompanied with deep water wave characteristics.

Early attempts to describe the wave breaking condition are all categorized as the geometric type. Stokes (1890) explained a wave breaking condition as the corresponding wave crest angle of  $120^\circ$ . Mitchell (1893) explained that this condition in deep water can be reformatted to the maximum wave steepness of the wave such as  $(H_0/L_0)_{max} = 0.142$ . For shallow water waves, McCowan (1894) gave the depth limit criterion calculated from the Stokes’ criterion, such as  $H_b/d_b = 0.78$ . Many researchers proposed different critical values for the depth limit criterion, in the range of from 0.73 to 1.03 (Komar, 1998). For the case of the solitary wave it could be more than 2.0, but McCowan’s 0.78 is the most common value.

The applicable area of these conditions is restricted in either deep water or shallow water. They are not universal. Miche (1944) extended Mitchell’s equation to the intermediate and shallow water waves,

$$\left(\frac{H}{L}\right)_{max} = 0.142 \tanh\left(\frac{2\pi d}{L}\right) \quad (2.19)$$

This equation includes both wave steepness criteria and depth limit criteria, which are

connected by hyperbolic tangent function. Therefore, it can be applied to any kind of state of the wave, though the depth limited condition ( $H_b/d_b$ ) becomes slightly bigger (0.89) than the commonly used value (0.78).

The second types are formulated in the form of the breaking wave height ratio against the deep water wave. For example, Munk (1949) derived a following expression by equating energy fluxes at the breaker zone and the deep water accompanied with the depth limit criterion,  $H_b/h_b = 0.78$  as the wave breaking condition,

$$\frac{H_b}{H_0} = \frac{1}{3.3(H_0/L_0)^{1/3}} \quad (2.20)$$

These types are intended for use in applications without computer assistance by embedding wave shoaling effect in the equation. But they are of no use for this study because the Boussinesq equation computes the wave transformation.

Lastly, wave breaking indexes on the sloped bottom is reviewed briefly. It is known that the wave breaking location would shift on a different bottom slope. However, none of the wave breaking conditions mentioned above include a term related to the bottom slope in the equation. Goda (1970) compiled a number of data sets from wave tank experiments by several researchers. The range of beach slope in those experiments are from 1:9 to 1:100. Then several wave breaking trigger index curves in different expressions are established with including the bottom slope effect. For more details about these index curves, see Goda (1970). Other wave breaking indexes including the slope effect can be seen in SPM (1984) and CEM (2002).

### 2.3.2 Phase-resolving Type Wave Breaking Trigger

Phase resolving wave breaking criteria were developed for the Boussinesq equation model because the Boussinesq equation computes phase resolved information of the wave which is hard to determine by physical experiment. The Boussinesq Equation does not

have an inherent wave breaking mechanism because of the difference of the physics between the breaking wave and the non-breaking wave. Therefore, the model has to include an additional momentum term to describe the energy dissipation due to the wave breaking, and the wave breaking event should be controlled by a certain wave breaking trigger mechanism to realize the initiation and termination of the wave breaking.

There are three types of additional momentum evaluation methods for wave breaking; surface roller model (Schäffer et al., 1993; Madsen et al., 1997a,b; Sørensen et al., 1998; etc.), vorticity model (Svendsen et al., 1998), and eddy viscosity model (Kirby et al., 1998; Chen et al., 1999; Kennedy et al., 2000; etc.). There are only three phase resolving wave breaking criteria. Two of them are closely related to the establishment of energy dissipation methods mentioned above.

Schäffer et al. (1993) introduced the front face angle method schematized in Fig. 2.1. This is associated with the surface roller model. The parameter of this method is the

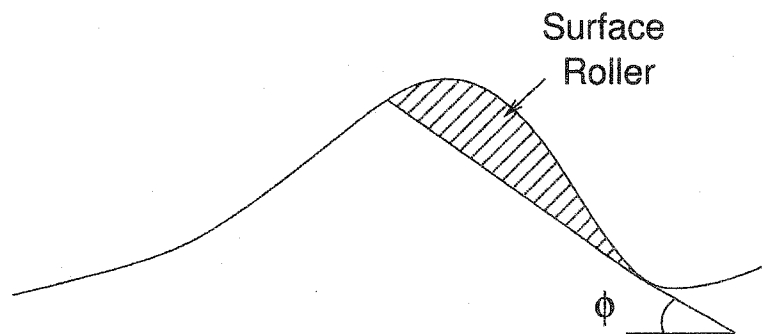


Figure 2.1: Definition sketch of surface angle method (From Schäffer et al., 1993)

local slope angle of the front face of the wave. The surface roller area is defined as an area surrounded by the free surface and the critical condition line with angle  $\phi$ , as seen in Fig. 2.1, and the extra momentum term is added to the equation at the calculation

nodes designated as the surface roller area. The critical condition is controlled by three parameters in this model. They are the initiation condition,  $\phi_B$ , the termination condition,  $\phi_0$ , and the duration or the time scale for the development of the roller,  $t^*$ . For nonbreaking waves, the critical condition stays at the initiation value. When the local slope angle at any part of the front face exceeds the initiation condition, the critical condition line is drawn in the wave profile and it makes a surface roller area, as shown in Fig. 2.1, which means the initiation of the wave breaking.

After the wave breaking is started, the critical condition varies in time with the following expression,

$$\tan \phi = \tan \phi_0 + (\tan \phi_B - \tan \phi_0) \exp \left[ -\ln 2 \frac{t - t_b}{t^*} \right] \quad (2.21)$$

where,  $t_b$  = the time at the wave breaking is initiated. During wave breaking, the critical condition line is drawn from a point where the local slope angle matches to the critical condition defined by Eqn 2.21 to make a tangential line. Note that the critical condition  $\phi$  does not represent the maximum local slope angle after wave breaking initiates. Wave breaking is terminated when the local slope angle at the all nodes in the front slope of the wave has a smaller value than the critical condition given by Eqn 2.21 so that the surface roller area cannot be formed.

The number set of three control parameters introduced by Schäffer et al. (1993) is  $(\phi_B, \phi_0, t^*) = (20^\circ, 10^\circ, T/5)$  and this set is also used by Madsen et al. (1997a). This set is a default value which does not guarantee the result to fit with the experimental results universally. Madsen et al. (1997a) showed that the default set gives good agreement with experimental result for spilling breaker on the plane slope beach but adjustment of  $\phi_B$  to  $25^\circ$  and  $t^*$  to  $T/10$  is needed for plunging breaker. Also, they concluded that

$(\phi_B, \phi_0) = (14^\circ, 7^\circ)$  gives good agreement for the case on bar-trough beach profile. Because the governing equation of this model is the flux type (e.g. Eqn. 2.1), the calculated shoaling is underestimated (Madsen et al. (1997a)). Therefore, the calibrated initiation value,  $\phi_B$  is smaller ( $20^\circ$ ) than the theoretical limit in the cnoidal wave theory ( $26^\circ$ ). Sørensen et al. (1998) modified the governing equation to correct the underestimation and recalibrated the initiation condition. Using a new equation set, the calibrated initiation condition  $\phi_B$  was redefined to  $32^\circ$ .

The second phase-resolving criterion is the method used in FUNWAVE. The energy dissipation mechanism associated with this wave breaking trigger is the eddy viscosity model. The control parameter of this model is the vertical acceleration of the free surface of the water,  $\eta_t$ . The structure for controlling the critical condition in this model is similar to the previous method. It requires three key control values to control the critical condition after the wave breaking. The eddy viscosity has nonzero value when the vertical acceleration of free surface,  $\eta_t$  exceeds a critical value, then the critical value varies with time controlled by the three control values as following;

$$\eta_t^* = \begin{cases} \eta_t^{(F)} & t - t_b \geq T^* \\ \eta_t^{(I)} + \frac{t - t_b}{T^*}(\eta_t^{(F)} - \eta_t^{(I)}) & 0 \leq t - t_b < T^* \end{cases} \quad (2.22)$$

where  $\eta_t^{(I)}$  is the initiation value,  $\eta_t^{(F)}$  is the termination value,  $T^*$  is the transition time(duration), and  $t_b$  is the time when the wave breaking is initiated. The default values of the initiation value and the termination value are  $0.35\sqrt{gh} \sim 0.65\sqrt{gh}$  and  $0.15\sqrt{gh}$ , respectively. The default value for the transition time is  $5\sqrt{h/g}$ . These values are, again, not the universal values applicable for any kind of wave conditions. Therefore, calibration of these three coefficients is needed to match experimental data.

The biggest difference in the frameworks of these two trigger mechanisms, other than

the control parameter, is the determination of the location at which the extra momentum term should be added inside of the breaking wave. We call them here the breaking nodes. For the surface roller model, the breaking nodes are the ones between where the local slope is equal to the critical value given by Eqn 2.21 to where the tangential line intersects again with the free surface. So, each node in the roller is not needed to exceed the critical value. On the other hand, in the model used in FUNWAVE, the breaking nodes are independently determined at each node as a result of Eqn 2.22. For a more detailed comparison of the existing phase-resolving type wave breaking trigger and the energy dissipation mechanism, see Svendsen et al. (1996).

#### 2.4 Relative Trough Froude Number Theory

The fundamental idea of the RTFN is to consider wave breaking as a moving hydraulic jump or bore, and taking the Froude number just as in the open channel hydraulics. Using the analogy to the moving hydraulic jump itself is not a new idea (for example, Peregrine and Svendsen (1978) and Basco and Svendsen (1984)), and the similarity of the wave breaking and the moving hydraulic jump in terms of hydraulics has been widely used for the analysis of the wave breaking, e.g. the surface roller model mentioned in the previous section is based on this concept.

Utku (1999) first related the Froude number as a wave breaking index under the moving hydraulic jump concept. Fig. 2.2 shows the definition sketch of the relative trough Froude number theory. The moving frame with the speed of the wave celerity,  $C$ , gives the relative velocity, and the conservation laws with respect to the moving frame can be applied under the Galilean transformation. Therefore, the Froude number with respect to the moving frame can be written,

$$Fr_t = \frac{u_{trough} + C}{\sqrt{gD}} \quad (2.23)$$

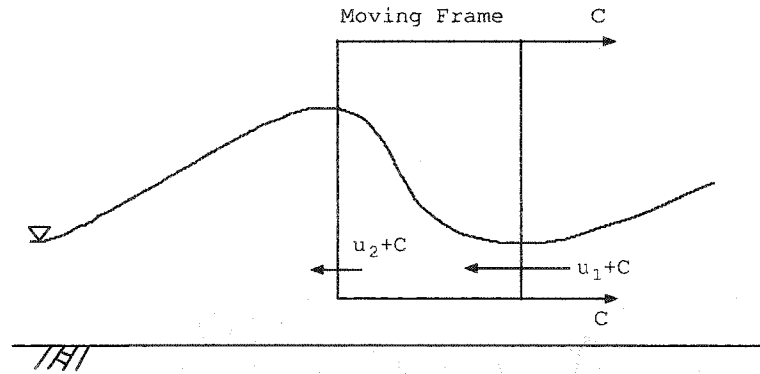


Figure 2.2: Definition sketch of the RTFN (From Utku and Basco, 2002)

where  $u_{trough}$  is a depth averaged particle velocity at the trough and  $D$  is the relative length scale, which is the water depth at the trough in shallow water.

Wave breaking begins when the RTFN exceeds the critical value and ceases when it becomes lower than the critical value. Wave tank experiments performed by Utku revealed that the critical relative trough Froude number is about 1.36, which gives a good agreement to the value for the stationary hydraulic jump at which the surface roller starts to build.

The most important feature of the RTFN theory is that it realizes wave breaking with only one coefficient. Another advantage of the RTFN formulation is inclusion of the upstream boundary condition. Because of this, the RTFN can handle explicitly the shift of the wave breaking location against the opposing current or the following wind over the wave. The other method can handle these problems as a result of the wave-current or wave-wind interaction. Utku (1999) examined four opposing current conditions (none, quarter, half, and full) and confirmed that regardless the existence of the opposing current or the strength, the critical RTFN (CTFN) was consistent.

## 2.5 Properly-posed Boundary Value Problem

Lastly, the properly-posed boundary value problem is discussed to state what kind of

condition should be included in a wave breaking trigger mechanism. As Abbott (1966) pointed out, all hydraulic problems have to satisfy properly-posed boundary value at the boundary of the model, depending on the direction of the characteristic function. Considering wave breaking as a shock problem, i.e. hydraulic jump, as widely accepted, three conditions have to be stated properly in the model; two from the upstream, i.e. onshore side, and one from the downstream, i.e. offshore side.

Existing wave breaking trigger models only satisfy these conditions implicitly. For example, slope angle of the front face of the wave is determined from the elevation and the location difference between the crest and the trough and the wave-current interaction (including zero wave-current interaction for the absence of the current). This includes one downstream condition (crest elevation) and two upstream conditions (trough elevation and current in front of the wave). But these are implicitly indicated in a variable called front slope angle as a result of wave transformation. All the other mechanisms related to the free surface geometry are in the same manner.

On the other hand, the RTFN trigger explicitly contains three conditions at the proper side of the boundary because the formulation itself is derived from the hydraulic jump. Since the RTFN trigger directly involves boundary conditions, the accuracy of the wave transformation in the wave model does not give a direct impact to the accuracy of the determination of the wave breaking location specially if a current exists in the field. This will be a theoretical advantage for the RTFN wave breaking trigger model.

## CHAPTER III

### THEORETICAL ANALYSIS

#### 3.1 Overview

The experimental work by Utku (1999) proved that the critical relative trough Froude number (CTFN) is consistent for different wave breaking conditions. However, from the theoretical view point, Utku (1999) only pointed out the similarity between the wave breaking initiation and the development of the surface roller in the undular hydraulic jump in the open channel flume for the explanation of the critical value of the RTFN. A quantitative approach to explain the critical condition for the RTFN theory was not included. In this chapter, a theoretical analysis to find the critical condition of the RTFN is performed under several simplified assumptions, and the results show that the RTFN theory is also theoretically sound for any kind of wave condition.

#### 3.2 Redefinition of the RTFN

The most fundamental definition for the Froude number is the ratio of the inertia force and the gravity force in the fluid. It is also defined as the ratio of the velocity of the disturbance source and the propagation celerity of the disturbance. It is called the Froude number when this concept is applied to the shallow water equation. Since the hydrostatic pressure is one of the basic assumptions for open channel hydraulics, the reference celerity in the denominator is always  $\sqrt{gd}$ , which is the wave celerity in very shallow water. However, the disturbance propagation speed (the wave celerity) in the ocean varies with the relation between the water depth and the wave characteristics. Therefore, it is inappropriate to use  $\sqrt{gd}$  as the reference speed for ocean waves, thus the

RTFN is redefined as following;

$$Fr_t = \frac{C_{crest} - u_{trough}}{C_{trough}} \quad (3.1)$$

where  $C_{crest}$  is the wave celerity at the crest and  $C_{trough}$  is the wave celerity at the trough. With this definition, the RTFN theory can be applied also to the deep water wave breaking because the limitation factor appeared as  $\sqrt{gd}$ , which is the shallow water wave celerity, is removed from the equation. However, this equation only shows a framework of the RTFN concept so that it is required to combine wave theory to obtain the analytical formula.

### 3.3 The RTFN with Linear Wave Theory

Linear wave theory is employed as a first examination of the theoretical analysis. The wave celerities at the crest and the trough are assumed to be same because of the infinitesimally small wave amplitude.

$$C = \frac{gT}{2\pi} \tanh\left(\frac{2\pi d}{L}\right) \quad (3.2)$$

where  $T$  = the wave period,  $d$  = water depth, and  $L$  = the wave length. The particle velocity in linear wave theory is described as

$$u = \frac{gH}{2} \frac{T}{L} \frac{\cosh k(z+d)}{\cosh kd} \cos(kx - \sigma t) \quad (3.3)$$

where  $H$  = the wave height,  $k$  = the wave number =  $2\pi/L$ , and  $\sigma$  = the radian frequency =  $2\pi/T$ . For the same reason mentioned above, the trough velocity is taken at the still water level,  $z = 0$ . Thus, the particle velocity at the wave trough can be calculated from Eqn 3.3 as,

$$u_{trough} = -\frac{gHT}{2L} \quad (3.4)$$

Substituting Eqn 3.2 and 3.4 into Eqn 3.1 gives the theoretical RTFN,  $Fr_t$ , as follows;

$$Fr_t = \frac{\pi H/L + \tanh(kd)}{\tanh(kd)} \quad (3.5)$$

This shows the RTFN in any kind of linear wave. To determine the critical condition, the Miche formula given as Eqn 2.19 is applied for the kinematic wave breaking condition. Substituting Eqn 2.19 into Eqn 3.5 provides the CTFN from linear wave theory.

$$Fr_{tc} = CFTN = \pi\alpha + 1 \quad (3.6)$$

where  $\alpha$  is the coefficient in Miche formula, and  $\alpha = 0.142$  is most often applied. Applying  $\alpha = 0.142$  to Eqn 3.6 provides 1.4461 for the CTFN with the linear wave theory. Notice that this value is independent of any wave characteristic so that it is the universal constant for any kind of wave condition.

Based on Miche formula, a constant CTFN value can serve as the critical condition for both deep and shallow water wave breaking. However, another wave breaking index,  $H/d = 0.78$  is preferred in many occasions for shallow water wave breaking, rather than using  $H/d = 0.892$  derived from Miche formula. Applying this condition to Miche formula gives  $\alpha = 0.1241$  and CTFN becomes 1.39 for shallow water wave breaking. The reason for this difference is because the Miche formula is based on a deep water wave breaking criterion by Michelle (1893) and extend it to intermediate and shallow water wave breaking, while  $H/d = 0.78$  is established as a shallow water wave breaking index. The effect of beach slope on the wave breaking index in shallow water will be discussed in a later section.

### 3.4 The RTFN with Stokes Second Order Wave Theory

Stokes wave theory is the most commonly used nonlinear wave theory. There are several different orders of the equation and as the order gets higher the accuracy is increased. However, the second order equation is employed for this analysis because of its simplicity. The second order equation is only effective for deeper water due to the limitation of the convergence of the expanded series (Dean and Dalrymple, 1984). Therefore, Stokes second order wave theory is used only for the deep water wave, then

solitary wave theory will be examined for the shallow water wave in the next section.

The linear dispersion relationship is valid up to the second order equation in Stokes wave theory; therefore, the wave celerity is same as the Eqn 3.2. The horizontal particle velocity at the trough for the Stokes second order wave is given as;

$$u_{trough} = -\frac{gH \cosh(k(z+d))}{2 \cosh(kd)} + \frac{3}{4} \left(\frac{\pi H}{L}\right)^2 C \frac{\cosh(2k(z+d))}{\sinh^4(kd)} \quad (3.7)$$

where  $C$  is the wave celerity. Substituting Eqn 3.7 and Eqn 3.2 into Eqn 3.1 and applying Miche formula, the CTFN equation with the Stokes second order wave is

$$Fr_{tc} = 1 + \pi\alpha \frac{\cosh(k(z+d))}{\cosh(kd)} - \frac{3}{4} (\pi\alpha)^2 \frac{\cosh(2k(z+d))}{\cosh^2(kd) \sinh^2(kd)} \quad (3.8)$$

The wave now has a finite amplitude in the Stokes theory. Therefore, the free surface location at the trough has to be determined for the analysis. The Stokes second order wave theory gives the displacement at the trough as,

$$\eta_{trough} = -\frac{H}{2} \left( 1 + \pi \left(\frac{H}{L}\right) \frac{\cosh(kd)(2 + \cosh(2kd))}{\sinh^3(kd)} \right). \quad (3.9)$$

Miche formula is applied again to Eqn 3.9 for the wave breaking condition, then it is substituted into Eqn 3.8

$$Fr_{tc} = 1 + \pi\alpha \frac{\cosh(kd - \chi\pi\alpha \tanh(kd))}{\cosh(kd)} - \frac{3}{4} (\pi\alpha)^2 \frac{\cosh(2(kd - \chi\pi\alpha \tanh(kd)))}{\cosh^2(kd) \sinh^2(kd)}, \quad (3.10)$$

where

$$\chi = f(kd) = 1 - \pi\alpha \frac{2 + \cosh(2kd)}{\sinh^2(kd)}. \quad (3.11)$$

This time, the CTFN is not a constant. Eqn 3.10 only depends on the relative depth,  $kd$ .

Fig. 3.1 shows Eqn 3.10 for  $kd > \pi/2$  (deep water), where the convergence condition is well satisfied. CTFN converges to 1.426 as the relative depth gets larger. The CTFN at the deep water wave limit,  $kd = \pi$ , is 1.440 so that it is quite uniform in deep water wave

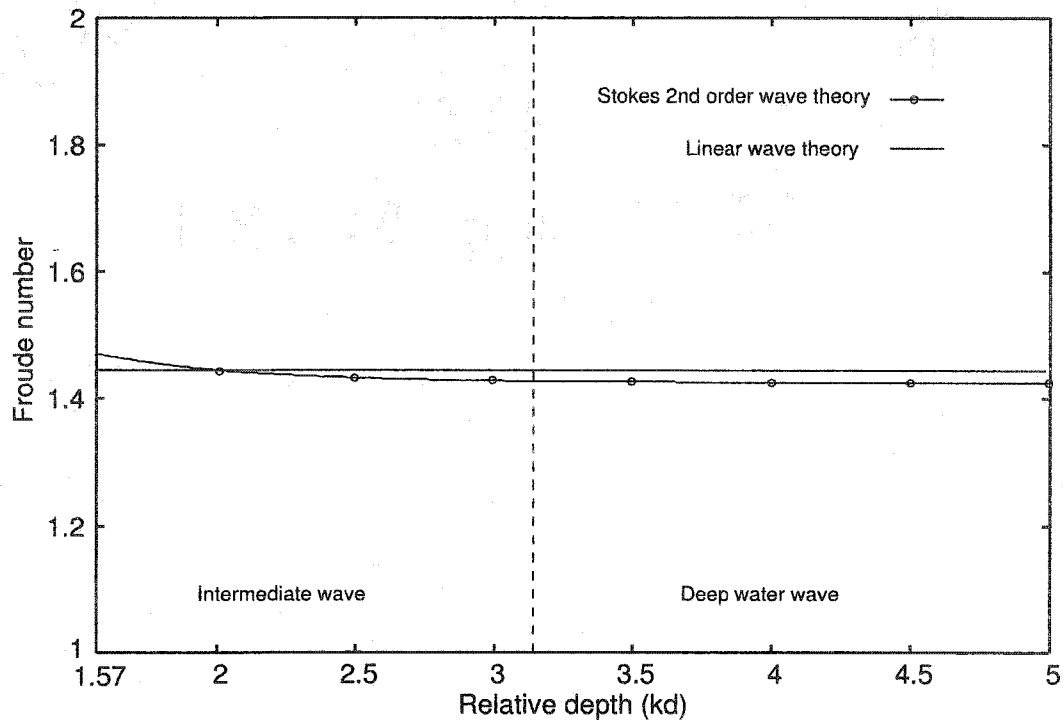


Figure 3.1: The CTFN with Stokes second order wave theory

region. In the intermediate water wave region, the CTFN gets bigger as the relative depth becomes shallower but the rate of the change is small. Therefore, it can be concluded the CTFN is still about 1.45 in the deeper water section even coupling with a nonlinear deep water wave theory.

### 3.5 The RTFN with Solitary Wave

A solitary wave is not an oscillatory wave but it is normally considered as a wave which has infinite wave length, so that it is a special form of very long/shallow water wave ( $kd \ll 1$ ). A sketch of the solitary wave is shown in Fig. 3.2. The solitary wave celerity is defined as (Dean and Dalrymple, 1984);

$$C = \sqrt{gd} \left( 1 + \frac{a}{2d} \right) \quad (3.12)$$

where  $a$  is the amplitude which is the difference between the crest height and the still

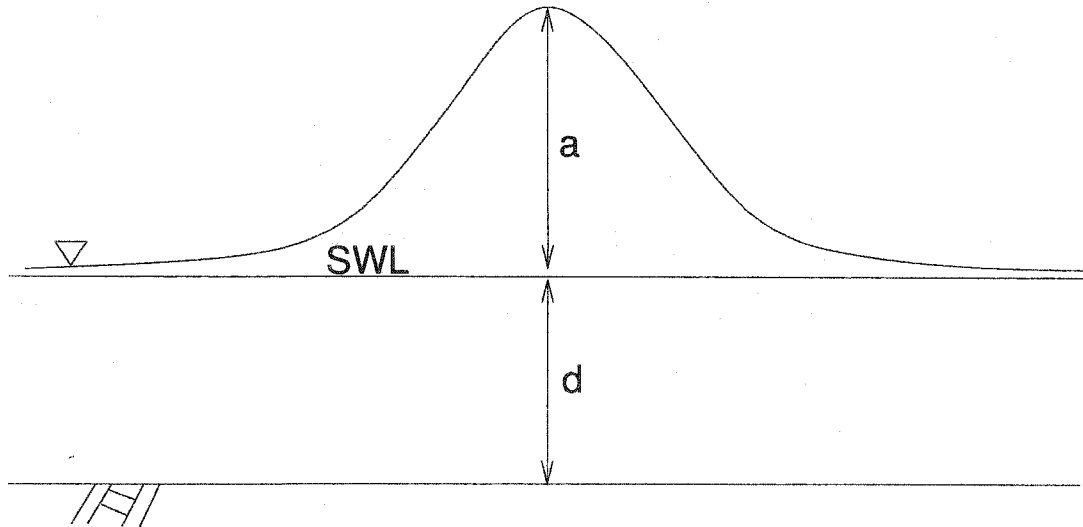


Figure 3.2: Definition sketch of solitary wave case

water level and  $d$  is the still water depth. There is no trough for solitary wave theoretically. Therefore, the point which is infinitely far ahead from the crest location is considered as the trough. Since the water is just still water with depth of  $d$  at the trough position, the particle velocity at the trough is assumed to be 0.

$$u_{trough} = 0 \quad (3.13)$$

The absence of the free surface disturbance recovers the hydrostatic pressure assumption at the trough. It makes the reference speed (trough celerity) the original Froude number equation,

$$C_{trough} = \sqrt{gd}. \quad (3.14)$$

Again, substituting these values into Eqn 3.1 gives the RTFN with solitary wave.

$$Fr_t = \frac{\sqrt{gd}(1 + (a/2d)) - 0}{\sqrt{gd}} = 1 + \frac{a}{2d} \quad (3.15)$$

Since the still water level is designated as the wave trough in this analysis, the amplitude,

$a$ , is the same as the wave height,  $H$ . So, applying Miche formula for a shallow water wave, the wave breaking index,  $H/d = 0.89$ , gives the CTFN as,

$$Fr_{tc} = 1.445. \quad (3.16)$$

### 3.6 The CTFN and Wave Breaking Indexes in Shallow Water on Sloping Bottom

From the theoretical analysis in the previous sections, it can be concluded that the CTFN = 1.45 is a decisive number for any kind of wave condition as long as Miche formula is valid as a wave breaking condition. However, Miche formula does not represent the wave breaking state correctly in shallow water. As mentioned in Section 4,  $H/d = 0.78$  is more accepted in shallow water than  $H/d = 0.892$ . Another case that the  $H/d$  ratio does not agree with the Miche formula can be found in the solitary wave breaking on the sloped bottom (Weggel, 1972).

The reason for the discrepancy between the Miche formula and other indexes in shallow water can be explained as follows. In shallow water, the wave celerity is a function of the water depth. Therefore, the wave celerities at the crest and the trough are different on the sloped bottom because the water depths at the crest and the trough are different on the sloped bottom. However, wave theories assume a flat bottom for their derivation so that the wave celerity is assumed to be same at any point within one cycle. Therefore, this celerity difference leads to the discrepancy in the critical depth-wave height ratio.

Strictly speaking, it is incorrect to apply a wave theory on a sloped bottom because of this limitation; however, the theory shows fair agreement with the observations with very gentle slopes ( $m \gg \gg 1$ ). So, the following discussion explains this problem mathematically by evaluating the RTFN formula on a very gently sloped bottom. Fig. 3.3 shows a sketch of the analysis, here  $m$  denotes the bottom slope angle in the cotangent

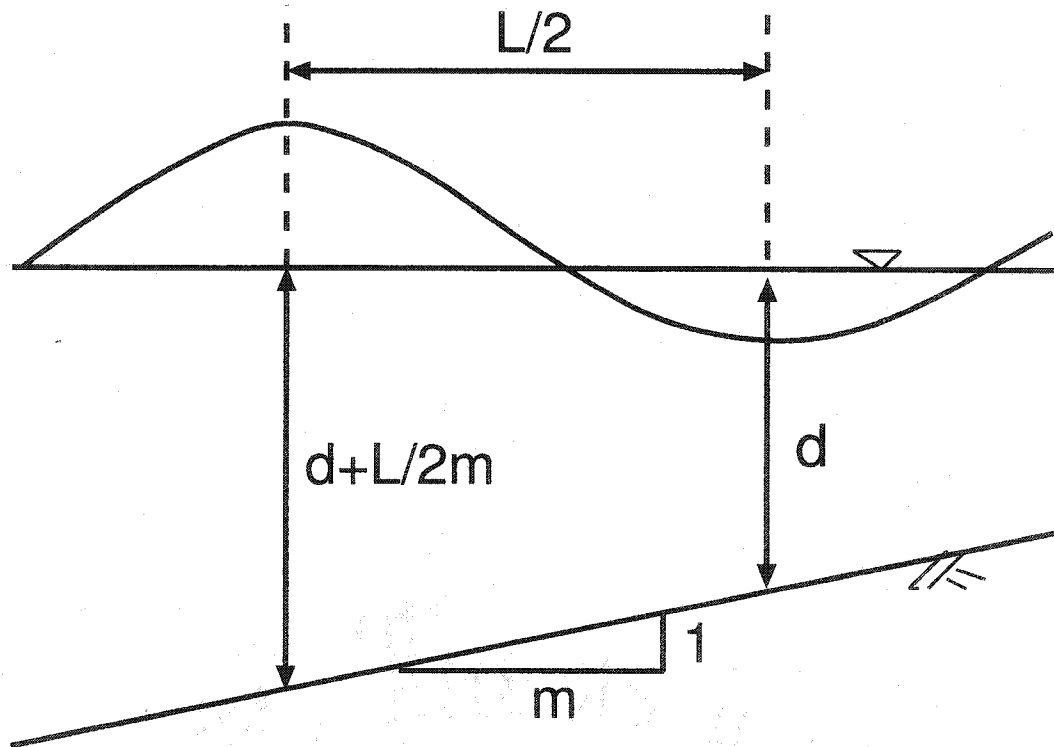


Figure 3.3: Definition sketch for sloped bottom

function. The linear wave theory is employed in this analysis to determine the wave celerity and the particle velocity because of its simplicity. The only difference from the previous analysis on the flat bottom is that the water depth at the crest is replaced by  $d + L/2m$ , rather than  $d$ . The celerity at the crest becomes  $\tanh(k(d + L/2m)) = \tanh(2\pi(d/L) + \pi/m)$ . Evaluating by the same procedure, the RTFN on the very gentle slope is expressed as;

$$Fr_t = \frac{\pi(H/L)}{\tanh(2\pi(d/L))} + \frac{1 + \tanh(\pi/m)/\tanh(2\pi(d/L))}{1 + \tanh(\pi/m) \cdot \tanh(2\pi(d/L))}. \quad (3.17)$$

Because of the very gentle slope,  $\pi/m$  is very small so that Eqn 3.17 can be reduced to

$$Fr_t = \frac{\pi(H/L)}{\tanh(2\pi(d/L))} + \frac{1 + (\pi/m)/\tanh(2\pi(d/L))}{1 + (\pi/m) \cdot \tanh(2\pi(d/L))}. \quad (3.18)$$

For deep water waves, the hyperbolic tangent function reduces to one because  $2\pi(d/L)$

is large. The second term in the right hand side of Eqn 3.18 becomes one, and  $Fr_t$  is independent of the slope,  $m$ . This result agrees with the fact that the deep water wave does not *feel* the bottom so that it is not affected by the bottom bathymetry. For shallow water waves,  $2\pi(d/L)$  is small and the hyperbolic tangent function reduces to  $2\pi(d/L)$ . Since both  $(\pi/m)$  and  $2\pi(d/L)$  are very small, the product of these two term can be neglected. This leads to the following expression:

$$\frac{H}{d} = 2(Fr_t - 1) - \frac{1}{2m(d/L)} \quad (3.19)$$

The first term on the right hand side of the equation becomes 0.89 when the CTFN is equal to 1.446. By the contribution of the second term, the  $H/d$  ratio on a very gentle slope becomes smaller than that on a flat bottom. Note that Eqn 3.19 recovers the flat bottom condition  $H/d = 0.89$  as  $m \rightarrow \infty$ . This result explains why  $H/d = 0.78$  shows better agreement with observations than the Miche formula. The Miche formula neglects bottom slope effect for shallow water wave breaking. For deep water wave breaking, bottom bathymetry does not affect to the wave breaking condition because waves do not feel the bottom as discussed above. And the Miche formula is extended from a deep water wave breaking condition given by Mitchell (1893). And one critical condition, CTFN=1.45, connects two different conditions.

This argument is, however, only approximate, even though the analytical condition is restricted to a very gentle bottom slope, for two reasons; (1) linear wave theory does not support the sloped bottom, (2) linear wave theory neglects all the shallow water wave transformation. The wave shoaling and the asymmetry in the wave shape will affect the RTFN calculation but there is no means to evaluate these effect analytically, other than solving the Boussinesq equation numerically. Therefore, we will not discuss this point further.

### 3.7 Summary for Theoretical Analysis

Several cases of theoretical analysis for the RTFN theory were performed in this chapter. All the analysis coupled with the linear wave theory, Stokes' second order wave theory, and the solitary wave theory give similar numbers for the critical condition,  $Fr_{tc} = 1.45$ , under the following two conditions:

1. the wave breaking condition follows Miche (1944), and
2. the particle velocity is taken at the free surface.

The analysis on the sloped beach is not sufficient for conclusion because of the limitation of the wave theories and the nonlinear shallow water wave transformation. Since theoretical analysis does not work for this case, more experimental measurements are needed in order to find out the existence of the slope effect in the CTFN for shallow water wave breaking. The result shows the possible slope effect for the shallow water wave breaking by keeping CTFN a universal constant.

It is concluded from this analysis that the *theoretical* value of the CTFN is 1.45 regardless of the state of the wave.

## CHAPTER IV

### WAVE TANK EXPERIMENT

#### 4.1 Introduction

Though the theoretical analysis implies that the CTFN is quite stable for a range of wave conditions, it is unknown for the case of a nonlinear shallow water wave transformation. Therefore, a wave tank experiment was performed for the calibration of the CTFN and application in a numerical model. Because the main purpose of this experiment is for calibration, measurements are only taken at the location where the wave breaking begins. Flow characteristics, which are needed in order to determine the CTFN, will be calculated by the numerical model as explained below.

#### 4.2 Experimental Setting

The experiment is performed in a wave tank in the Coastal Engineering Centre at Old Dominion University in Norfolk, Virginia. The wave tank is 3ft×3ft×60ft and is equipped with a piston-type wave generating paddle, which has a capability to generate irregular waves. The wave tank operation system is updated to DHI Wave Synthesizer for Windows NT/2000. With this new system, the generation of the wave is fully controlled from the software. The embedded beach section has 1:20 plane slope. A wave gauge is installed at the toe of the beach slope to measure the actual wave motion so that the adjustment of the input wave height for the numerical model can be made. Fig. 4.1 schematically shows the wave tank setting.

Three wave heights, three wave periods, and three water depths (a total of 27 cases) are chosen for the experiment. Wave periods and water depths are determined from the scale of the wave tank. After several preliminary numerical model tests, it was found that FUNWAVE cannot handle some higher wave heights for given wave periods and water

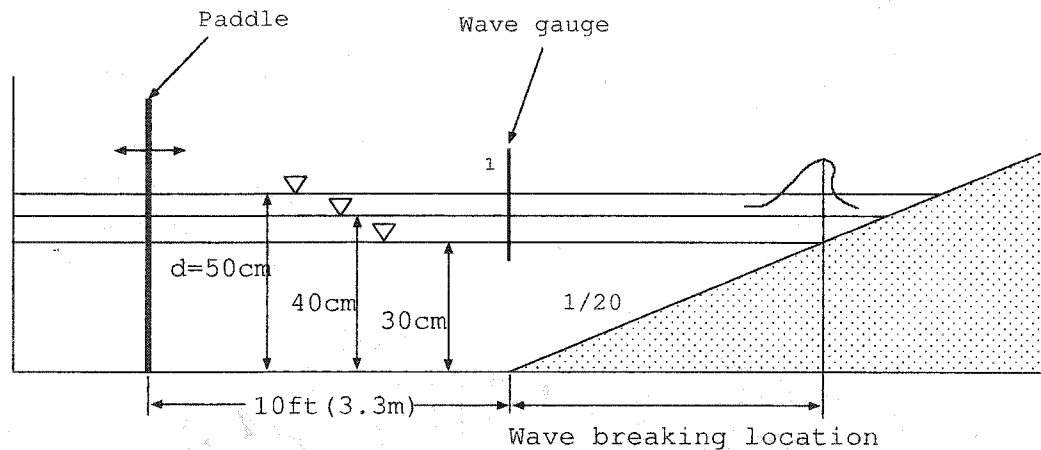


Figure 4.1: Wave tank setting

depths. The numerical model either crashed in the middle of the calculation or generated higher frequency waves. The reason is the source function method, which is the wave input method for the FUNWAVE, is based on the linear wave theory (Wei et al., 1999). A wave with a large wave height cannot be treated as a linear wave. In this situation, a finite amplitude wave has to be represented by the composite of harmonics. But, the input wave is a sinusoidal curve because the source function method can only introduce waves generated from linear wave theory. Therefore, the higher harmonics are separated from the main trunk of the wave in order to adjust the wave shape to what it should be. The preliminary numerical model tests suggest that the wave height of 6 cm is about the largest wave height with which the higher harmonics do not significantly affect the result. This forces the input wave condition to be small. Each condition is listed below;

Wave height : 2 cm 4 cm 6 cm

Wave period : 1.0 sec 1.5 sec 2.0 sec

Water depth : 30 cm 40 cm 50 cm

Note that these input wave conditions are regular waves. Because of small wave height

condition, the breaker type of 27 cases all fall into the spilling breaking by the classification of Battjes (1974). Each run is three minutes long and is recorded on digital video camcorder, which has a capability to shoot a movie as a series of still pictures. This way, clear still images can be used for the analysis. In this experiment, the movie is recorded with 30fps resolution.

### 4.3 Results

Wave height at the toe of the beach slope is important for a calibration. When the wave starts to climb up the beach slope and it *feels* the bottom, it starts to shoal. Asymmetry of the bottom in different sections of the wave causes nonlinear processes. In other words, since the water depth varies within one phase cycle, wave processes cannot be approximated to a linear process. So, the toe of the beach slope is the last place where two wave heights in the numerical model and the physical experiment can be adjusted. Wave gauge records reveal that wave height at the toe of the beach slope is smaller than the design wave height set by the control program. Fig. 4.2 shows an example of wave gauge record for the case of  $H=2$  cm,  $T=1.0$  sec, and  $d=40$  cm. The wave height is reduced to about 1.6 cm at the toe of the beach slope. All experiments had smaller wave height than the design wave height. Therefore, the input wave conditions in the numerical model have been adjusted to 1.6 cm, 3.5 cm, and 5.2 cm for the cases of 2 cm, 4 cm, and 6 cm respectively.

The wave breaking locations are determined by observation of the recorded digital video data on a frame-by-frame. A sample image capture of the digital video recording is shown in Fig. 4.3. The frame in which the wave just starts to tip over at the crest is considered as the initiation frame and the crest location in the initiation frame is taken as the initiation location of the wave breaking for the wave condition. The wave breaking

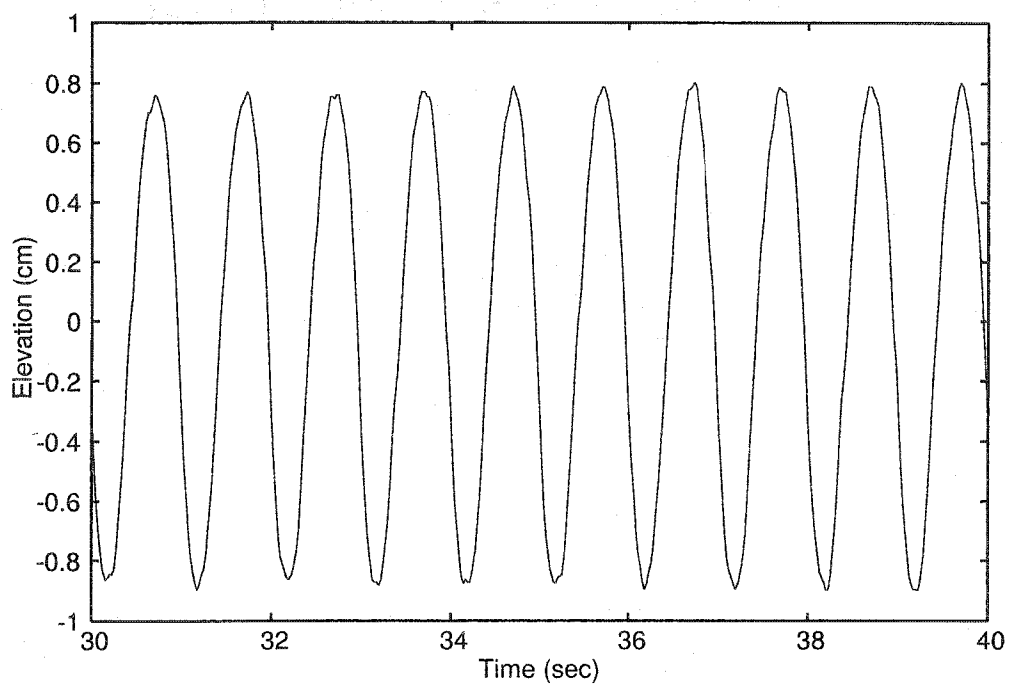


Figure 4.2: Wave gauge record

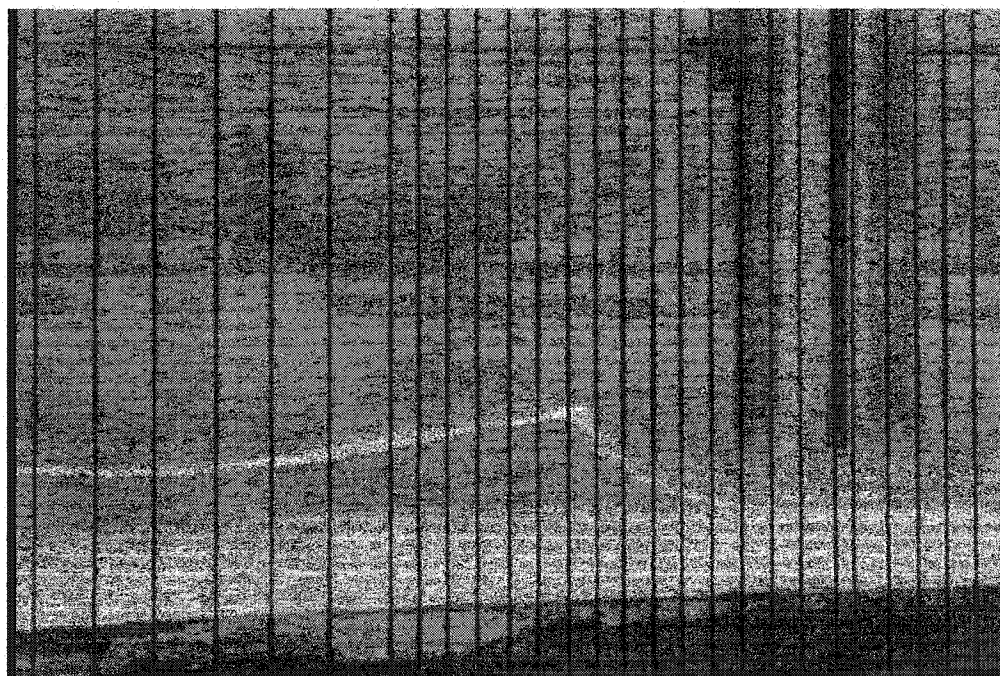


Figure 4.3: Wave breaking location analysis on digital video record

location here is defined as a horizontal distance from the toe of the slope to the crest of the wave, as shown in Fig. 4.1. Seven samples are randomly selected from the three minute record, then five of them are averaged to determine the initiation location of the wave breaking after the maximum and the minimum values are discarded from the data set.

Results are shown in Tables 4.1, 4.2, and 4.3 for the case of the water depth of 30 cm, 40 cm, and 50 cm respectively. This data set will be used in Chapter VI for the calibration of the RTFN trigger model.

Table 4.1: Wave breaking location(m), d=30cm

Wave height	T=1.0sec	1.5sec	2.0sec
2cm	5.06	4.97	4.87
4cm	4.45	4.36	4.20
6cm	3.92	3.79	3.70

Table 4.2: Wave breaking location(m), d=40cm

Wave height	T=1.0sec	1.5sec	2.0sec
2cm	7.08	6.98	6.86
4cm	6.62	6.33	6.07
6cm	5.96	5.79	5.50

Table 4.3: Wave breaking location(m), d=50cm

Wave height	T=1.0sec	1.5sec	2.0sec
2cm	9.01	8.87	8.80
4cm	8.50	8.32	8.17
6cm	8.09	7.85	7.69

## CHAPTER V

### CALCULATION METHODS

#### 5.1 Introduction

This chapter discusses how to actually calculate the RTFN and formulate it as a wave breaking trigger in a numerical model. Most of the chapter is devoted to the evaluation of the wave celerity calculation methods because it is the most important element for the RTFN calculation.

#### 5.2 The Calculation Procedure of the RTFN

Initially, the location of the trough and the crest are determined and paired together. Since the numerical model is a one dimensional and regular waves are tested in this work, a simple procedure is employed to locate the crest and trough. A window with a fixed width moves in the calculation domain. The index number for the window is taken at the center of the window. The maximum value of  $\eta$  within the window is compared with  $\eta$  at the center of the window. If the two values are identical, the node is considered to be the crest. The benefit of this method is that it filters out short oscillations generated for various reasons. It is important for correctly pairing crest and trough location to eliminate short oscillations from the determination procedure. The trough location is simply taken as a node where  $\eta$  has the minimum value between two crests. In this study,  $\Delta x = 0.025$  m and  $\Delta t = 0.01$  sec are fixed for all the numerical experiments discussed in the next chapter.

Once the crest and trough locations are determined, the flow characteristics at both locations are taken from the model parameters or calculated from the obtained parameters. The particle velocity is the dependent variable of the Boussinesq equation so that it is simply taken at the trough location. Here, the particle velocity is the one at the

arbitrary depth,  $z_\alpha$ , and  $z_\alpha/h = -0.531$  as discussed in Chapter II. On the other hand, a computation is required to obtain the wave celerities at the crest and trough locations. The calculation method for the wave celerity will be discussed in detail later.

The RTFN is calculated from the data, and checked for the critical condition. If the RTFN exceeds the predetermined critical condition, the extra momentum term due to the wave breaking is added to the Boussinesq equation. The RTFN theory is purely for the triggering mechanism. It does not include the theory for the energy dissipation inside of the wave breaking. In short, the RTFN can determine which wave is breaking but cannot calculate the wave changes. Therefore, the additional momentum term is added at all nodes between the crest and the trough. This procedure was simply adopted for easy calculation and will be discussed later in Section 5 in Chapter VI. The calculation of the eddy viscosity and the momentum term were not changed from those in the original FUNWAVE model. For more details about the original momentum sink mechanism due to the wave breaking, see Kirby et al. (1998).

### 5.3 Implementation into FUNWAVE

FUNWAVE is a 1D/2D wave model based on the Boussinesq equation developed by the University of Delaware. The source code was obtained from the University of Delaware and modified to apply the RTFN theory as a wave breaking trigger, using the above mentioned procedure. However, since FUNWAVE has a fixed boundary condition for  $\eta$ , there is no clear crest–trough–crest structure at the right hand side boundary of the domain. Thus, the determination of the wave crest and trough position is different at this location from the one explained in the previous section. The moving window technique is applied to find the trough location first, then the corresponding crest position is determined using the same technique.

The modified source code is presented in Appendix A for the trigger mechanism subroutines. The full FUNWAVE code is available from the University of Delaware ([chinacat.coastal.udel.edu/kirby/programs/funwave/funwave.html](http://chinacat.coastal.udel.edu/kirby/programs/funwave/funwave.html)).

#### 5.4 Wave Celerity Calculation

Computation of the wave celerity at the crest and trough is required for the RTFN calculation. Utku and Basco (2002) found that 90% of the RTFN calculation is due to the contribution of the celerity. Therefore, it is very important to calculate wave celerity accurately. Four methods to calculate the wave celerity are investigated and tested for suitability. There are two requirements for the calculation method. One is applicability and availability: (1), the method must apply to a calculation for any kind of wave condition and the calculation has to be done with variables available in the numerical model. The second one is robustness: i.e. (2), the method has to calculate stable result so that the result does not cause an illegal operation, which means a wave breaking event occurs where it should not be or vice versa.

The four alternatives are:

1. analytical formula from wave theories,
2. pure advection equation,
3. tracking crest and trough position, and
4. least square estimation method (Misra et al., 2003).

These four alternatives are tested on a 1:20 plane slope beach. The incident wave condition is  $T=1.5$  sec and  $H=4$  cm.

##### 5.4.1 Analytical Formula

Using the analytical formula derived from a wave theory is the first alternative for the wave celerity calculation. Four different formulations, two equations and two conditions, are tested here. Two equations are both taken from the linear wave theory. One is shallow water wave celerity ( $\sqrt{gd}$ ) and the other is the general expression for the linear wave celerity ( $gT/2\pi \cdot \tanh(kd)$ ). Each equation is tested with and without the effect of surface displacement by the wave. The result is shown in Fig. 5.1. Note that the figure is a snapshot of the wave celerity for all the nodes at a certain time step.

Using the shallow water wave celerity makes the calculation procedure easy because it contains only variables provided by the FUNWAVE ( $h$  and  $\eta$ ) at that calculation node and at that time step. However, this equation is applicable only for shallow water waves. It does not represent the wave celerity correctly in deeper water. Fig. 5.1 shows the shallow water wave celerity and the general expression only matches in the region of very shallow water. Using the general expression provides better results for the wave range. However, including the wave period in the equation, not only the general expression of the linear wave celerity but also Stokes' wave celerity, makes the calculation difficult for irregular wave cases because there is no means to determine the wave period instantaneously from the data set computed in the numerical model. This experiment could be completed because it is conducted with a regular wave case so that the wave period information is provided externally.

#### 5.4.2 Using Pure Advection Equation

Sørensen et al. (1998) calculate the wave celerity for their roller model using the pure advection equation. Since the pure advection equation contains the surface disturbance propagation speed as a coefficient,

$$\frac{\partial \eta}{\partial t} + C \frac{\partial \eta}{\partial x} = 0, \quad (5.1)$$

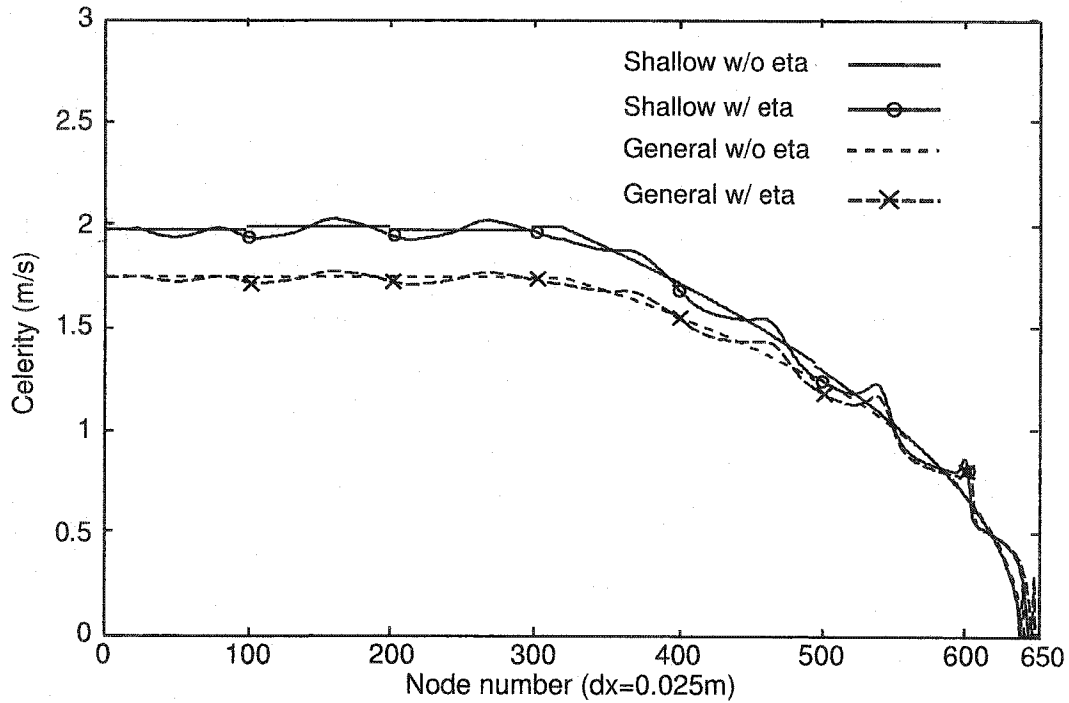


Figure 5.1: Wave celerity calculated by analytical formulas

the wave celerity can be calculated as

$$C = -\frac{\partial \eta}{\partial t} / \frac{\partial \eta}{\partial x}. \quad (5.2)$$

This method is easy to calculate because it only depends on  $\eta$ , and the time and spatial derivative of  $\eta$  are calculated by the numerical model in order to solve the Boussinesq equation.

The result with the pure advection equation method is shown in Fig. 5.2. This is again a snapshot of the celerity at a certain time step. However, as seen in the plot, the results are scattered. The method calculates more than 100 m/s or negative celerity at some nodes, but they are filtered out from the plot. Points where the scheme calculates these extreme values are the crest and trough nodes. This is because the spatial derivative, which is in the denominator of Eqn 5.2, at the crest and the trough is equal to zero.

Although in the actual calculation it does not become exactly equal zero, it is a very small number. Sørensen et al. (1998) apply this method at the steepest point in the wave front, therefore, it calculates the celerity with good accuracy. But it is not suitable for the calculation at the crest and the trough.

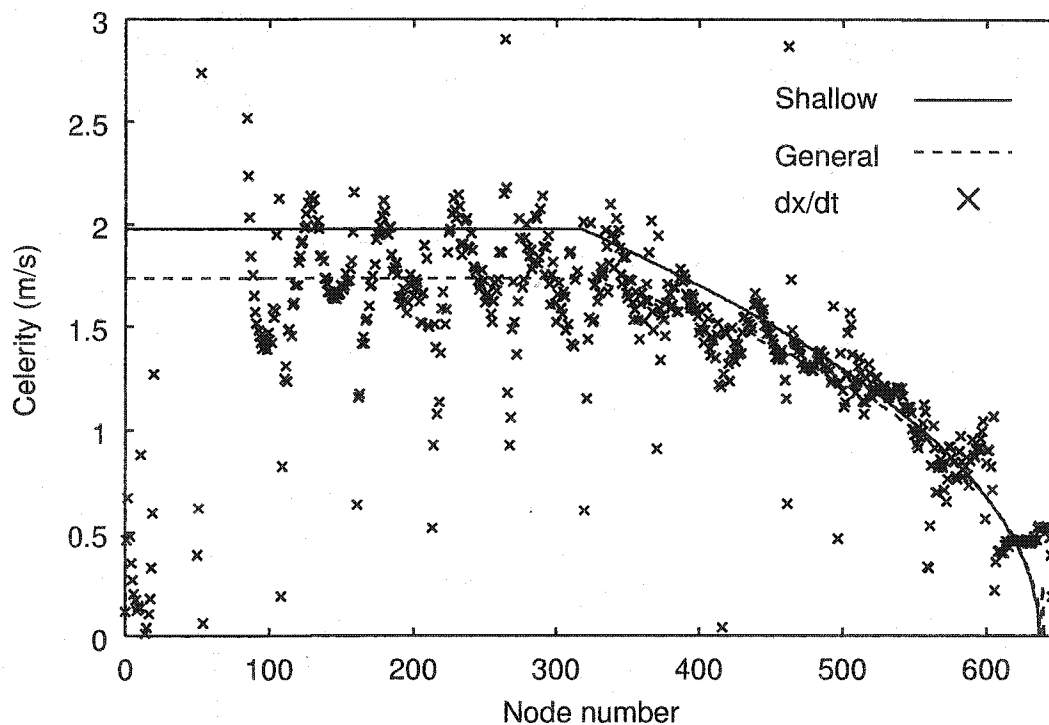


Figure 5.2: Wave celerity calculated from pure advection equation

#### 5.4.3 Tracking Crest and Trough Position

The third method calculates the wave celerity by locating the crest and trough positions at different times. The spatial difference between two time levels is divided by the time interval in between. The mathematical expression of this method can be defined as;

$$C = \frac{x_{i,k} - x_{i-n,k}}{n \cdot \Delta t} \quad (5.3)$$

where  $i$  is the current time step,  $k$  means the  $k$ th wave,  $n$  is the multiplication factor for

time interval.

For this method, the precise estimation for the location of the crest and the trough is needed, otherwise the resolution of the wave celerity calculation depends on the calculation node spacing of the numerical model. For example, using the space and time intervals of the FUNWAVE,  $\Delta x = 0.025$  m and  $\Delta t = 0.01$  sec, the minimum resolution of the wave celerity will be 2.5m/s if the time interval of the data is  $\Delta t$ . Longer time intervals make the resolution lower, but it averages out the information.

Several cases for the wave celerity calculation were tested with different interpolation methods and curve fitting techniques. The result does not change much with different interpolation method. Fig. 5.3 shows the result with a parabolic curve fitting method.

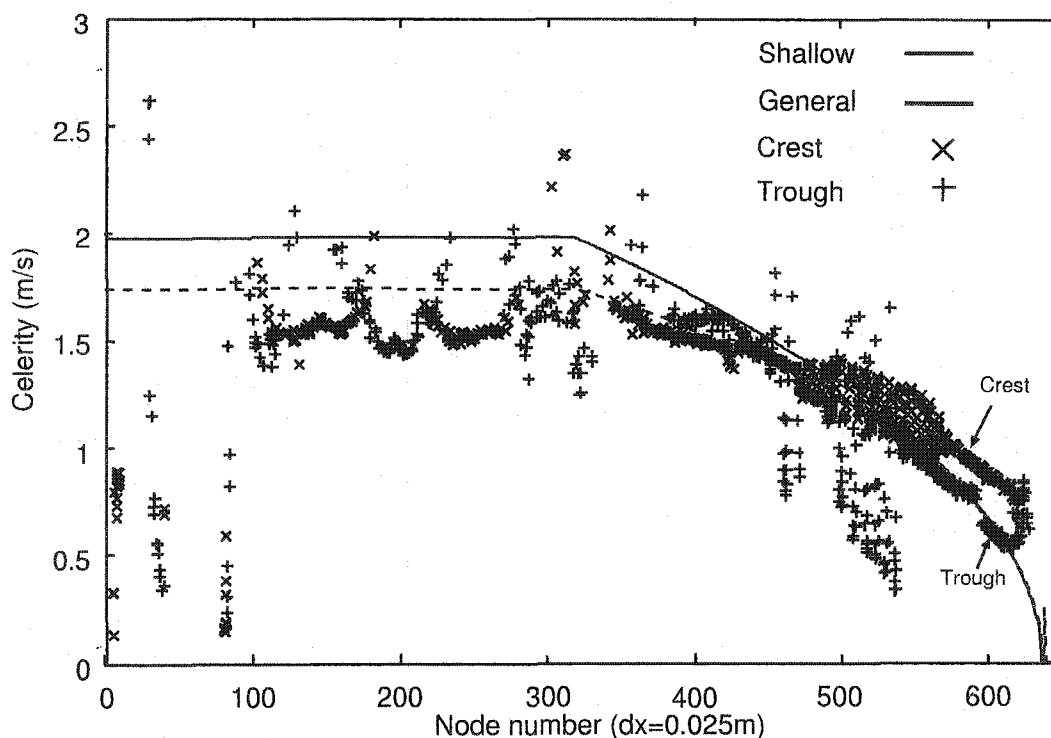


Figure 5.3: Wave celerity calculated by tracking method

This plot shows the celerity only at the crest and the trough over the one wave period. The agreement to the linear wave celerity is better than using the pure advection equation formula; however, values are scattered around the location where wave breaking begins. This instability is critical because of the location.

#### 5.4.4 Least Square Estimation

The least square estimation method was formulated for finding the wave celerity from a remotely-sensed photograph by Misra et al. (2003). The fundamental concept of this method is the same as the tracking method. The distance between two target locations taken from different time levels is divided by the time interval between the two. This method, however, is a variant of the cross-correlation estimation and uses the least square error estimation to find the distance between the most correlated points from two data sets. The least square error between two functions/data sets is calculated by the following equation:

$$\varepsilon(\xi) = \int_0^{W-\xi} \{f(x) - g(x + \xi)\}^2 dx \quad (5.4)$$

where  $f(x)$  is a function at a certain time level,  $g(x)$  is a function at the other time level,  $\xi$  is a spatial lag and  $W$  is a window size. In this case,  $f(x)$  and  $g(x)$  are the free surface profile,  $\eta(x, t)$ , at two time levels. The window here is defined as a finite calculation region originated from the location where we want to calculate the celerity. The most correlated point is found at the location where the least square error gives the minimum value,  $\xi_{min}$ .

Then the celerity is calculated as;

$$C = \frac{\xi_{min}}{n \cdot \Delta t} \quad (5.5)$$

Since the target function is not an analytical equation but data sets in this case, analytical methods cannot be used for finding  $\xi_{min}$ . Therefore, numerical integration computes the least square error,  $\varepsilon(\xi)$  until it finds the  $\xi$  which gives the minimum error.

To do this, a fine grid system for  $\xi$  is introduced for the calculation. The grid spacing for  $\xi$  is 0.001 m. This gives the minimum celerity of 0.025m/sec with the time interval of  $4\Delta t$ . For the subgrid system, the parabolic curve interpolation estimates the free surface displacement,  $\eta(\xi)$ , between the calculation nodes. The least square estimation has higher accuracy and is more stable, regardless the window size, in the results compared to the conventional cross-correlation estimation. According to Misra et al. (2003), the phase error of the estimated wave celerity from the exact celerity is about 0.5% for the sine wave signal and about 0.1% for the cosine wave signal when the wave length is chosen as the window size. For more detail about the accuracy of the least square estimation method, see Misra et al. (2003). Therefore, the distance between the current crest/trough to the adjacent crest/trough (i.e. the wave length) is taken as the window size in this calculation because the locations of the adjacent crest and trough are already found through the RTFN calculation process.

Fig. 5.4 shows the result of the celerity calculation using the least square estimation method. The scheme slightly underestimates the celerity comparing to the linear wave celerity. Specifically, the agreement of the trough celerity around the breaking zone is poor. The possible reason of this underestimation is the shape of the wave. At the trough in the shallow water, the free surface gradient is very flat as a result of the wave transformation. This makes the detection of the correlation point difficult. And the small oscillation separated from the main trunk of the wave due to the wave breaking makes the determination of the correlation point even more difficult.

To avoid this problem, a combination method of the least square estimation and the analytical formula is employed for the calculation of the trough celerity. There are supporting facts for using  $\sqrt{gd}$  in the shallow water. Madsen et al. (1997a) reports that

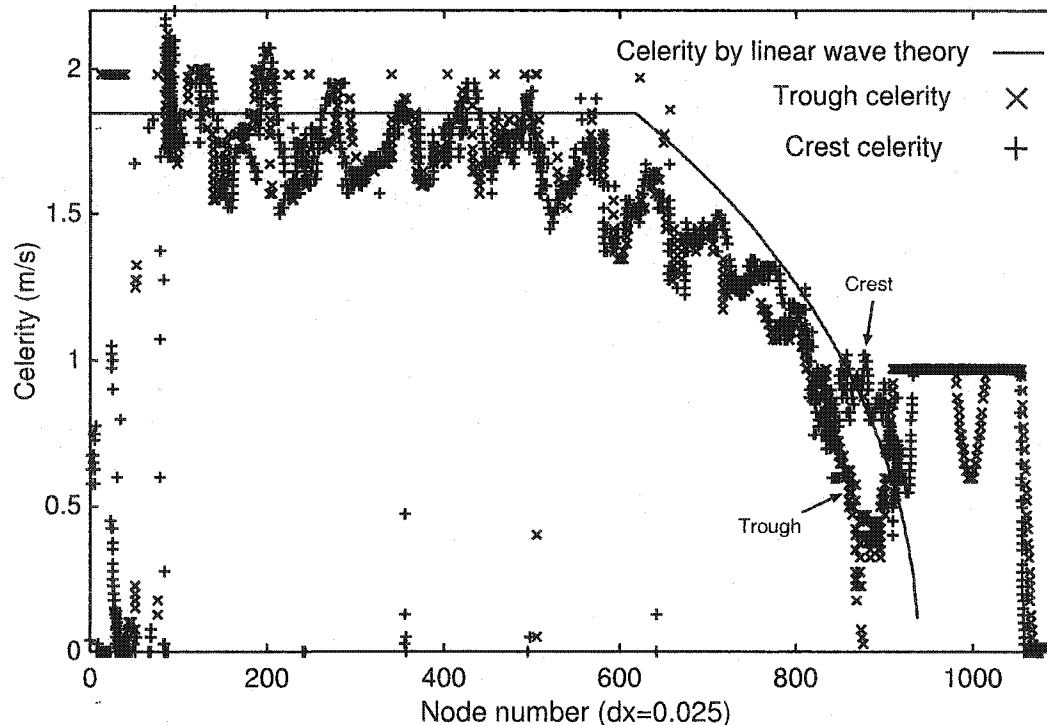


Figure 5.4: Wave celerity calculated by least square estimation

wave breaking accelerates the wave celerity by 30% in the surf zone. This acceleration is captured by the tracking method in the last section (See Fig. 5.3). The crest celerity by the tracking method is accelerated by the wave breaking in the surf zone, even though it is scattered by the instability of the method. So, it can be said that the tracking method can calculate the wave celerity trends correctly but the convergence is poor. It is shown in Fig. 5.3 that the trough celerity computed by the tracking method is not accelerated in the surfzone and follows the theoretical celerity. This means that the trough celerity is not affected by the wave transformation or breaking. Also, the theoretical analysis in Chapter III shows that applying  $\sqrt{gd}$  at the trough position for the solitary wave, which has flat shape at the trough, gives good agreement in the result with the other formulation. These

facts suggest the usage of  $\sqrt{g(h + \eta)}$  for the shallow water wave celerity at the trough position would not introduce new problems into the scheme. This procedure also includes the wave set-up effect in the calculation.

The Ursell number ( $aL^2/h^3$ ) is employed for the switch between the calculation methods. The Ursell number is a dimensionless number used for finding the nonlinearity of the wave or the applicable area of a shallow water wave theory. The applicable area of the cnoidal wave theory, which is a nonlinear shallow water wave theory, is  $Ur > 26$ . Therefore, it is fair to consider a wave as a shallow water wave when the Ursell parameter is more than 30. Under the condition,  $Ur > 30$ , the threshold value and the transition area of two calculation methods are determined by trial and error method in order to make a smooth transition between two calculation methods. The least square estimation calculates the trough celerity when the Ursell number is less than 40, and the analytical formula gives the celerity with  $Ur > 60$ . Between the two numbers, it is a transition area. Both methods calculate the trough celerity, and the results are blended with the weighted average method. This way, this hybrid method satisfies two conditions: a stable trough celerity in the shallow water region and a calculation method which is applicable for the entire wave range out to deep water.

Fig. 5.5 shows the results with the combined method. A significant improvement is achieved from the previous result. The trough celerity in shallow water is very stable because it is now calculated by an analytical formula. The least square estimation still underestimates the trough celerity just before the calculation method is changed to the analytical formula (around node 750), but it is not so significant because it does not turn on a wave breaking that is unrealistic. This time, the wave celerity acceleration, due to the wave breaking, is captured in the surf zone. This is because the improved trough

celerity prevents turning on wave breaking where it should not happen.

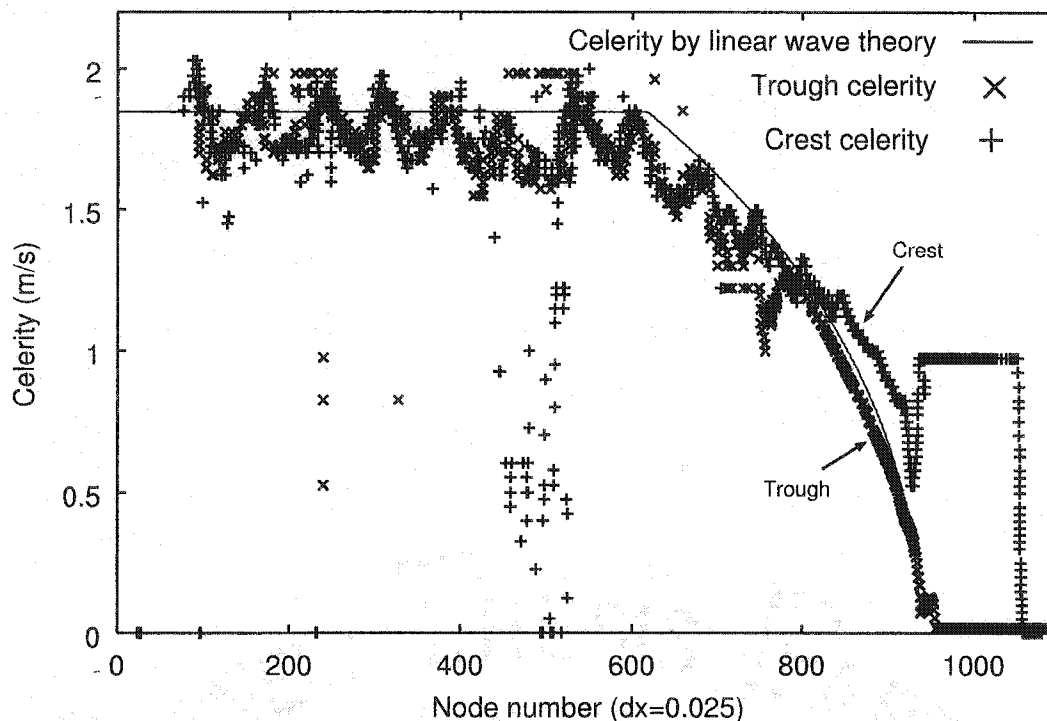


Figure 5.5: Wave celerity calculated by least square method and analytical formula

Even though the combined method gives better results than the other calculation methods, there are still some problems. The first one is that the least square estimation method is not completely stable for all types of situations. Many calculation failures for the crest celerities are found around node 500 in Fig. 5.5. These calculation failures do not affect the result because the underestimation for the crest celerity at these points does not trigger an illegal operation of the wave breaking. This implies, however, that the least square estimation is very sensitive because a small instability in the wave shape influences the results. The second one is that this calculation method requires much more computer resources. The measurement of the calculation time, neither actual time nor CPU time, was not performed, so that the quantitative comparison cannot be shown here. But the

actual calculation time becomes an order of hours from an order of minutes, comparing to the one with analytical formulas. The numerical integration and the iteration steps to find the most correlated point make the wave celerity calculation time to be very expensive.

#### **5.4.5 Summary for Wave Celerity Calculation**

Four calculation methods for the wave celerity calculation are tested in this chapter. The least square estimation method with analytical formula for the trough celerity in shallow water achieves the best results for two conditions, the applicability/availability and the robustness against the wave breaking, among the five test cases. Therefore, this method will be used for the wave celerity calculation in numerical experiments discussed in the next chapter. However, some experiments conducted in the early stage of this research were performed using the analytical formula method.

## CHAPTER VI

### NUMERICAL EXPERIMENTS

#### 6.1 Introduction

This chapter summarizes the numerical experiments performed for this research. The qualitative studies are the initial investigations and demonstrate how the RTFN behaves with nonlinear wave transformation effects. Model calibration is then performed to determine the CTFN for a numerical model with the experimental data discussed in Chapter IV. Then additional investigations for the characteristics of the RTFN theory are performed with the calibrated CTFN.

#### 6.2 Qualitative Study

Chapter III analyzed the theoretical wave breaking condition with the RTFN theory. The analysis only considered the moment when the wave breaking is about to begin in the theoretical analysis. In this section, however, our interest is mainly on the change of the RTFN in time and space over various bathymetries. It is very important to see how the RTFN changes as a wave approaches the shore, but this kind of analysis is only possible with assistance of the numerical model.

Another purpose of the qualitative study is to find whether the CTFN established by Utku(1999) from his experimental study could work as a proper critical value for the wave breaking in the numerical model. His  $Fr_{critical} = 1.36$  is the only number confirmed by the actual wave tank experiment; however, slight differences in measurement of the particle velocity and the wave celerity between the physical measurement and the values in the numerical model could affect the critical value. This is not a model calibration, so the wave breaking locations initiated by  $CTFN=1.36$  are evaluated qualitatively.

Three cases are tested for this purpose; plane slope beach, bar-trough profile composed

with straight slopes, and one tenth scaled real bathymetry taken at Duck, North Carolina. A brief explanation of the bathymetry shapes and the input wave conditions for three test cases is listed as follows:

Case 1 : Uniform slope (1:20) laboratory scale

$$d = 0.4m, H = 0.04m, T = 1.5sec$$

Case 2 : Bar-trough beach, laboratory scale

$$1:40 \text{ slope plus bar, } d = 0.5m, H = 0.04m, T = 1.3sec$$

Case3 : Real bar-trough beach profile(Duck, NC), 1/10 scale

December 8, 1999, Profile P188

Note that all the input waves are regular waves for all the numerical experiments conducted in this research.

This series of experiments is performed with the analytical equation for the wave celerity calculation. Therefore, the RTFN in these calculations is given as follows:

$$Fr_t = \frac{\sqrt{g(h_i + \eta_i)} + u_j}{\sqrt{g(h_j + \eta_j)}} \quad (6.1)$$

where the subscript  $i$  indicates the crest node and  $j$  indicates the trough node. The CTFN for these numerical experiments is 1.36, which is determined by Utku(1999) from his wave tank experiment. The results are only qualitative but demonstrate basic principles.

### 6.2.1 Plane Slope Beach

The first test case is a plane slope beach. The bathymetry model is taken from the ODU wave tank (See Fig. 4.1 for details). On a plane slope beach, wave input from one end of the domain simply shoals up when approaching to the shoreline, then it breaks at a certain point or depth and the breaking continues until the wave reaches the shoreline. The RTFN theory interprets this phenomenon as follows. The RTFN exceeds 1.36 at a certain point on the slope, and before that it stays below the critical value and after

the breaking initiation it never returns below 1.36 until the wave reaches the shoreline. Now, the behavior of the RTFN is computed with wave transformations calculated by the nonlinear Boussinesq model and examined whether it could satisfy the conditions mentioned above.

Fig. 6.1 shows the RTFN against the wave trough location. The RTFN stays about 1.1 when the wave is in the flat bottom part ( $i < 320$ ). Then it starts increasing gradually as the wave approaches the shore. At around node 500, where the water depth is about 17cm, the RTFN exceeds the critical value, 1.36. The RTFN continues to increase even after wave breaking begins. Behavior of the RTFN shown in Fig. 6.1 satisfies the condition mentioned above, namely, smaller RTFN for non-breaking waves and bigger RTFN for breaking waves. This result confirms that the RTFN can actually work as a wave breaking trigger index in a numerical model.

It is shown that the RTFN evolution in the Boussinesq equation model behaves as the theory requires. This implies that the wave breaking trigger “correctly” turns on a wave breaking at a certain point on the slope, and as a result, the wave starts to decay. Fig. 6.2 displays the wave profile envelope over one wave period. Fig. 6.2.a displays the result with the RTFN trigger and Fig. 6.2.b is that calculated with the FUNWAVE original trigger for reference.

Both results reproduce fundamental wave transformation processes in the surf zone, which are shoaling, wave set-up, and wave breaking. The difference between the two profiles can be seen at the peak wave crest elevation and its location. The profile envelope for the RTFN trigger does not have a sharp spike shape peak for the wave crest found in the FUNWAVE profile envelope. However, envelopes once separated at the wave breaking location match up again near the shoreline. This implies that the RTFN trigger initiates

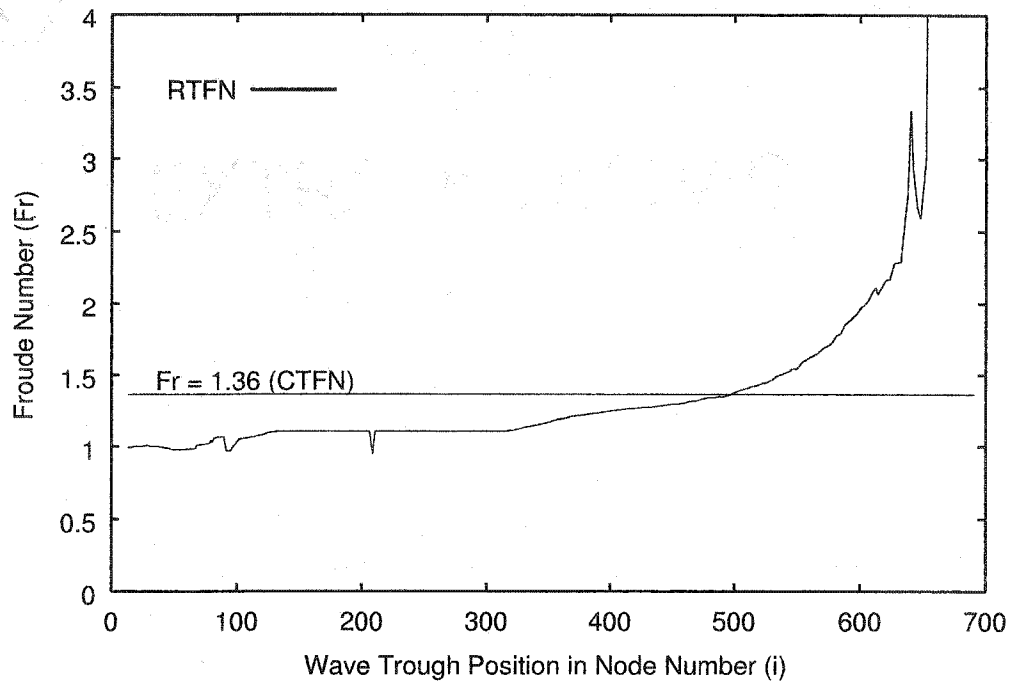
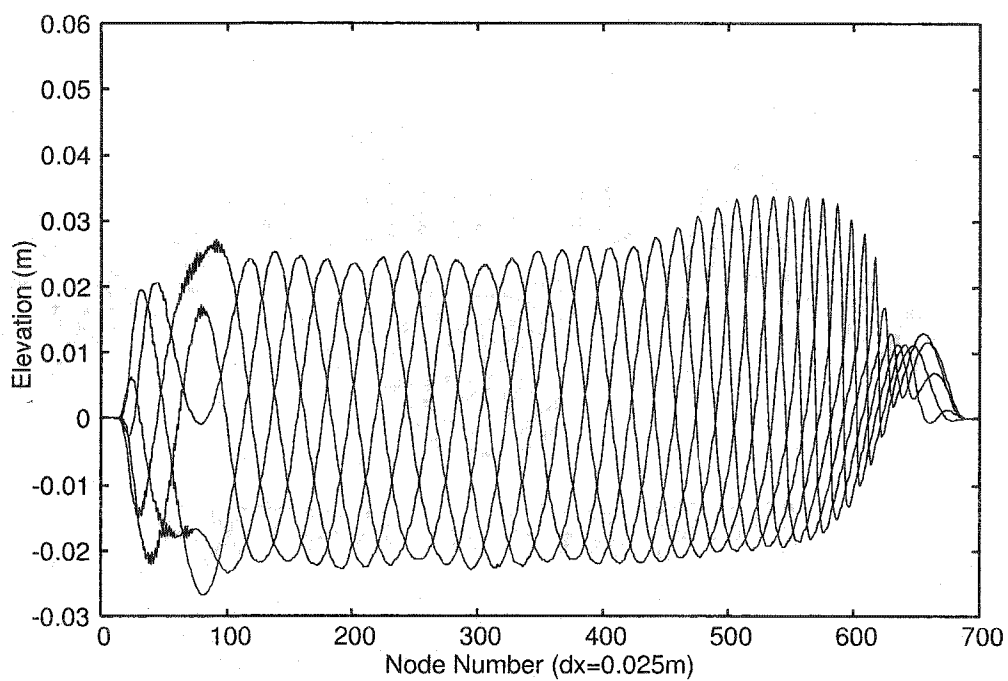


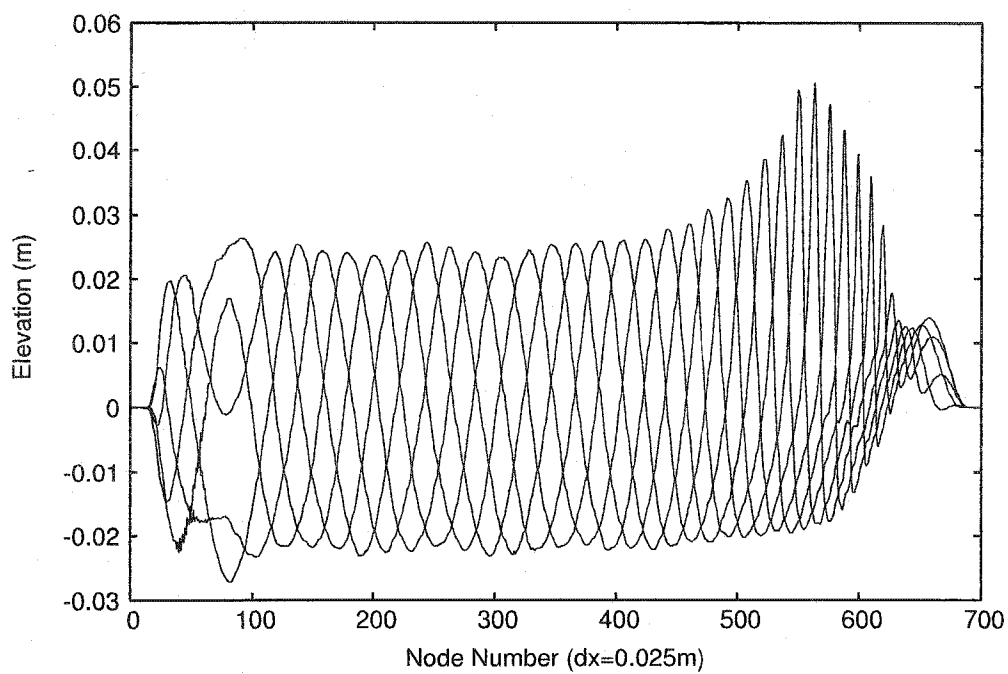
Figure 6.1: The RTFN evolution on a plane slope

the wave breaking event earlier than the FUNWAVE trigger does so that wave decay starts earlier. Therefore, the elevation of the top of the wave crest is lower than the FUNWAVE trigger case. Since wave breaking event is initiated earlier and because the wave height at the breaking point given by the RTFN is smaller than the FUNWAVE breaking wave height, the energy dissipation caused by the wave breaking is smaller.

To see the actual evidence of energy dissipation in a breaking wave, the eddy viscosity is plotted in Fig. 6.3. The result from the FUNWAVE trigger case is displayed again for the reference. Comparison to the FUNWAVE trigger case clearly reveals that the RTFN initiates the wave breaking event earlier than the FUNWAVE trigger does. And it also gives us evidence of the slow wave decay mentioned above. The magnitude of the eddy viscosity term is relatively small in the region where only the RTFN trigger turns on the

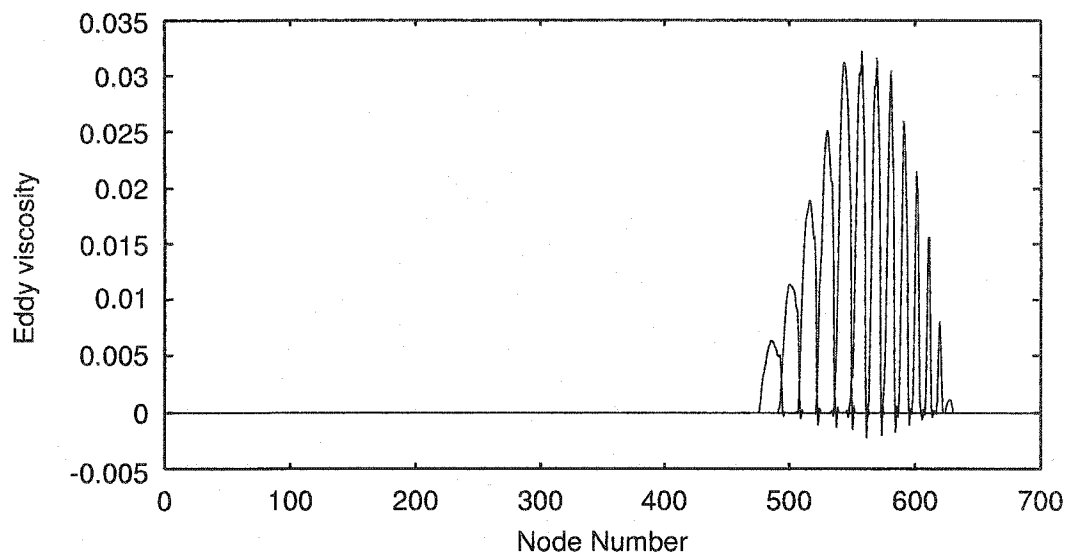


(a) The RTFN trigger

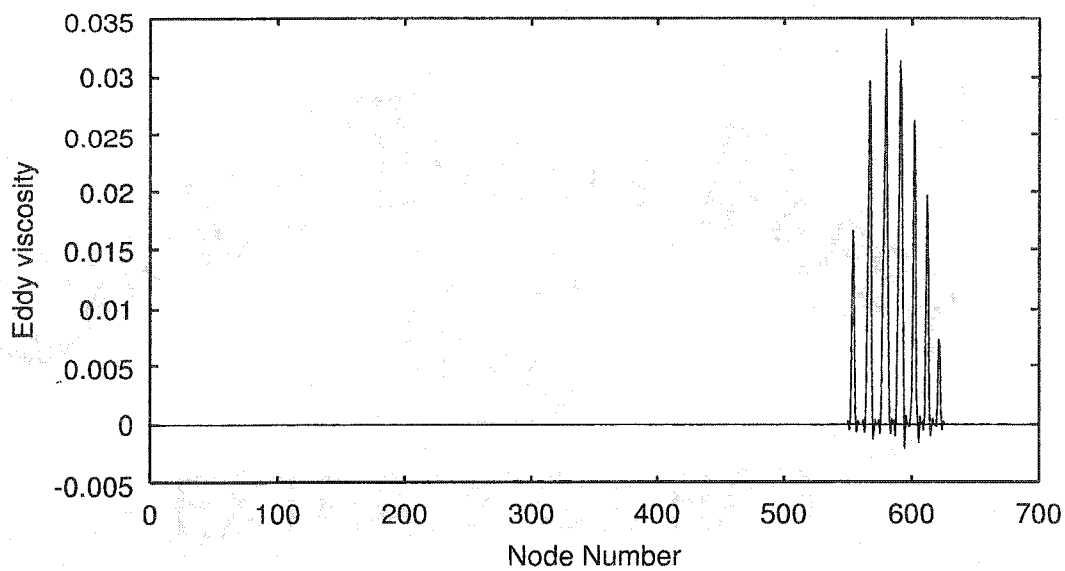


(b) FUNWAVE original trigger

Figure 6.2: Wave profile envelopes on plane beach



(a) The RTFN trigger



(b) FUNWAVE original trigger

Figure 6.3: Eddy viscosity generated by wave breaking : plane slope

wave breaking.

As a result, it can be concluded that the RTFN trigger works in the right direction, however, it starts a wave breaking event earlier. Since the energy dissipation effect by the wave breaking is small at the beginning of the wave breaking event and therefore it is canceled out by the wave shoaling effect, the wave crest elevation retains a similar height in the earlier stage of wave breaking. The difference of wave breaking location will be discussed in the later section.

### 6.2.2 Bar-Trough Beach

The second test is performed on a bar-trough shaped beach modeled after an imaginary laboratory wave tank basin. The base slope of the beach is 1:40 and a bar component which has 1:15 front slope is placed on the base slope. See Fig. 6.4 for more details, and a snapshot of the wave profile at time step 9001.

One noticeable feature in the wave profile in this figure is that the wave amplitude between the bar and the shoreline is amplified by the reflected wave energy. This does not affect much the RTFN calculation at this point, however the RTFN evolution becomes unstable as seen in Fig. 6.5. This is because the irregular shape of the wave profile resulting from the interaction between incoming wave and reflected wave makes detection of the true positions of wave crest and trough difficult. The trapped reflected wave will become a minor problem later when the wave celerity calculation method is switched to the least square estimation method; however, this will be discussed in a later section.

Fig. 6.5 shows the RTFN evolution over the domain. Up to the bar, the RTFN varies as in the plane slope beach case. The RTFN exceeds 1.36 before the wave trough passes the bar, and it drops to about 1.1 when the wave trough enters the trough region. In the trough region, the RTFN oscillates due to the reflected wave but it basically stays under

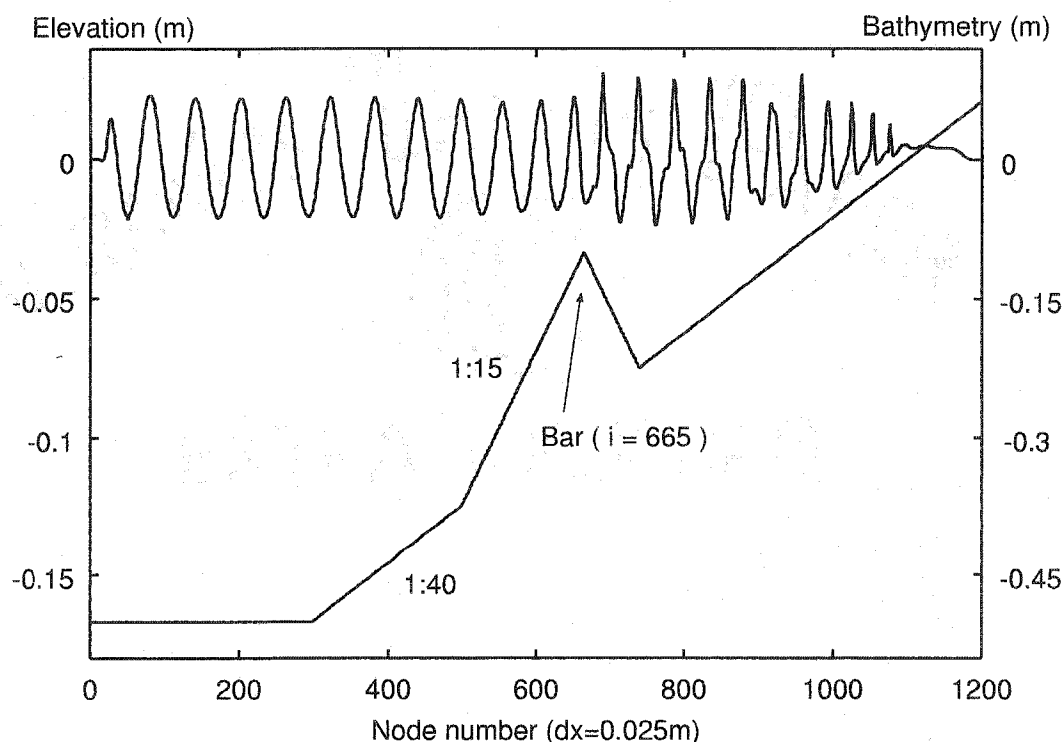


Figure 6.4: Bathymetry setting and water surface profile : bar-trough beach

the critical value. The RTFN again exceeds 1.36 when the wave reaches the very shallow water region near the shoreline. The RTFN stays greater than the critical value until the wave reaches the shoreline.

The eddy viscosity plot is again used to see where the actual energy dissipation is due to the wave breaking occurs (See Fig. 6.6). As expected, eddy viscosity has a non-zero value around the bar ( $i = 650$ ), which means the RTFN trigger actually turns on a wave breaking event and momentum sink term in the equation takes momentum out from the wave around the bar. The eddy viscosity is zero in the trough region, node 700 to 800, which indicates that the RTFN trigger ceases wave breaking in the trough so that the momentum sink term is excluded from the basic equation. As we have seen, the RTFN

trigger automatically turns on and turns off the wave breaking event at the bar and the trough according to the magnitude of the RTFN.

However, the comparison to the FUNWAVE case reveals that only the RTFN trigger makes wave breaking around the bar position. Also the RTFN trigger initiates wave breaking earlier than the FUNWAVE trigger. This is the same trend as seen in the plane slope case. It is not our intent here to discuss the accuracy of these results, but to confirm whether the new wave breaking trigger model works in the numerical model.

### 6.2.3 Real Bathymetry

The third test for this qualitative study is performed on a scaled, real bathymetry. Since the main purpose of this test is to check the ability of the RTFN trigger model on a complex bathymetry qualitatively, the scale ratio is chosen without the practical meaning.

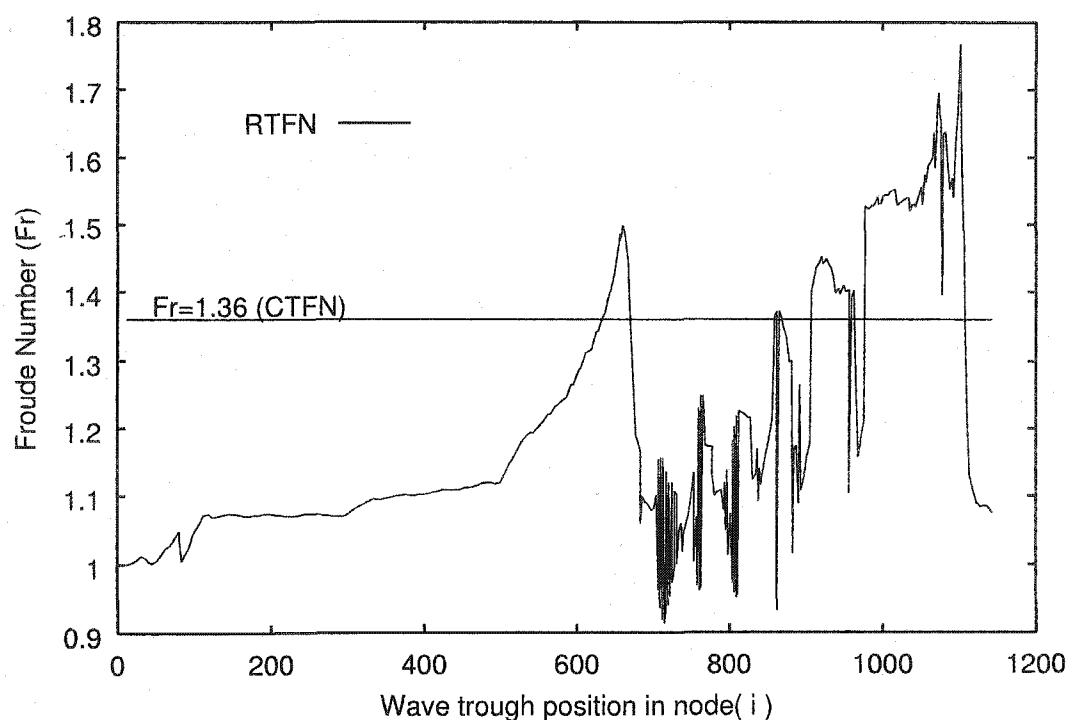
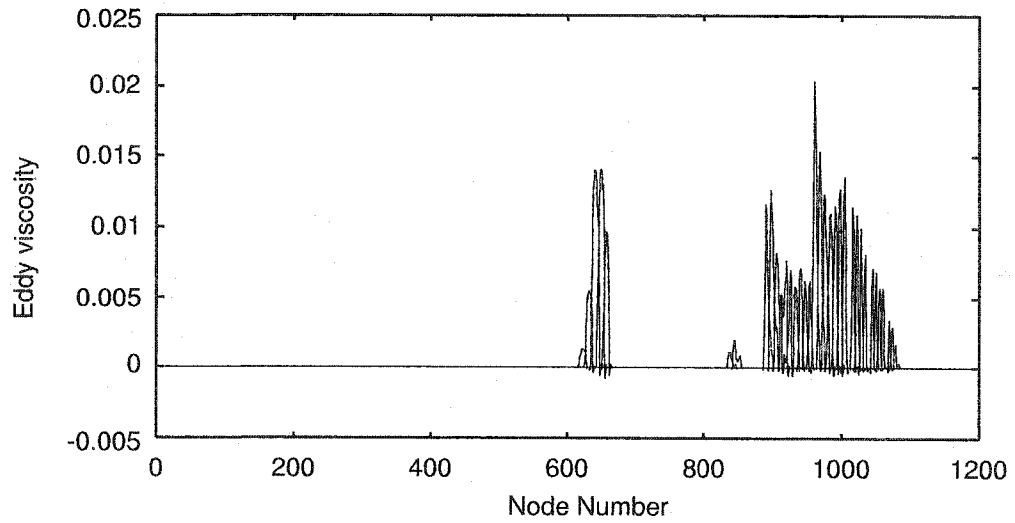
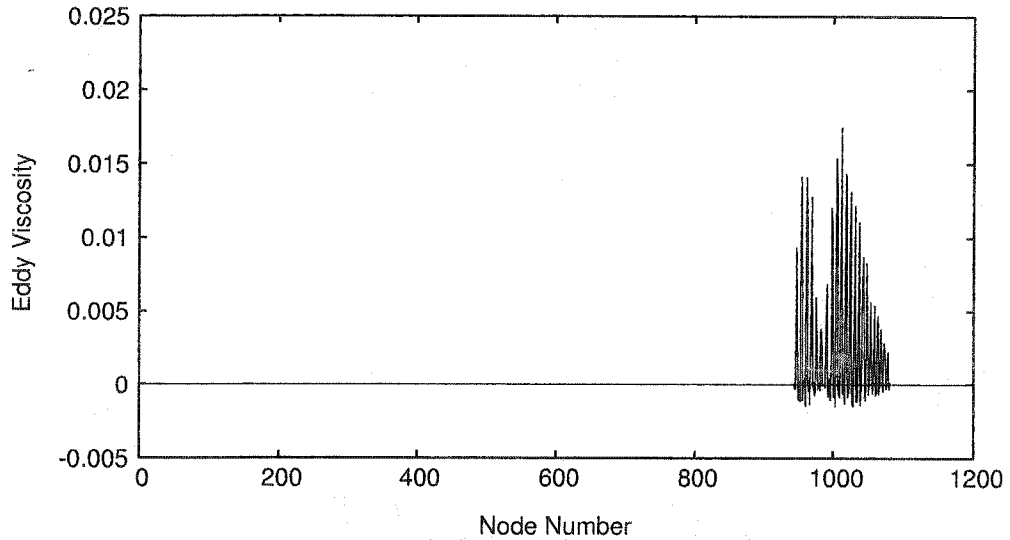


Figure 6.5: The RTFN evolution on a bar-trough beach



(a) The RTFN trigger



(b) FUNWAVE original trigger

Figure 6.6: Eddy viscosity generated by wave breaking : bar-trough beach

To make the wave generation easy, water depth at the offshore boundary is determined a similar to the other test cases. As a result, 1/10 scale is chosen for this test. The bathymetry data was surveyed by the Field Research Facility (FRF) of the U.S. Army

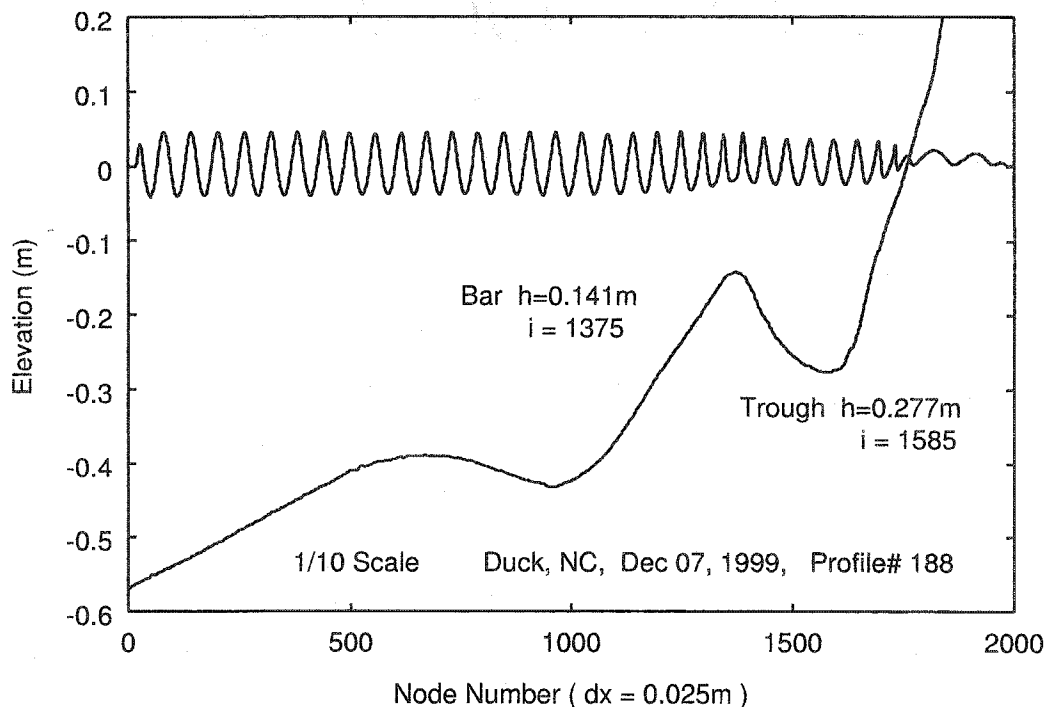


Figure 6.7: Bathymetry setting and water surface profile : real bathymetry

Corps of Engineers at Duck, North Carolina. The bathymetry data is available for the public and can be obtained from their web site at [www.frf.usace.army.mil](http://www.frf.usace.army.mil). A profile taken at December 1999 is chosen for this experiment because it has well-developed bar-trough formation. It actually has a double bar-trough formation in the profile, as seen in Fig. 6.7, which also shows a snapshot of the wave profile at timestep 9000. In this case, the reflected wave energy is not trapped between the bar and the shoreline. So, a smooth wave profile and the RTFN evolution are obtained for this case.

Fig. 6.8 displays the RTFN evolution plot on the real bathymetry. The RTFN does not change so much over the first bar which is located around node 600. However, the RTFN increases rapidly when the wave approaches the second bar which is at node 1300. The RTFN exceeds 1.36 before the wave reaches the peak of the second bar ( $i = 1375$ ), then

it drops down to about 1.2 at node 1400. And the RTFN stays about 1.2 while the wave is in the trough region. The RTFN evolution along the profile means that waves break at the second bar and wave breaking ceases in the trough. Since the overall tendency in the RTFN evolution is the same as the previous case, a comparison to the FUNWAVE trigger case is not made for this experiment. It is confirmed that the RTFN trigger gives reasonable RTFN evolution even on a complex bathymetry.

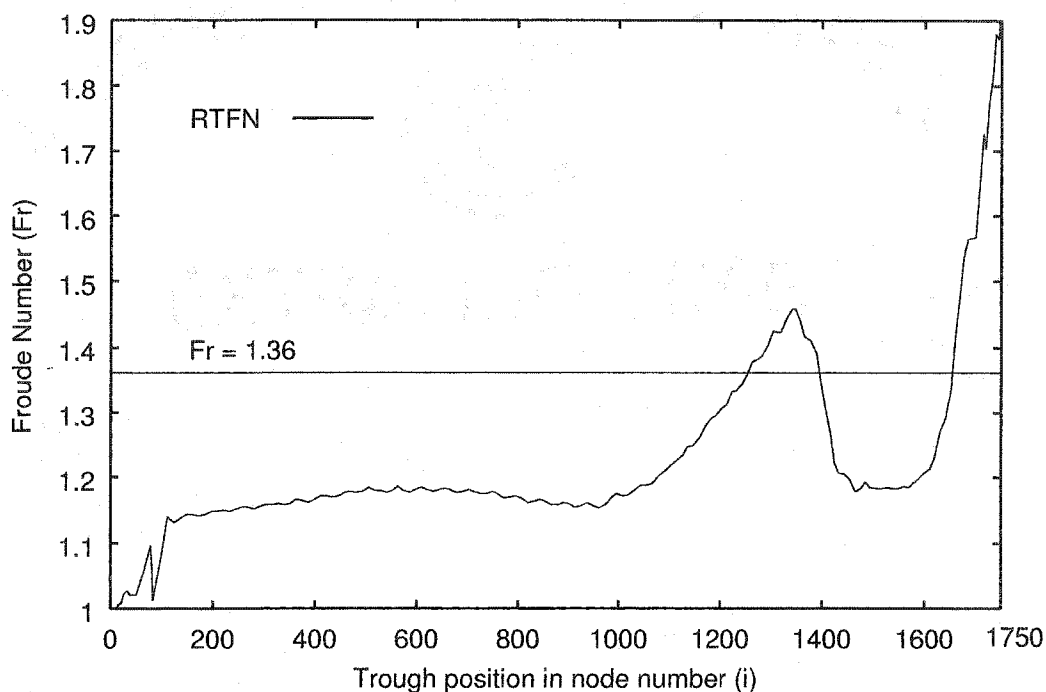


Figure 6.8: The RTFN evolution on a real bathymetry

#### 6.2.4 Summary of Qualitative Studies

For all three cases, the behavior of the RTFN along the domain is quite satisfactory as a wave breaking trigger index. It increases as the wave approaches to a bar or shoreline, and decreases when the wave is in the trough region. The RTFN stays higher than the

critical value ( $Fr = 1.36$  in this section) at the inner surfzone, even though the energy dissipation due to wave breaking makes the wave height lower in this region. Therefore, it is now confirmed that the RTFN theory can be used as a wave breaking trigger for phase-resolving wave model.

However, we also have learned that the RTFN trigger initiates wave breaking earlier than the FUNWAVE trigger. This implies that the critical condition ( $Fr = 1.36$ ), which is determined from wave tank experiment, may not be suitable for the numerical model. Therefore, a model calibration with physical wave tank data is required to establish new CTFN condition, which is suitable for numerical modeling.

### 6.3 Calibration of the CTFN

The qualitative studies successfully showed that the behavior of the RTFN in the numerical model is reasonable to use as a parameter for a wave breaking trigger. However, the discrepancy in the initiation location of the wave breaking between the RTFN trigger and the FUNWAVE trigger pose a new question. The question is whether the CTFN=1.36 which is confirmed from one wave tank experiment (Utku, 1999) also works as a proper CTFN for numerical modeling. To confirm this question, a calibration of the critical condition of the RTFN theory is performed with data from the physical experiment. Note that we assume in this study that all the wave breaking events occur in the shallow water region for simplicity, even though the RTFN theory itself can handle deep water wave breaking theoretically as discussed in Chapter III. Also note that the wave celerity calculation method is the analytical formula as shown in Eqn 6.1.

We have previously discussed the setting and the results of the wave tank experiment in Chapter IV. A total of 27 cases were simulated in the numerical model. Adjustments of input wave heights are made for numerical modeling according to the wave gauge record

placed at the toe of the beach slope (See Fig. 4.1 for details) so that two wave heights are identical just before wave starts to shoal. There is one case in which the numerical model crashed in the middle of the calculation because of the instability of the model ( $H=6.0$  cm,  $T=2.0$  sec, and  $d=30$  cm). Therefore, 26 cases are compared in the wave breaking initiation location between the numerical model and the physical experiment. FUNWAVE wave breaking trigger also calculates the 26 cases, and the results are compared to the physical experiment for reference purposes.

The wave breaking location,  $X_b$ , is defined as the distance from the toe of the beach slope to the wave crest location where a wave breaking event is initiated. Tables 6.1, 6.2, and 6.3 show wave breaking locations for 26 cases with the RTFN trigger. Tables 6.4, 6.5, and 6.6 are wave breaking locations for the FUNWAVE trigger cases. Physical experimental results are found in Tables 4.1, 4.2, and 4.3 in Chapter IV.

For simplicity, the comparison of wave breaking locations calculated in the numerical model against those observed in the physical experiment are plotted in Fig. 6.9. The least square linear fits are superimposed on the plot to obtain a better understanding of how the numerical results are related to the physical experimental data. Since the calculated results and the observed data are ideally the same but different methodologies, the ideal fit line is  $y = x$ .

The FUNWAVE trigger predicts wave breaking locations very well for all 26 cases. The least square fit line is very close to  $y = x$ , which is the ideal matching between two data sets. On the other hand, the RTFN trigger cases shows earlier initiation than it should. Also, Fig. 6.9 clearly reveals the tendency of earlier breaking for the RTFN trigger cases. It is confirmed that the CTFN determined from wave tank experiment ( $Fr=1.36$ ) is not suitable for the critical value in the numerical model.

Table 6.1: Wave breaking location(m), d=30cm (RTFN)

Wave height	T=1.0sec	1.5sec	2.0sec
2cm	4.28	3.63	2.88
4cm	3.13	2.33	0.50
6cm	1.95	1.58	N/A

Table 6.2: Wave breaking location(m), d=40cm (RTFN)

Wave height	T=1.0sec	1.5sec	2.0sec
2cm	6.25	5.73	5.00
4cm	5.03	4.25	3.95
6cm	3.93	3.23	2.70

Table 6.3: Wave breaking location(m), d=50cm (RTFN)

Wave height	T=1.0sec	1.5sec	2.0sec
2cm	8.38	7.63	6.75
4cm	7.28	6.28	5.23
6cm	6.05	4.85	3.90

Table 6.4: Wave breaking location(m), d=30cm (FUNWAVE)

Wave height	T=1.0sec	1.5sec	2.0sec
2cm	5.23	5.00	5.00
4cm	4.50	4.35	4.08
6cm	3.78	3.60	N/A

Table 6.5: Wave breaking location(m), d=40cm (FUNWAVE)

Wave height	T=1.0sec	1.5sec	2.0sec
2cm	7.18	7.10	6.90
4cm	6.48	6.23	6.05
6cm	5.73	5.48	5.25

Table 6.6: Wave breaking location(m), d=50cm (FUNWAVE)

Wave height	T=1.0sec	1.5sec	2.0sec
2cm	9.20	9.00	8.93
4cm	8.55	8.18	8.05
6cm	7.80	7.38	7.30

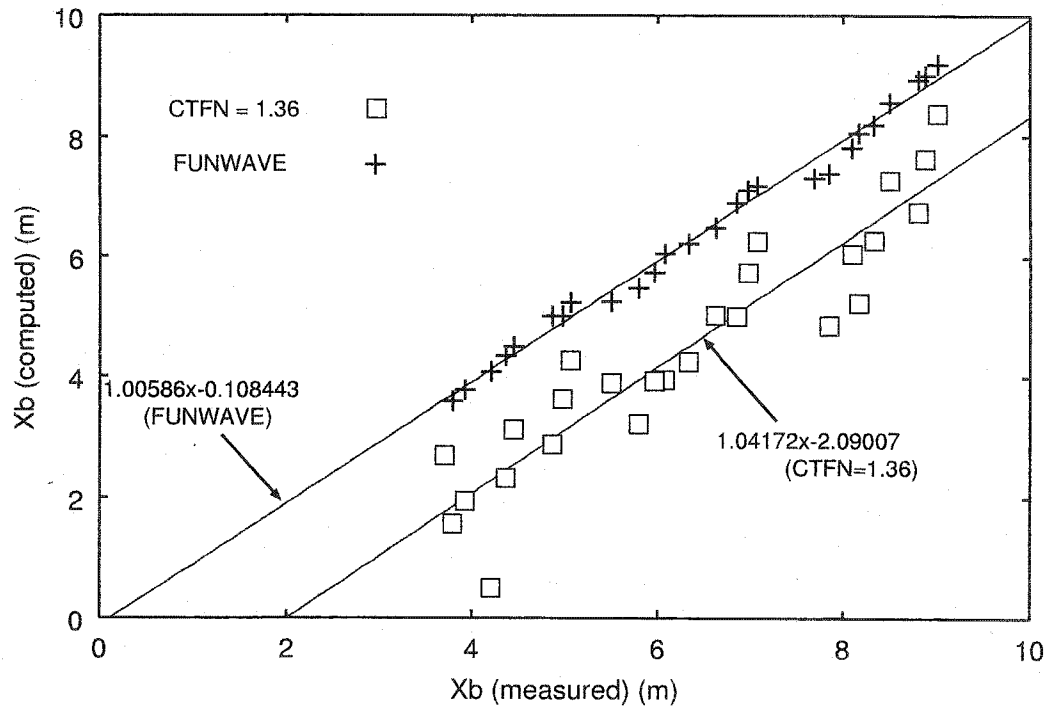


Figure 6.9: Wave breaking location comparison (CTFN=1.36 & FUNWAVE)

Now the establishment of a new CTFN which gives reasonable wave breaking location in the numerical model is needed. A closer look at the plot and the least square fit line gives an idea of how to determine the new CTFN for the numerical model. The least square fit line for the RTFN trigger case provides a very close number to 1 in the slope (1.04172) but the intercept is far away from 0 (-2.09007). This indicates the RTFN trigger with CTFN=1.36 initiates wave breaking events always 2 m earlier than it should. The fact that the discrepancy from the physical data is relatively constant tells us the RTFN trigger mechanism works consistently but low CTFN makes earlier initiation. Therefore, it can be easily assumed that higher CTFN would give better consistency to the physical data.

Therefore, RTFN values at the locations where the physical experiment indicates the

Table 6.7: RTFN value at the wave breaking location in physical experiment (30cm)

Wave height	T=1.0sec	1.5sec	2.0sec
2cm	1.588	1.703	1.742
4cm	1.604	1.746	1.739
6cm	1.575	1.730	N/A

Table 6.8: RTFN value at the wave breaking location in physical experiment (40cm)

Wave height	T=1.0sec	1.5sec	2.0sec
2cm	1.606	1.700	1.773
4cm	1.627	1.718	1.693
6cm	1.588	1.708	1.666

Table 6.9: RTFN value at the wave breaking location in physical experiment (50cm)

Wave height	T=1.0sec	1.5sec	2.0sec
2cm	1.580	1.630	1.783
4cm	1.611	1.711	1.751
6cm	1.598	1.721	1.810

Table 6.10: Wave breaking location(m), d=30cm (CTFN=1.68)

Wave height	T=1.0sec	1.5sec	2.0sec
2cm	5.10	4.90	4.75
4cm	4.50	4.23	4.00
6cm	3.95	3.80	N/A

Table 6.11: Wave breaking location(m), d=40cm (CTFN=1.68)

Wave height	T=1.0sec	1.5sec	2.0sec
2cm	7.10	6.98	6.65
4cm	6.50	6.18	6.00
6cm	5.98	5.55	5.13

Table 6.12: Wave breaking location(m), d=50cm (CTFN=1.68)

Wave height	T=1.0sec	1.5sec	2.0sec
2cm	9.10	9.00	8.68
4cm	8.53	8.23	7.80
6cm	7.95	7.53	6.83

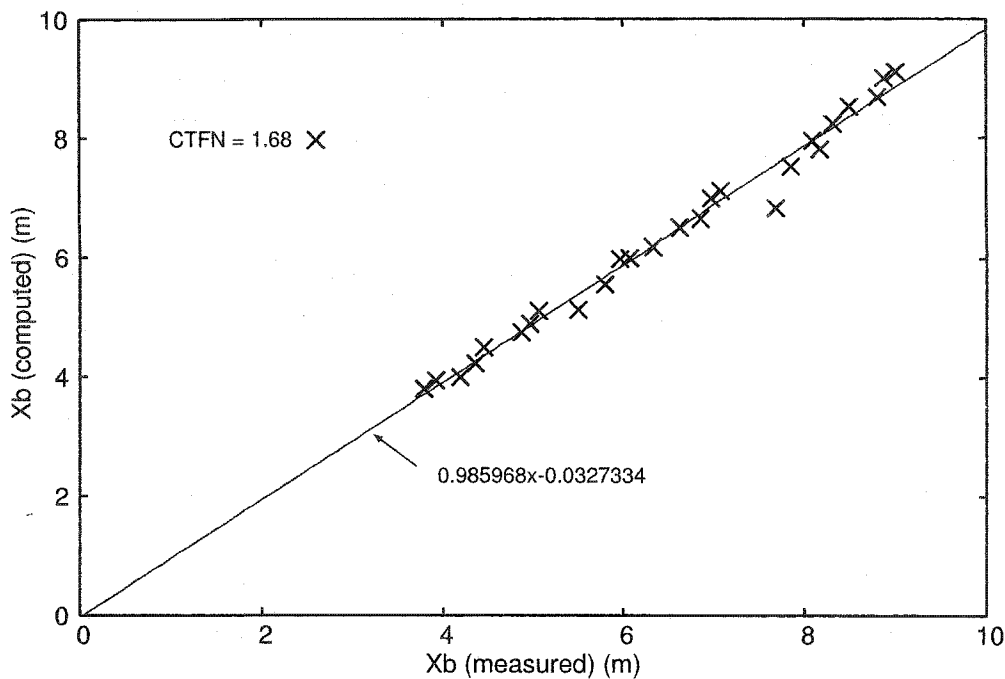


Figure 6.10: Wave breaking location comparison (CTFN=1.68)

wave breaking initiates are investigated in each case. Tables 6.7, 6.8 and 6.9 display the RTFN values at those locations for 26 cases. The averaged value of these 26 cases is 1.68. So, it is expected that using CTFN=1.68 in the model would give us better consistency against the physical experimental result than using CTFN=1.36. Wave breaking locations calculated by the RTFN trigger with CTFN=1.68 are listed in Tables 6.10, 6.11, and 6.12, and the comparison plot is shown in Fig. 6.10.

As seen in Fig. 6.10, consistency against the physical experiment is much improved by employing the new CTFN value. The least square fit line becomes very close to the ideal matching,  $y = x$ . And the scatter around the least square fit line is also improved. The standard deviation from the least square fit line is reduced to 0.202 from 0.719 in the case of CTFN=1.36. This is because RTFN evolution is a nonlinear process. As displayed in Fig. 6.1, the slope of the RTFN evolution line gets steeper as the wave approaches to the

shoreline because square root function is in the denominator of the equation. Therefore, even though 1.68 is an averaged value so that there is some difference between the actual RTFN value at the wave breaking location indicated by the physical experiment and the averaged value, making CTFN higher and, because of that, making wave breaking initiation later reduces the scatter in space, comparing to the case of CTFN=1.36.

This result is quite satisfactory in terms of matching numerical result to the physical experimental data. However, the new CTFN value, 1.68, is higher when compared to the theoretical value 1.45. This could be caused by using an improper RTFN calculation method in the model.

For this reason, the representative water depth in the wave celerity calculation formula is reconsidered. Since an analytical formula has been used for the wave celerity calculation, determination of the water depth is very important in the shallow water region, because shallow water wave celerity depends on the water depth. As discussed in Chapter III, the solitary wave theory provides a good approximation for waves in very shallow water region. A combination of the solitary wave theory and an approximation relation,  $(1+\varepsilon)^\alpha = 1+\alpha\varepsilon$ , leads us to conclude that it is theoretically proper to apply  $\sqrt{g(h+\eta)}$  for both wave crest celerity and wave trough celerity, and this formulation is represented in Eqn 6.1. However, this formulation requires high CTFN value to match the result to wave tank experiment data. Due to complex nonlinear processes in shallow water region, it is impossible to determine what causes the difference between theory and application.

Consider linear wave theory as an alternative. Theoretically speaking, the linear wave theory is not the most appropriate wave model for wave celerity calculation in shallow water region because the wave definitely has finite wave amplitude. But the celerity formula,  $\sqrt{gh}$ , is widely accepted in many application and it is the linear approximation

of all of the nonlinear wave celerity in shallow water. Therefore, it is fair to use linear wave celerity in this case. One inferior point with using  $\sqrt{gh}$  is that this formulation does not include any nonlinear effect happening in the nearshore region, which is an important factor for the RTFN calculation. Therefore, we have to consider some way to avoid excluding all nonlinear effects from the formulation.

From the discussion mentioned above, it is determined that  $\sqrt{gh}$  should be used for the wave crest celerity calculation; however, a wave celerity calculation method including free surface displacement is employed also in this formulation for the wave trough celerity in order to have a nonlinear effect in the RTFN calculation. The reason for using the nonlinear wave celerity for wave trough is that the wave has very flat free surface geometry around wave trough in shallow water region, and has a uniform horizontal velocity distribution under the wave trough caused by shallow water wave motion. This geometrical and velocity distribution condition is similar to the open channel flow. So, we are going to use actual water depth, not theoretical still water depth as implied from linear wave theory. For the wave trough section, this gives a closer appearance to the moving hydraulic jump used for the establishment of the RTFN theory.

The CTFN with this new formulation is determined by trial and error using the physical wave tank data. Several test cases are executed with different CTFN values and it was found that CTFN=1.47 works very well for the new RTFN calculation method. Wave breaking locations with CTFN=1.47 are summarized in Tables 6.13, 6.14, and 6.15, and the comparison to the physical data is plotted in Fig. 6.11. The new CTFN for numerical model is very close to the theoretical CTFN found in Chapter III, as a result. The consistency to the physical data is also good by using the new combination of RTFN calculation method and the CTFN. The least square fit line is again very close to the ideal

Table 6.13: Wave breaking location(m), d=30cm (CTFN=1.47)

Wave height	T=1.0sec	1.5sec	2.0sec
2cm	5.10	4.70	4.53
4cm	4.43	4.05	3.78
6cm	4.00	3.30	N/A

Table 6.14: Wave breaking location(m), d=40cm (CTFN=1.47)

Wave height	T=1.0sec	1.5sec	2.0sec
2cm	7.10	6.83	6.43
4cm	6.58	6.20	5.93
6cm	5.90	5.50	5.38

Table 6.15: Wave breaking location(m), d=50cm (CTFN=1.47)

Wave height	T=1.0sec	1.5sec	2.0sec
2cm	9.10	8.75	8.33
4cm	8.53	8.18	7.53
6cm	8.05	7.50	6.80

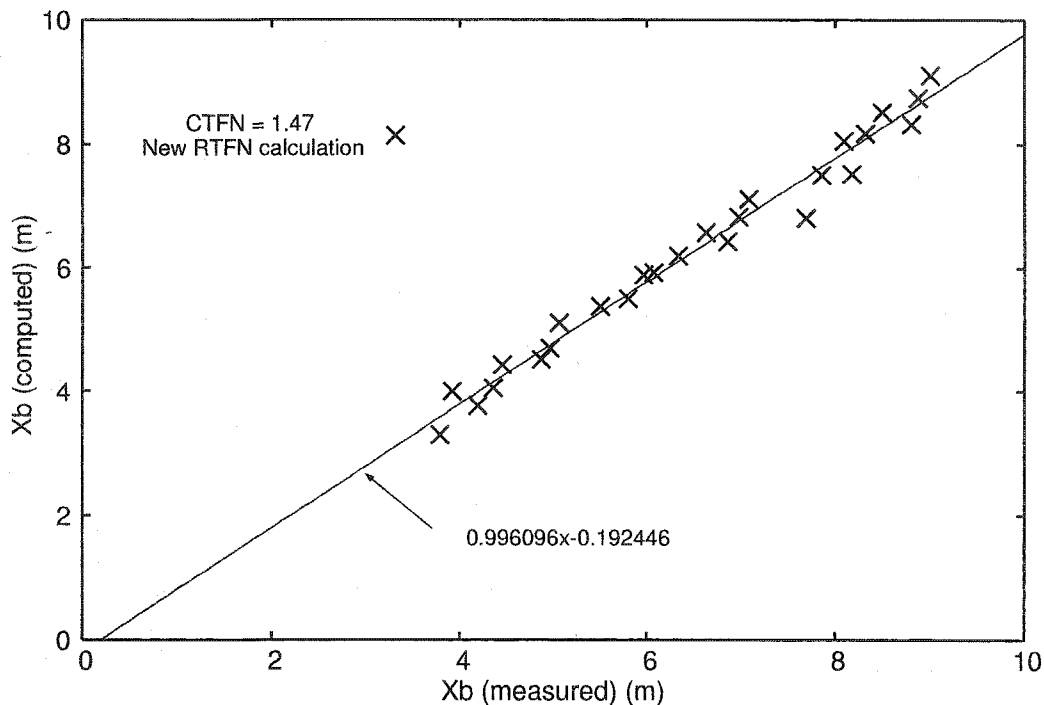


Figure 6.11: Wave breaking location comparison (CTFN=1.47)

fit, but the interception is slightly off from the origin (0.192446) and the standard deviation from the least square line becomes 0.240 which is slightly worse than the previous case (0.202).

However, this formulation satisfies both agreement with the physical experimental data for the wave breaking initiation location, and the theoretically predicted CTFN value. It is fair to say that this is a reasonable method for the RTFN calculation. However, this scheme has theoretical weakness as discussed above. The weakness comes from the fact that even though it is assumed that all the wave breaking events would happen in a shallow water region so that wave definitely has finite wave amplitude, the formulation contains a part derived from the linear wave theory. To remove the linear wave theory from the formulation and avoid theoretical failure, the least squared, cross-correlation estimation

method (Misra et al., 2003) discussed in Chapter IV is introduced to estimate the celerity at the wave trough.

This free-surface-geometry-based calculation method will permit the deeper water condition to be calculated. Since the model relies solely on the free surface geometry calculated by the Boussinesq equation model, the accuracy of wave celerity calculation follows from the phase accuracy of the Boussinesq model. Therefore, it has virtually no limit against the deeper water, even though deep water wave breakings are not tested in this study, as long as the Boussinesq equation can serve correctly for a given domain. Because it has some difficulty for the implementation of the least square estimation method, the model used in the actual calculation is a hybrid model of the least square estimation method and analytical formula modified by the Ursell number, as explained in Chapter V.

In this experiment, the CTFN value is assumed to be 1.47 and the experiment is executed only with this value because this number is theoretically appropriate and gave a good agreement to physical tank result in the previous case. Wave breaking locations calculated with the least square estimation method and CTFN=1.47 are listed in Tables 6.16, 6.17, and 6.18 and the comparison plot is shown in Fig. 6.12.

Resulting accuracy with this formulation is extremely good. The least square fit line is almost perfect,  $y = 1.00097x - 0.082635$ , and the scatter around the fit line is reduced to 0.235, compared to 0.240 for the analytical formula case. It has more scatter than the case with FUNWAVE trigger (0.182) and the case with CTFN=1.68 (0.202). However, this is the best formulation among all the test cases examined in this section. Since the formulation with the least square estimation method also gives consistent result with CTFN= 1.47, it can be concluded the proper CTFN value for numerical model is about

Table 6.16: Wave breaking location(m), d=30cm (Least square estimation)

Wave height	T=1.0sec	1.5sec	2.0sec
2cm	5.10	4.90	4.40
4cm	4.53	4.35	3.58
6cm	4.15	3.80	N/A

Table 6.17: Wave breaking location(m), d=40cm (Least square estimation)

Wave height	T=1.0sec	1.5sec	2.0sec
2cm	7.10	6.85	6.58
4cm	6.63	6.30	5.88
6cm	6.15	5.90	5.45

Table 6.18: Wave breaking location(m), d=50cm (Least square estimation)

Wave height	T=1.0sec	1.5sec	2.0sec
2cm	9.13	8.93	8.43
4cm	8.65	8.35	7.70
6cm	8.25	7.88	7.20

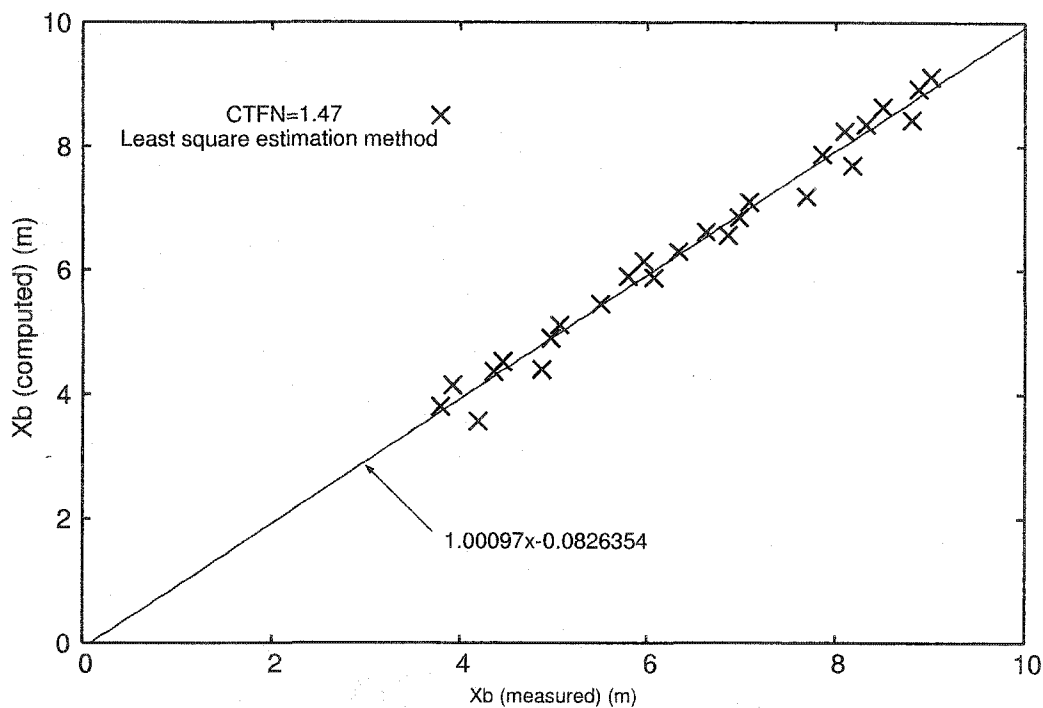


Figure 6.12: Wave breaking location comparison (Least square estimation method)

1.47 for plane slope beach.

Last of all for the calibration, least square fit lines and the standard deviations around the line are listed as a summary of all the methods above.

Calibration scheme	Least square fit line	Standard deviation
FUNWAVE	$y = 1.00586x - 0.108443$	0.182
RTFN (Analytical I, 1.36)	$y = 1.04172x - 2.09007$	0.719
RTFN (Analytical I, 1.68)	$y = 0.98597x - 0.03273$	0.202
RTFN (Analytical II, 1.47)	$y = 0.99610x - 0.192446$	0.240
RTFN (Least sq. est., 1.47)	$y = 1.00097x - 0.082635$	0.235

#### 6.4 Slope Effect

One advantage of using the numerical model in research is that once the model is calibrated, you can easily apply it to other domains. In this section, a number of numerical experiments are performed with different beach slope settings. It is known that wave breaking location is altered by the effect of a sloping bottom (Goda, 1970). However, the RTFN theory is only confirmed physically on 1:20 slope beach so that the effect of sloping bottom to the RTFN theory is unknown.

Seven different beach slope settings are prepared for this analysis. Four wave periods and two wave height are chosen for wave input condition. Beach slope conditions and input wave conditions are listed below.

Beach slope : 1/10 1/15 1/20 1/25 1/30 1/35 1/40

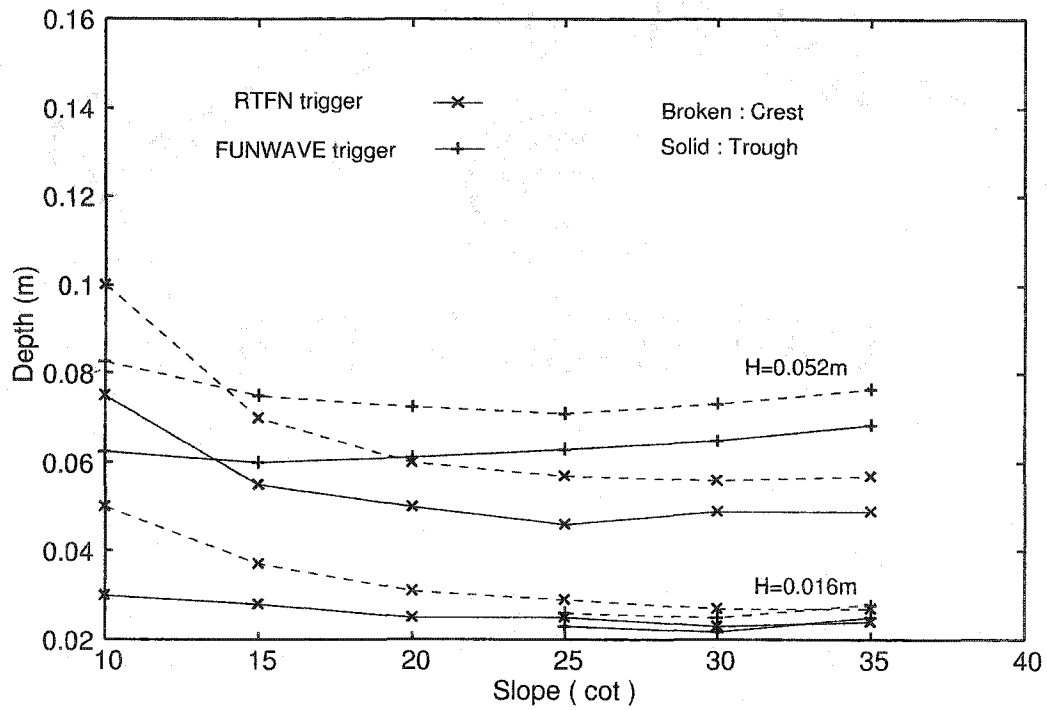
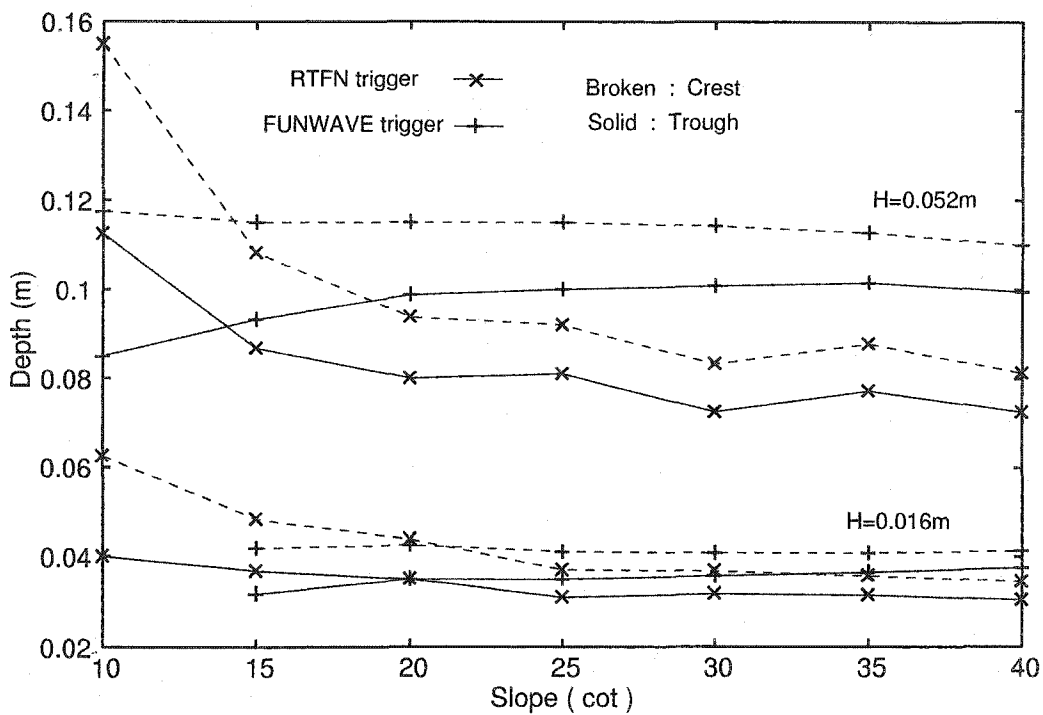
Wave period : 0.75 1.0 1.5 2.0 (sec)

Wave height : 0.016 0.052 (m)

Therefore, a total 56 cases are tested, and the same number of test cases are executed with the FUNWAVE original breaking trigger for comparison. Wave crest and trough location at the initiation of wave breaking are determined by looking through the eddy viscosity record. Then the depths at both locations are determined from the bathymetry data. For the case of  $H_0 = 0.016m$ , the wave breaking heights are also calculated from the surface displacement at the crest and trough.

The depth at the wave crest and the wave trough location is used for the comparison between the RTFN trigger and the FUNWAVE trigger in this analysis, because unlike the calibration performed in the previous section, wave breaking location from the toe of the beach slope is not comparable among different beach slope settings.

Results are shown in Fig. 6.13, 6.14, 6.15, and 6.16 for the case of  $T=0.75$  sec, 1.0 sec,

Figure 6.13: Slope effect on breaking depth ( $T=0.75\text{sec}$ )Figure 6.14: Slope effect on breaking depth ( $T=1.0\text{sec}$ )

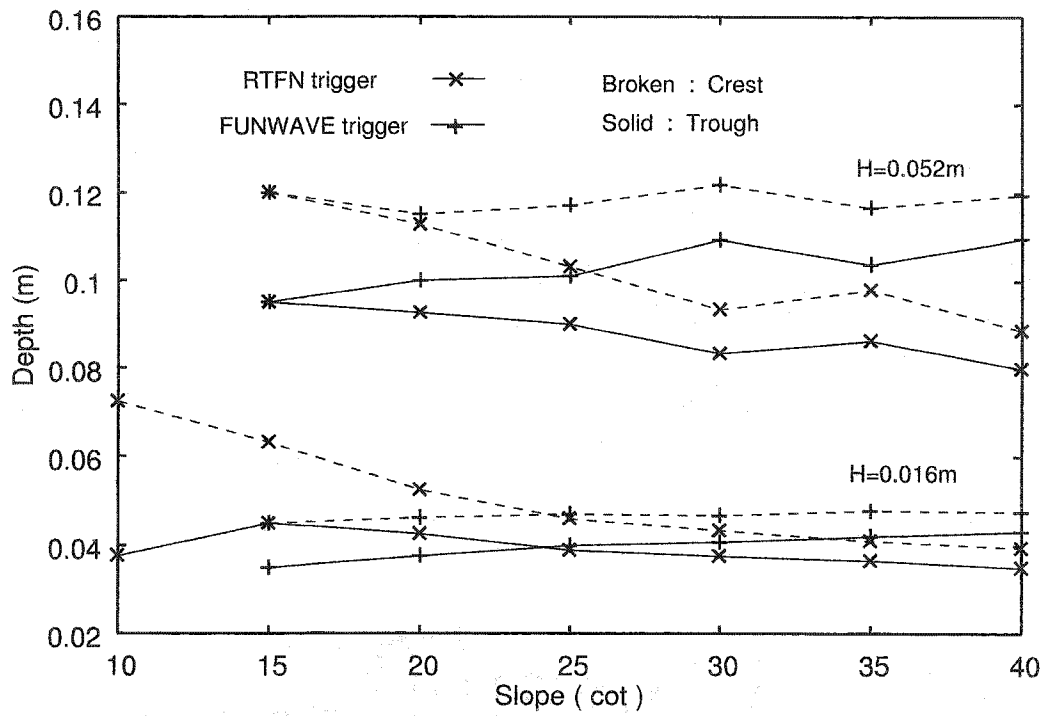


Figure 6.15: Slope effect on breaking depth ( $T=1.5$ sec)

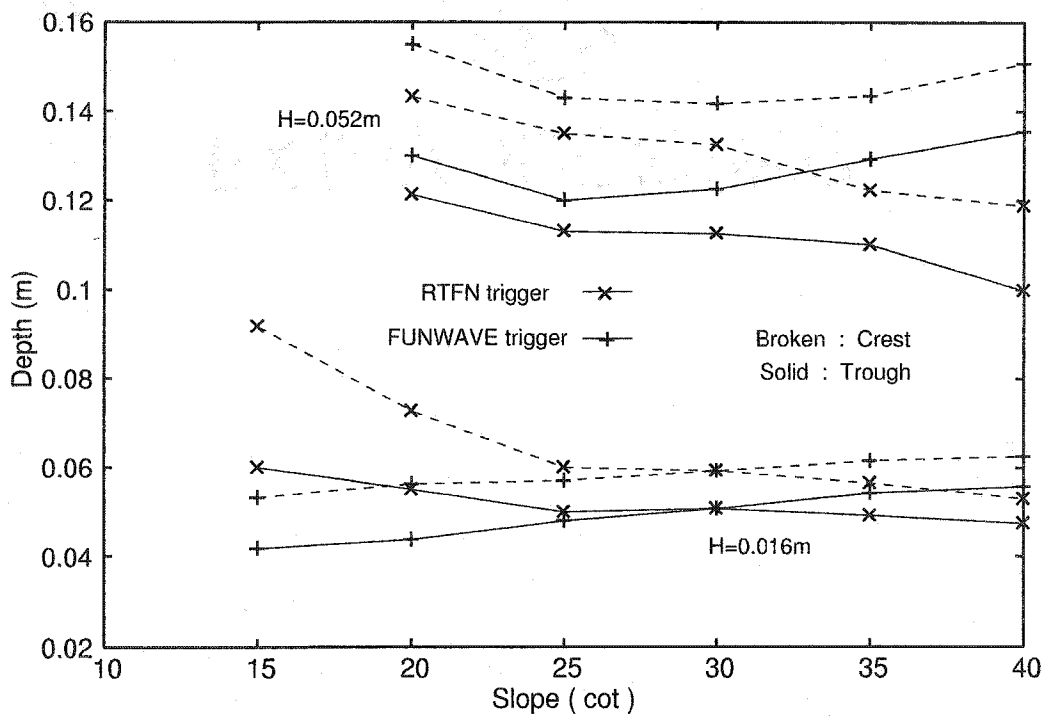


Figure 6.16: Slope effect on breaking depth ( $T=2.0$ sec)

1.5 sec, and 2.0 sec, respectively. Tabulated results are also displayed in Appendix B. As a general trend, the RTFN trigger makes the breaking position (depth) shift towards to the shoreline as the slope gets flatter. On the other hand, the FUNWAVE trigger makes the breaking position shift away from the shoreline as the slope gets flatter. Results show completely opposite directions between two trigger formulations, but it cannot be determined here which one is closer to the actual phenomena because there is no physical data set for this case. Therefore, we compare these results to the existing theory for phase-averaged waves.

Goda (1970) compiled a number of wave tank experiment data and established several forms of the wave breaking index curve with bottom slope effect. One of the results can be seen in Fig. 6.18. This is the most widely accepted wave breaking index on a sloped bottom. This index curve is chosen as a reference. Here, the FUNWAVE trigger has a problem. As shown in Fig. 6.17, the wave height continues to increase for more than ten time steps after the FUNWAVE trigger initiates the wave breaking event. From our experience during the wave tank experiments, it was almost impossible to catch the moment when the top of the crest starts tip over without the assistance of the video recording. Considering the time when data for Goda (1970) was taken (1960 - 1970's), it is reasonable to consider that the use of the wave height at the point where it becomes maximum is more proper rather than using the point where the FUNWAVE trigger starts wave breaking. And from the figure in Goda (1970), the still water depth,  $h_b$ , is taken at the crest position.

The ratio of breaking height over breaking depth ( $H_b/h_b$ ) is the most popular index for the wave breaking in shallow water so that the calculation results are superimposed into this index curve. Fig. 6.18 shows wave breaking height ratio calculated by the RTFN

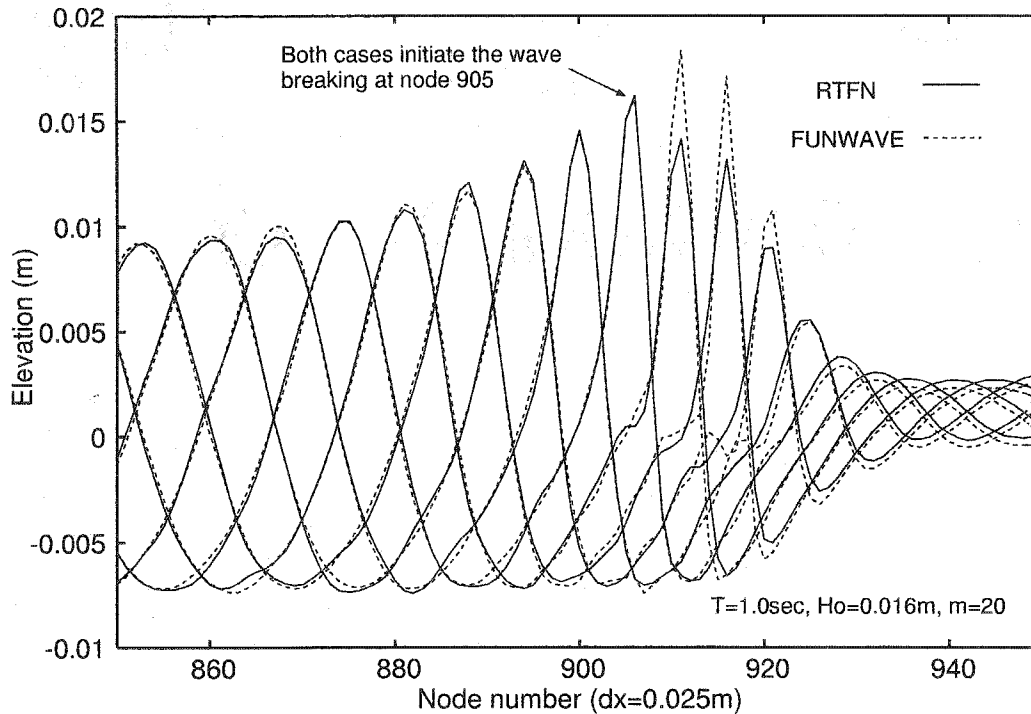


Figure 6.17: Determination of wave breaking height

trigger and the FUNWAVE trigger, and also shows the wave breaking index curve given by Goda (1970). Neither of the two numerical result matches to the wave breaking index by Goda (1970). Wave breaking height ratio against the relative depth is much smaller than the index curve suggested. This means, in general, both numerical models initiate wave breaking events earlier than the index curve suggests.

There is a difference between the RTFN trigger and the FUNWAVE trigger. The RTFN trigger gets more influence from the change of the bottom slope. On the other hand, the wave breaking height ratio calculated by the FUNWAVE trigger stays in about same range regardless the bottom slope. However, besides the rate of change, both triggers show the same trend in the breaking height ratio against the bottom slope; the wave breaking height ratio becomes higher as the bottom slope gets flatter. This is the opposite direction of

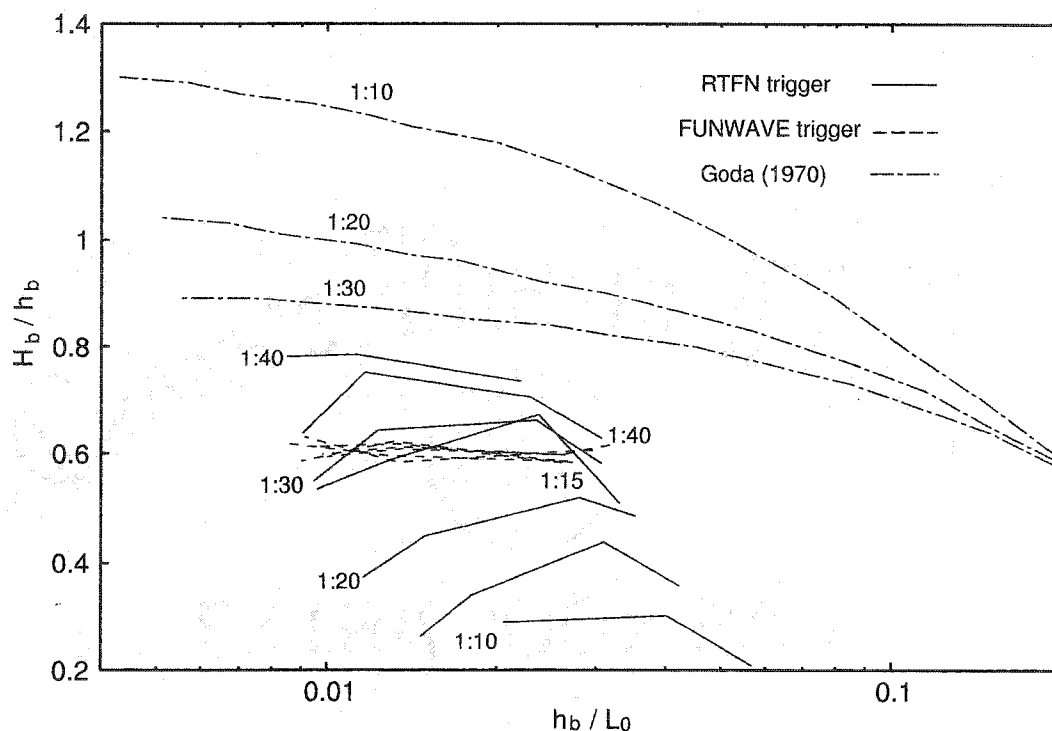


Figure 6.18: Slope effect : comparison with Goda (1970)

what is suggested in the wave breaking index curve by Goda (1970).

This difference may be caused by the difference of the scale. In fact, Goda (1970) excluded two data sets from his compiled data because of small wave height. Incident wave conditions employed here are smaller than the ones normally taken at wave tank experiments because of stability of the numerical model. In wave tank experiments, ten centimeters or more of the wave height and two second or more of the wave period are commonly used in wave tank experiment. But FUNWAVE could not make such a wave numerically. For example, the model went unstable for the case of  $H = 6$  cm,  $T = 2.0$  sec, and  $d = 30$  cm in the calibration. Therefore, relatively small input wave conditions are used in this research. This scale difference may cause a difference in the result but we cannot conclude at this time because there is no data sets which can be used for a direct

comparison.

A decision cannot be made for the slope effect on the wave breaking position at this time because of the lack of supported physical data. Therefore, a series of wave tank experiments are needed to make a direct comparison with numerical model results.

### 6.5 Duration of the Wave Breaking

Another unknown aspect for the RTFN trigger is the termination condition of the wave breaking. The initiation condition was confirmed through the calibration process discussed in this chapter. This is sufficient when the model computation is performed on a plane sloped beach, because the wave breaking never turns off once it started. However, the wave breaking trigger needs to turn off the wave breaking event correctly when it simulates a bar-trough shaped beach or real bathymetry. Theoretically speaking, a turbulent hydraulic jump ceases when the Froude number goes below the critical value so that it is natural to expect the same thing for the RTFN model because it is based on a moving hydraulic jump; however, no experimental work has been conducted on this problem.

When the model is executed on a bar-trough shaped beach, it can be realized that the RTFN trigger terminates wave breaking earlier than the FUNWAVE trigger. Fig. 6.19 shows an example of wave profile over the bar position. It also indicates the crest locations where the eddy viscosity term has a non-zero value. The top of the bar (0.05 m in depth) is located from node 530 to node 570 in this case.

As we have seen, both triggers initiate wave breaking at similar locations (around node 505), which is just before the top of the bar. Then the RTFN terminates the wave breaking around node 530 and starts it again at node 545 for a short time, while the FUNWAVE trigger keeps the wave breaking on until the wave trough reaches to node 575.

Also there is a difference between the RTFN trigger case and the FUNWAVE trigger

case in the wave profile evolution. The wave breaking gradually reduces the wave height over the entire bar section for the FUNWAVE trigger case. On the other hand, the RTFN trigger case shows more complicated evolution over the bar top. First, the wave height decays much faster than the FUNWAVE case during the wave crest travels between node 510 and node 530. Then the wave height grows until the wave crest reaches to node 545 and reduces the height throughout the rest of the bar section.

Considering both wave profile evolution and locations where the eddy viscosity term appears in the equation, this behavior can be explained as follows. The RTFN wave breaking model takes much more momentum out from the governing equation once the trigger initiates wave breaking. Therefore, the wave decays more than the FUNWAVE wave breaking model. Consequently, the wave cannot hold the state of wave breaking after

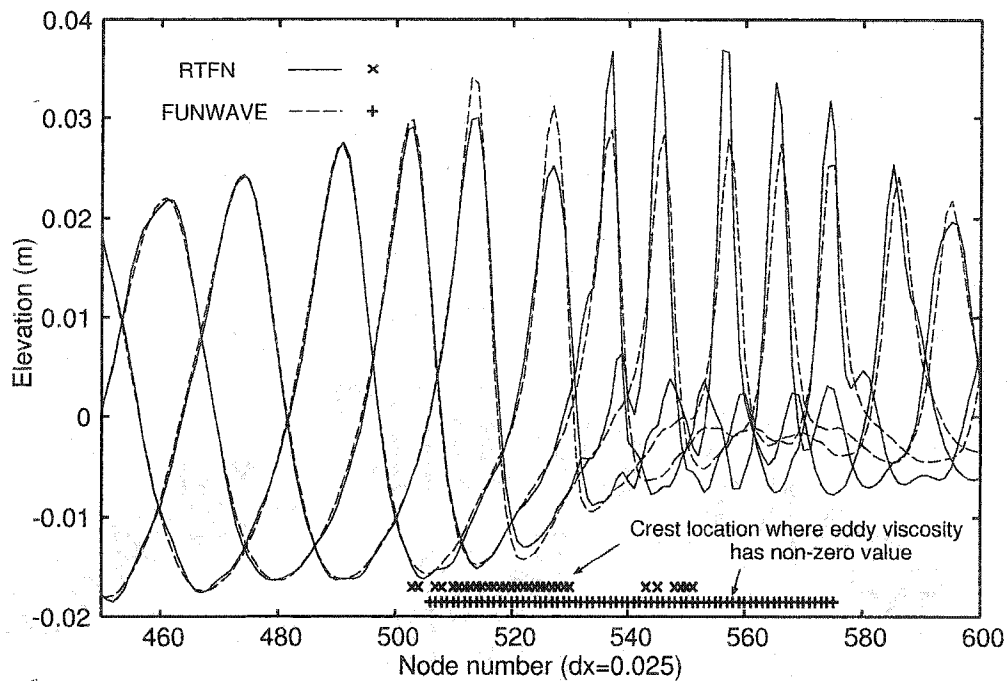


Figure 6.19: Example wave profile over the bar

it travels 25 nodes' length. So, the RTFN trigger terminates the wave breaking event at around node 530. However, the wave is still on the top of the bar and the water depth is very shallow so that the wave starts to increase in height again. Then at node 545 the wave once again becomes fully increased in height so that wave breaking begins again.

The problem is that the momentum sink relation of the RTFN model in the numerical model is too large. Since the RTFN theory only gives the condition of wave breaking, there is no effective theory to locate where the extra momentum term should be added in between the wave crest and the wave trough. Therefore, the eddy viscosity term is added at all the calculation nodes between the wave crest and the wave trough to turn on the wave breaking. This gives a difference in results for the two triggers. Because the FUNWAVE trigger determines the wave breaking condition node-by-node basis so that the distribution of the extra momentum term between the crest and the trough is different in the two models.

Therefore, an adjustment to the magnitude of the momentum sink during the wave breaking is taking place. Since there is no effective theory to identify which calculation node to be turned on, the adjustment of a mixing length coefficient in the momentum sink calculation is investigated. A preliminary test is performed qualitatively. Four different multiplication coefficients are chosen,  $\times 0.5$ ,  $\times 0.6$ ,  $\times 0.7$ , and  $\times 0.8$ . And, the model is executed on a plane slope bottom. Then the wave profile evolution after the wave breaking is compared to the FUNWAVE trigger case. The case with multiplication coefficient 0.7 gives similar wave profile evolution to the FUNWAVE case after the wave breaking so that chosen 0.7 for the test.

The test domain is a bar-trough profile with wide bar top. The width of the bar top is enough wide to cease the wave breaking within the bar top section (from node 530 to

590). For the case of the FUNWAVE trigger, the wave breaking starts around node 525 for the wave trough position and node 515 for the crest position, then it ceases at around node 585 for the trough position and node 575 for the crest position. Note that the bar top elevation has to be carefully chosen not to trap the reflected wave between the bar and the shoreline. The irregular shape of the wave profile leads to a miscalculation of the Ursell number, and that makes switching of calculation method misbehave and causes an illegal operation of wave breaking.

Wave profile evolutions for the RTFN trigger cases are plotted in Fig. 6.20. The wave decay is reduced by introducing the multiplication factor. However, the duration of the wave breaking event does not change so much from the original case with the reduced momentum sink. The RTFN evolution plotted in Fig. (6.21) reveals that the reduced momentum sink term helps to push up the RTFN slightly, especially in the later half on the bar top, but it is not enough to exceed the CTFN.

As a result, it is impossible to improve the duration problem by changing a mixing length coefficient, therefore, we have to establish our own system for identifying which calculation node has to include the extra momentum terms for wave breaking and which ones are not included between the wave crest and the wave trough. The turbulent mixing coefficient,  $\beta$ , may have an important role for the duration problem because wave breaking introduces intensive turbulence into the water column so that the velocity distribution is changed before and after wave breaking. However, establishing a new system requires more wave tank experiments and theoretical work. Therefore, this problem is left for future investigations.

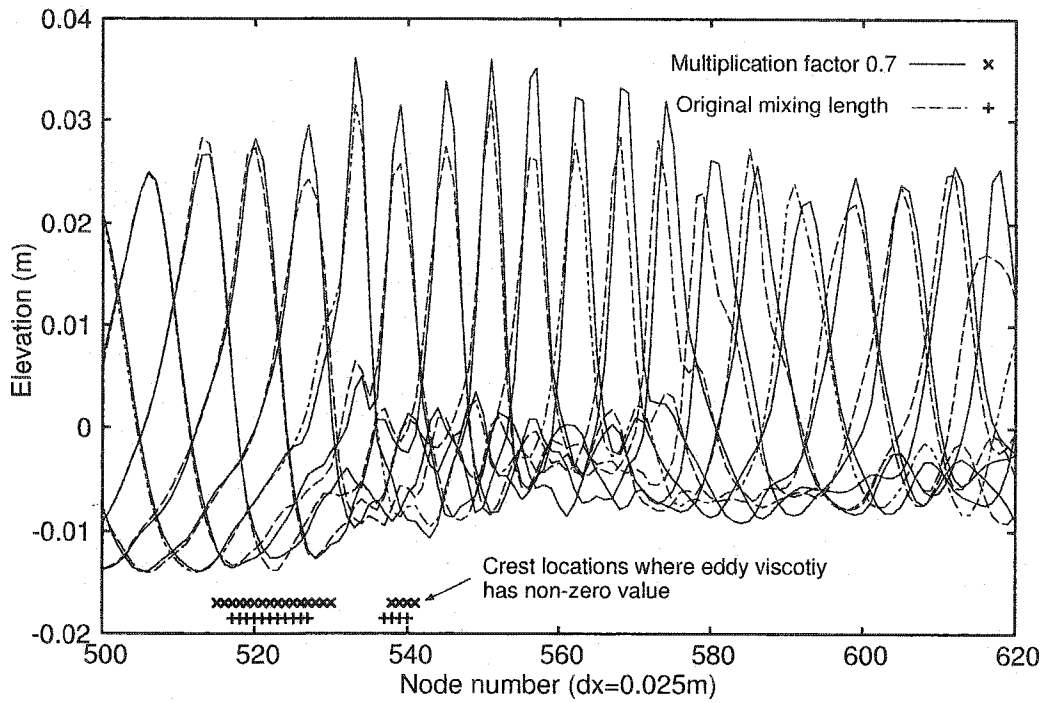


Figure 6.20: Wave profile evolution over a wide bar (RTFN)

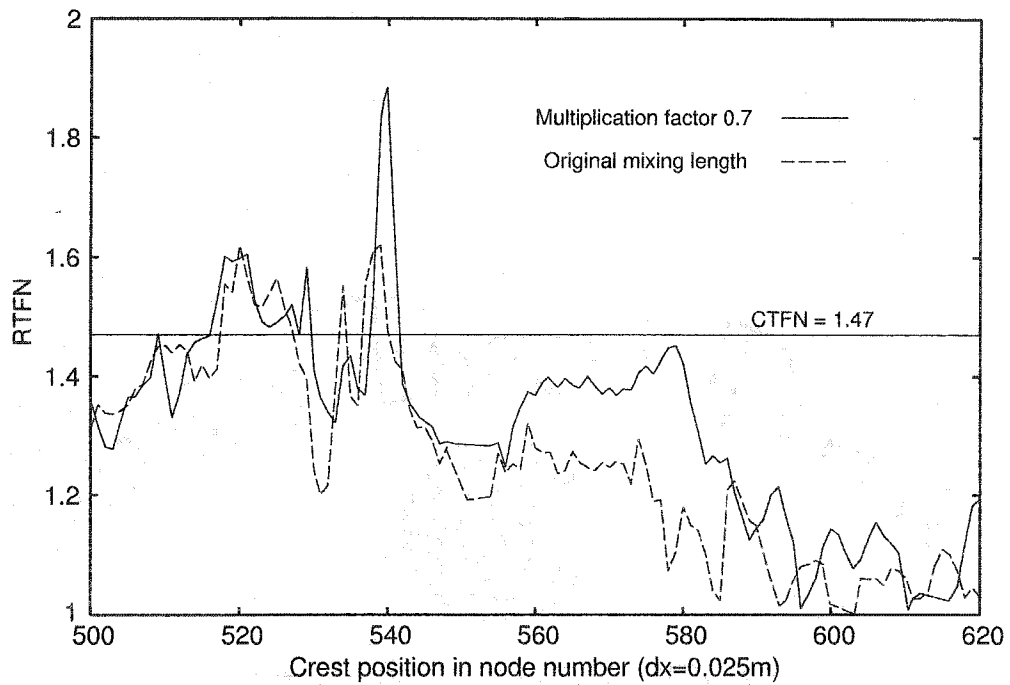


Figure 6.21: RTFN evolution over a wide bar

## CHAPTER VII

### CONCLUSIONS AND RECOMMENDATIONS

#### 7.1 Overview

Establishing an accurate wave breaking trigger mechanism has been one of the most fundamental problems in coastal engineering for more than one hundred years. A large research effort continues today. Development of computer resources and techniques requires new types of wave breaking trigger models for phase-resolving models.

The relative trough Froude number (RTFN) theory is the most recent wave breaking trigger mechanism introduced by Utku (1999). This model is approached from a completely different direction from the other wave breaking trigger models. Based upon a moving hydraulic jump, this model has theoretical basis when compared to the other, phase-resolving type, wave breaking trigger models. Satisfying the properly posed boundary conditions explicitly, the RTFN trigger model gives an appropriate solution for phase-resolving type numerical models.

This study is devoted to implementing a numerical wave breaking trigger mechanism based on the RTFN theory and confirming its functionality. A series of numerical experiments determine what is missing in the present formulation and will reinforce the RTFN theory when appropriate physical data is obtained. Also, this research reveals the analytical solution of the critical condition in the RTFN theory.

#### 7.2 Summary for the Entire Work

This study contains basically two parts: theory and numerical model. A wave tank experiment is also performed to obtain calibration data.

Firstly, existing wave breaking trigger models are reviewed and classified. The phase-averaged type is the classical form of the wave breaking trigger model, and phase-resolving

type is the newer kind and is required for the phase-resolving type numerical models. There are two types of phase-resolving type wave breaking triggers (Schäffer et al., 1993; Kirby et al., 1998). Both triggers are controlled by the free surface kinematics: the slope angle variation, or the vertical acceleration of the free surface. Both employ three control parameters for determination of the critical conditions, which are the initiation condition, the termination condition, and the duration time. The RTFN wave breaking trigger has a completely different structure. The RTFN is a dynamical parameter and stems from the theoretical background of the moving hydraulic jump, the RTFN trigger model requires one critical condition (CTFN). Based on the moving hydraulic jump also permits clarification as a properly-posed boundary value problem. This gives a theoretical advantage to the RTFN model.

The theoretical analysis focuses on the analytical formula, not a conceptual model, and the theoretical critical condition of the RTFN theory. For this purpose, the definition equation of the RTFN model is redefined by going back to the most fundamental definition of the Froude number calculation. Combining the RTFN equation and the appropriate wave theory provides the analytical form of the RTFN model. Importing a kinematic wave breaking condition given by Miche (1944) in the analytical equation gives the theoretical critical condition of the RTFN trigger model. Linear wave theory and two non-linear wave theories, Stokes second order wave theory for deeper water wave and solitary wave theory for shallow water wave, are tested in this manner. All three wave theories provide a similar number for the critical condition, namely 1.45.

The RTFN theory is used to explain the discrepancy between the shallow water wave breaking index derived from Miche (1944) and widely used  $H/d = 0.78$ . The wave breaking index is derived from the RTFN theory on a sloped bottom and it reveals that a constant

CTFN provides reasonable explanation for the discrepancy between two existing wave breaking indexes even though it is very limited in theory.

A wave tank experiment is conducted to obtain data for the calibration of the RTFN trigger in a numerical model. A total of 27 cases are executed and the initiation locations of the wave breaking, which is defined as a horizontal distance from the toe of the beach slope and the wave crest location at the initiation moment, are determined with the assistance of digital video recording. Also, the wave gauge record taken at the toe of the slope provides the input wave condition for the numerical model.

The calculation procedure of the RTFN in the numerical model is explained and the wave celerity calculation methods are intensively researched because 90% of the RTFN calculation is due to the contribution of the celerity (Utku and Basco, 2002). Four alternatives are tested. It turns out that, among them, only the least square estimation method can satisfy both the applicability and the robustness at same time. However, a relatively flat free-surface shape through the wave trough in shallow water region makes the least square estimation inaccurate. Therefore, a hybrid method is employed for the trough celerity calculation. The analytical formula takes over for shallow water wave calculation and the two methods are defined by the Ursell number. This method realizes high applicability and robustness at the same time and also includes the non-linear effect caused by wave transformation and breaking, but it requires extensive computing power.

Numerical experiments are then performed in this research. They can be classified into three stages; confirmation, calibration, and verification. Qualitative studies are performed for the confirmation of the model functionality. A series of experiments confirm that the RTFN evolution over the domain satisfies the condition required to be a wave breaking trigger, i.e. the RTFN should be greater than the CTFN for breaking waves and

smaller than the CTFN for non-breaking waves. Qualitative studies also reveal that the RTFN trigger with  $CTFN=1.36$ , which was determined by Utku (1999) from wave tank experiments, seems to initiate a wave breaking event earlier than it should.

Calibration of the CTFN is executed with a data set obtained from the wave tank experiment mentioned above. It turns out that the  $CTFN=1.36$  is too low for numerical model. Calibration of the model gives 1.68 for the critical condition. Even though the wave breaking location given by  $CTFN=1.68$  agrees well with the physical data, it is too high to be consistent with the theoretical CTFN. Therefore, the RTFN calculation is reformatted to achieve two conditions: agreement with the physical data and consistency to the theoretical value, to be satisfied at the same time.

Excluding the surface displacement term from the analytical equation, the CTFN is reduced through the calibration process to 1.47, which is very close to the theoretical value, without losing the agreement with the physical data. However, it has a theoretical weakness by introducing the linear wave theory into the formulation. Also, to continue using the analytical formula for the RTFN calculation does not solve the applicability problem so that the least square estimation method for the RTFN calculation is introduced. The  $CTFN=1.47$  gives excellent agreement with the physical data also for this case.

Finally, numerical experiments with different bathymetry are examined under the calibrated CTFN for verification of the model. Firstly, the bottom slope effect against the wave breaking location is tested by running the model on plane slope beaches with different beach slope angles. Results show a different trend between the RTFN trigger and the original FUNWAVE trigger. Neither of them agree with the breaking index curve given by Goda (1970).

The second test for the verification is concerned with duration of wave breaking. Numerical experiments on a bar-trough shaped beach reveals that the RTFN trigger and the original FUNWAVE trigger initiate the wave breaking about same location, but the RTFN trigger terminates the wave breaking earlier than the FUNWAVE trigger. When comparing the wave profile evolution over the bar, it is revealed that the RTFN trigger extracts too much momentum during the wave breaking event. Therefore, the mixing length coefficient in the extra momentum term due to the wave breaking is adjusted. Results on plane slope beach shows fair agreement in wave profile evolution to the case with the original FUNWAVE trigger case, but it does not improve the duration over a bar-trough profile.

### 7.3 Conclusions and Recommendations

A theoretical study for this research reformats the theoretical framework of the RTFN theory and provides the analytical forms of the RTFN by combining both linear and nonlinear wave theories. Importing the kinematic wave breaking condition given by Miche (1944) provides the theoretical critical condition of the RTFN theory. All the theoretical cases agree with 1.45 as a theoretical CTFN and, from the applicable area of the wave theory, we conclude  $CTFN=1.45$  is a universal constant under these conditions: (1) Miche formula is valid as as wave breaking criteria, and (2) the velocity is taken at the free surface.

The RTFN wave breaking trigger model is implemented in a phase-resolving type, Boussinesq equation based numerical model called FUNWAVE. Qualitative study of the numerical experiment confirms the evolution of the RTFN along with wave transformation satisfies the requirement to be a wave breaking trigger. The calibration of the model provides  $CTFN=1.47$  for the numerical model. This shows good agreement with the

theoretical value. But bottom slope effects against the wave breaking location and the duration of the wave breaking are unsolved problems in this research because of the lack of supported physical data.

The slope effect and the duration of the wave breaking need physical experimental data to confirm the physics of these problems. A momentum sink distribution mechanism also has to be established for numerical modeling. Therefore, future recommendations are:

1. conduct wave tank experiments with various bed slopes to verify the bottom slope effect against the RTFN theory;
2. conduct wave tank experiments with a bar-trough shaped beach to confirm the termination condition of the RTFN theory;
3. formulate the theory to locate where the extra momentum term due to the wave breaking should occur between the wave crest and the trough; and
4. implement the RTFN wave breaking trigger mechanism into both a one-dimensional and a two-dimensional, horizontal, numerical models.

## REFERENCES

- Abbott, M.B., 1966, *An Introduction to the Method of Characteristics*, American Elsevier, New York
- Abbott, M.B. and D.R. Basco, 1989, *Computational Fluid Dynamics: An Introduction for Engineers*, Longman, England
- Basco, D.R. and T. Okamoto, 2002, "A New Wave Breaking Trigger Criteria for Phase-Resolving Numerical Models", *Proceedings of 28<sup>th</sup> ICCE (Wales)*, ASCE, New York, 319–331
- Basco, D.R. and I.A. Svendsen, 1984, "Modeling Turbulent Bore Propagation in the Surf-zone", *Proceedings of 19<sup>th</sup> ICCE (Houston)*, ASCE, New York, 99–114
- Battjes, J.A., 1974, "Surf Similarity", *Proceedings of 14<sup>th</sup> ICCE (Copenhagen)* ASCE, New York, 466–479
- Boussinesq, J.V., 1872, "Theory of Waves and Surges which Propagate the Length of a Horizontal Rectangular Canal, Imparting to the Fluid Contained Within the Canal Velocities that are Sensibly the Same from Top to Bottom", *Jour. Math. Pures Appliquees, Series 2, Vol. 17*, 55–108
- Chanson, H. and J.S. Montes, 1995, "Characteristics of Undular Hydraulic Jumps: Experimental Apparatus and Flow Patterns", *Journal of Hydraulic Engineering, ASCE, Vol 121, no 2*, 129–144
- Chen, Q., P.A. Madsen, O.R. Sørensen, and D.R. Basco, 1996, "Boussinesq equations with improved doppler shift and dispersion for wave/current interaction", *Proceedings of 25<sup>th</sup> ICCE (Orlando)*, ASCE, New York, 1060–1073
- Chen, Q., R.A. Dalrymple, J.T. Kirby, A.B. Kennedy, and M.C. Haller, 1999, "Boussinesq Modeling of Rip Current System", *Journal of Geophysical Research, Vol. 104, No. C9*, 20,617–20,637
- Chen, Q., J.T. Kirby, R.A. Dalrymple, A.B. Kennedy, and A. Chawla, 2000a, "Boussinesq Modeling of Wave Transformation, Breaking, and Run-Up. II: 2D", *Journal of Waterway, Port, Coastal, and Ocean Engineering, Vol. 126, No. 1, January/February*, 48–56 No. C9, 20,617–20,637
- Chen, Q., J.T. Kirby, R.A. Dalrymple, A.B. Kennedy, E.B. Thornton, and F. Shi, 2000b, "Boussinesq modeling of waves and longshore currents under field conditions", *Proceedings of 27<sup>th</sup> ICCE, (Sydney)*, ASCE, New York
- Dean, R.G., and R.A. Dalrymple, 1984, *Water Wave Mechanics for Engineers and Scientists*, World Scientific, Singapore
- Goda, Y., 1970, "A Synthesis of Breaking Indices", *Transactions of JSCE, Vol.2, Part 2*, 39–49, 1970 (in Japanese)

- Kaminsky, G. and N.C. Kraus, 1993, "Evaluation of Depth-Limited Wave Breaking Criteria", *Waves '93*, ASCE, 180-193
- Kennedy, A.B., Q. Chen, J.T. Kirby, and R.A. Dalrymple, 2000, "Boussinesq Modeling of Wave Transformation, Breaking and Runup I: 1D", *Journal of Waterway, Port, Coastal and Ocean Engineering*, ASCE, Vol. 126, No. 1, January/February, 39-47
- Kirby, J.T., G. Wei, Q. Chen, A.B. Kennedy, and R.A. Dalrymple, 1998, "FUNWAVE 1.0 Fully Nonlinear Boussinesq Wave Model Documentation and User's Manual", Research Report No. CACR-98-06, Center for applied coastal research, University of Delaware, Newark, Delaware
- Komar, P.D., 1998, *Beach Processes and Sedimentation: Second Edition*, Prentice Hall, New Jersey
- LeMéhauté, B. and R.C.Y. Koh, 1967, "On the Breaking of Waves Arriving at an Angle to the Shore", *Journal of Hydraulic Research* 5, 541-549
- Madsen, P.A., R. Murray, and O.R. Sørensen, 1991, "A New Form of the Boussinesq Equations with Improved Linear Dispersion Characteristics", *Coastal Engineering*, 15, 371-388
- Madsen, P.A., and O.R. Sørensen, 1992, "A New Form of the Boussinesq Equations with Improved Linear Dispersion Characteristics. Part 2. A Slowly-Varying Bathymetry", *Coastal Engineering*, 18, 183-204
- Madsen, P.A., B. Banijamali, H.A. Schäffer, and O.R. Sørensen, "Boussinesq Type Equations with High Accuracy in Dispersion and Non-Linearity", 1996, *Proceedings of ICCE (Orlando)*, ASCE, New York, 95-108
- Madsen, P.A., H.A. Schäffer, and O.R. Sørensen, 1997a, "Surf Zone Dynamics Simulated by a Boussinesq Type Model. Part II: Model Description and Cross-Shore Motion of Regular Waves", *Coastal Engineering*, 32, 255-288  
"Swash Oscillations for Wave Groups and Irregular Waves", *Coastal Engineering*, 32, 289-319
- Madsen, P.A., O.R. Sørensen, and H.A. Schäffer, 1997b, "Surf Zone Dynamics Simulated by a Boussinesq Type Model. Part II: Surf Beat and Swash Oscillations for Wave Groups and Irregular Waves", *Coastal Engineering*, 32, 289-319
- Madsen, P.A. and H.A. Schäffer, 1998, "Higher-Order Boussinesq-type Equation for Surface Gravity Waves - Derivation and Analysis". *Phil. Trans. Royal Soc., London*, 356, 1-59
- Madsen, P.A. and H.A. Schäffer, 1999, "A Review of Boussinesq-type Equations for Gravity Waves", in *Advances in Coastal and Ocean Engineering*, edited by P.L.-F. Liu, World Scientific, River Edge, NJ
- McCowan, J., 1894, "On the Highest Wave of Permanent Type", *Philosophical Magazine, Journal of Science*, Vol.38

- Miche, R., 1944, "Movements Ondulatoires des Mers en Profondeur Constante ou Decroissante", *Annales des Ponts et Chaussees*, May-June, July-August, 25-78, 131-164, 270-292, 369-406
- Misra, S.K., A.B. Kennedy, and J.T. Kirby, 2002, "An Approach to Determining Nearshore Bathymetry Using Remotely Sensed Ocean Surface Dynamics", *Coastal Engineering* (in press)
- Mitchell, J.H., 1893, "On the Highest Waves in Water", *Philosophical Magazine*, Series 5, 36: 430-437
- Munk, W.H., 1949, "The Solitary Wave Theory and Its Application to Surf Problems", *Annale of the New York Academy of Science*, 51, 376-462
- Nwogu, O., 1993, "Alternative Form of Boussinesq Equation for Nearshore Wave Propagation", *Journal of Waterway, Port, Coastal, and Ocean Engineering*, Vol. 119, No. 6, November/December, 618-638
- Ohtsu, I., Y. Yasuda, and H. Gotoh, 2001, "Hydraulic Condition for Undular-Jump Formation", *Journal of Hydraulic Research*, vol 39, no 2
- Peregrin, D.H., and I.A. Svendsen, 1978, "Spilling breaker, bores and hydraulic jumps", *Proceedings of 16<sup>th</sup> ICCE (Hamburg)*, ASCE, New York, 540-550
- Press, W.H., S.A. Teukolsky, W.T. Vetterling, B.P. Flannery, 1992, *Numerical Recipes in Fortran 77: The Art of Scientific Computing (Vol. 1 of Fortran Numerical Recipes) Second Edition*, Cambridge University Press, Cambridge, UK
- Reinbauer, R.R. and W.H. Hager, 1995, "Non-breaking Undular Hydraulic Jump", *Journal of Hydraulic Research*, 33, 683-704
- Schäffer, H.A., P.A. Madsen, and R.A. Deigaard, 1993, "A Boussinesq Model for Wave Breaking in Shallow Water", *Coastal Engineering*, 20, 185-202
- Sørensen, O.R., P.A. Madsen, and H.A. Schäffer, 1998, "Nearshore Wave Dynamics Simulated by Boussinesq Type Models", *Proceedings of 26<sup>th</sup> ICCE, (Copenhagen)*, ASCE, New York, 272-285
- Sørensen, O.R., H.A. Schäffer, and P.A. Madsen, 1998, "Surf Zone Dynamics Simulated by a Boussinesq Type Model. III. Wave-induced Horizontal Nearshore Circulations", *Coastal Engineering*, 33, 155-176
- Stokes, G.G., 1880, "On the Theory of Oscillation Waves", In *Mathematical and Physical Papers*, Vol.1, 314-326, London, England: Cambridge University Press
- Svendsen, I.A., K. Yu, and J. Veeramony, 1996, "A Boussinesq Breaking Wave Model with Vorticity", *Proceedings of 25<sup>th</sup> ICCE, (Orlando)* ASCE, New York, 1192-1204
- U.S. Army Corps of Engineers, 1984, *Shore Protection Manual*, U.S. Army Corps of Engineers, Washington D.C., (in 2 volume)

- U.S. Army Corps of Engineers, 2002, Coastal Engineering Manual, Engineer Manual 1110-2-1100, U.S. Army Corps of Engineers, Washington D.C. (in 6 volume)
- Utku, M., 1999, "The Relative Trough Froude Number: A New Wave Breaking Criteria", unpublished Ph.D. dissertation, Civil Engineering Dept., Old Dominion University, Norfolk, Virginia
- Utku, M. and D.R. Basco, 2002, "A New Criteria for Wave Breaking Based on the Relative Trough Froude Number", Proceedings of 28<sup>th</sup> ICCE, (Wales), ASCE, New York, 258-268
- Weggel, J.R., 1972, "Maximum Breaker Height", Journal of the Waterways, Harbors, and Coastal Engineering Division, ASCE, 98, 529-548
- Wei, G., J.T. Kirby, S.T. Grilli, and R. Subramanya, 1995a, "A Fully Nonlinear Boussinesq Model for Surface Waves. Part 1. Highly Non-Linear Unsteady Waves", Journal of Fluid Mechanics, Vol. 294, 71-92
- Wei, G., and J.T. Kirby, 1995b, "Time-Dependent Numerical Code for Extended Boussinesq Equations", Journal of Waterway, Port, Coastal, and Ocean Engineering, ASCE, vol. 121, no. 5, September/October, 251-261
- Wei, G., J.T. Kirby, and A. Sinha, 1999, "Generation of Waves in Boussinesq Models Using Source Function Method", Coastal Engineering, 36, 271-299
- Zelt, J.A., 1990, "The Run-Up of Nonbreaking and Breaking Solitary Waves", Coastal Engineering, 15, 205-246

## APPENDIX A : SOURCE CODE (SUBROUTINES ADDED)

```

C* :20 *****
C      Subroutine for calculating momentum terms including
C      additional momentum term due to the wave breaking
C
      subroutine eval_f
C* 30: *****
C
*line 1990 "funwave1d.web"

      include 'param.h'
      implicit real(a-h,o-z)
      implicit integer(i-n)
      common/input1/ibe,imch,ianm,a0,h0,tpd,dx,dt,mx,nt,itbgn,itend,itde
&l,itscr,itftr,cbkv,ck_bt,delta,slmda,isltb,islte
      common/input2/isrc,swidth,cspg,cspg2,cspg3,isp(2),ngage,ixg(20),i
&t(6)
      common/input3/f1n,f2n,f3n,f4n,f5n,f6n,f7n
      common/input4/itide,tideco(3)
      common/const1/rdx,rdt,rx2,a1,a2,b1,b2,ga,pi,alpha,alpha1,clnr
      common/const2/m1,m2,m3,m4,idpc,it,ite,iwd,t,twrp,cph,omg
      common/const3/et_xc,cbreak,dmin,cbt,etem,uem,beta
      common/const4/p(7),q(7),ta(7),cb(4),td3(8),td4(8)
      common/const5/cf1(5),cf2(5),cf3(5),cf4(5)
      common/array1/etn(iq),un(iq),ete(iq),ue(iq),eto(iq),uo(iq)
      common/array2/et(4,iq),u(4,iq),e(4,iq),f(4,iq),f2(iq),e2(iq)
      common/array3/hu(iq),he(iq),p_x(iq),hpx(iq),heu_x(iq),epx(iq)
      common/array4/h(iq),za(iq),eta_x(iq),u_x(iq),u_xx(iq)
      common/array5/ft(4,iq),fgt(iq),fg(iq),u_t(4,iq)
      common/breaks/edvis(iq),fb(iq),fbt(iq),w1(iq),w2(iq),w3(iq)
      common/ludecs/a(2,iq),b(2,iq),c(2,iq),d(2,iq),adx(iq),bdx(iq)
      common/etaout1/ettg(6,iq),etxg(20,nq),s(nq)
      common/etastorage/ets1(iq),ets2(iq),ets3(iq),ets4(iq)
      common/celerity/celerityc,celerityt

      common/plotvar/xoff,hoff,eoff,fboff,amfh,amfx,amfet,amffb,etnum(12
&,iq),hreff

      common/runup/hs(iq),hcr(iq),fcbt(iq),corb(iq),ih0,nspg,irp,dlamda,
&dlt,cospg(iq),z0,idslot,pxtmp(iq)

```

```

common/brkn/et1,et2,cbrk,coeft,ddx,itbrk,itb(iq),ctb(iq)
character fin*30,f2n*30,f3n*30,f4n*30,f5n*30,f6n*30,f7n*30
C* :30 *
*line 1384 "funwave1d.web"

call preeval

eta_x(1)=(p(1)*etn(1)+p(2)*etn(2)+p(3)*etn(3)+p(4)*etn(4)+p(5)*etn
& (5))*rdx
eta_x(2)=(q(1)*etn(1)+q(2)*etn(2)+q(3)*etn(3)+q(4)*etn(4)+q(5)*etn
& (5))*rdx
eta_x(mx)=- (p(1)*etn(mx)+p(2)*etn(m1)+p(3)*etn(m2)+p(4)*etn(m3)+p(
& 5)*etn(m4))*rdx
eta_x(m1)=- (q(1)*etn(mx)+q(2)*etn(m1)+q(3)*etn(m2)+q(4)*etn(m3)+q(
& 5)*etn(m4))*rdx
do i=3,m2
eta_x(i)=(p(6)*(etn(i+1)-etn(i-1))-p(7)*(etn(i+2)-etn(i-2)))*rdx
enddo

u_x(1)=(p(1)*un(1)+p(2)*un(2)+p(3)*un(3)+p(4)*un(4)+p(5)*un(5))*rd
& x
u_x(2)=(q(1)*un(1)+q(2)*un(2)+q(3)*un(3)+q(4)*un(4)+q(5)*un(5))*rd
& x
u_x(mx)=- (p(1)*un(mx)+p(2)*un(m1)+p(3)*un(m2)+p(4)*un(m3)+p(5)*un(
& m4))*rdx
u_x(m1)=- (q(1)*un(mx)+q(2)*un(m1)+q(3)*un(m2)+q(4)*un(m3)+q(5)*un(
& m4))*rdx
do i=3,m2
u_x(i)=(p(6)*(un(i+1)-un(i-1))-p(7)*(un(i+2)-un(i-2)))*rdx
enddo

do i=2,m1
f(1,i)=-ga*eta_x(i)-un(i)*u_x(i)*clnr-w1(i)*un(i)+w2(i)*
& (u_xx(i))
enddo

c
c-----
c Select Breaking Trigger Type
c-----

open(548,file='breaking_trigger_type')
read(548,*) ibreaktrigger

```

```

close(548)
c
if(ibreaktrigger.eq.0) then
c-----
c   Original Breaking Mechanism
c-----
  izelt=0
  if(izelt.EQ.1)then
    itbrk=0
    do i=1,mx
      dp=max(ddx,h(i))
      et_tc=et_xc*sqrt(ga*dp)
      tmp=e(1,i)
      if(tmp.le.et_tc)then
        cbr=0.0
      elseif(tmp.le.2.0*et_tc)then
        cbr=tmp/et_tc-1.0
        itbrk=1
      else
        cbr=1.0
        itbrk=1
      endif
      edvis(i)=cbr*(cbreak**2*dp)*e(1,i)
    enddo
  else
    itbrk=0
    if(ite.EQ.1.OR.it.EQ.1)then
      do i=2,m1
        iage=min(itb(i+1),itb(i-1))
        iage=min(iage,itb(i))
        if(itb(i).LT.nt)then
          dp=max(ddx,h(i))
          trnt=coeft*sqrt(dp/ga)
          et_tc=et1-(et1-et2)*float(it-iage)*dt/trnt
          ctb(i)=max(et_tc,et2)
        else
          ctb(i)=et1
        endif
      enddo
    endif
    do i=2,m1
      dp=max(ddx,h(i))

```

```

    et_tc=ctb(i)*sqrt(ga*dp)
    tmp=e(1,i)
    if(tmp.LE.et_tc)then
        cbr=0.0
        itb(i)=nt
    else
        cbr=min(1.0,(tmp/et_tc-1.0))
        itbrk=1
        itb(i)=min(itb(i),it)
    endif
    edvis(i)=cbr*cbrk**2*dp*abs(e(1,i))
enddo
endif
else
c-----
c   Wave Breaking Based on Relative Trough Froude Number
c-----

    frcritical=1.47
    itbrk=0
    ipre=mx
    jpre=mx

c
    do iedd=4,m1-3
        edvis(iedd)=0.0
    enddo

c
c---- Calculate/Check critical condition of RTFN for first wave -----
c
    do i=m1-3,1,-1
        etalocalmin=min(etn(i-3),etn(i-2),etn(i-1),etn(i),etn(i+1),
&          etn(i+2),etn(i+3),etn(i-4),etn(i+4),etn(i-5),etn(i+5),
&          etn(i-6),etn(i-7),etn(i-8),etn(i-10),etn(i-12),
&          )
    if (etalocalmin.eq.0.0) goto 757
        if (etn(i).eq.etalocalmin.or.
&          (ipre.eq.mx.and.etn(i).lt.etn(i-5))) then
            do j=i,1,-1
                etalocalmax=max(etn(j-3),etn(j-2),etn(j-1),etn(j)
&          ,etn(j+1),etn(j+2),etn(j+3)
&          ,etn(j-4),etn(j-5),etn(j-6),etn(j-7)
&          ,etn(j-8),etn(j-10),etn(j-12)
&          )

```

```

if(etn(j).eq.etalocalmax) then
  ursell=(etn(j)-etn(i))*((jpre-j)*dx)**2/
    &      (max(h(i),ddx)**3)
  if(abs(etn(i)).lt.1.0e-6) then
    dp=max(ddx,h(j))
    celerityt=sqrt(ga*dp)
    wsize=(ipre-i)*dx
  elseif(ursell.gt.60.) then
    dp=max(ddx,(h(i)+etn(i)))
    celerityt=sqrt(ga*dp)
  else
    wsize=(ipre-i)*dx
    call celeritycalc(i,celerityt,wsize)
    if(ursell.gt.30.) then
      omega1=((ursell-30.)/30.)*0.5
      dp=max(ddx,(h(i)+etn(i)))
      celerityt=(1.-omega1)*celerityt+
        &      omega1*sqrt(ga*dp)
    endif
  endif
endif

c
wsizec=(jpre-j)*dx
call celeritycalc(j,celerityc,wsizec)
ipre=i
jpre=j
jpre1=j

c
if (celerityt.eq.0.0) then
  dp=max(ddx,h(i))
  celerityt=sqrt(ga*dp)
endif
froude=(celerityc-un(i))/celerityt
if(it.ge.itg(1).and.it.le.itg(6)) then
  write(*,*) it,i,celerityt,j,celerityc,un(i),froude
endif
if(froude.gt.frcritical) then
  iupper=int((i-j)/3)
  cbr=1.0
  itbrk=1
  do k=j,i
    dp=max(ddx,h(k))
    edvis(k)=cbr*cbrk**2*dp*abs(e(1,k))
  enddo
endif

```

```

        enddo
        endif
        i=j
        goto 758
    else
        etalocalminc=min(etn(j-1),etn(j-2),etn(j-3),
&         etn(j-4),etn(j-5),etn(j-6),etn(j-7))
        if(etalocalminc.lt.etn(i)) goto 757
    endif
    enddo
756    continue
    endif
757    continue
    enddo
758    continue
c
c---- Calculate/Check critical condition of RTFN for rest of the waves ---
c
    do j=jpre1,isrc+1,-1
        etalocalmin=100000.
        etalocalmax=max(etn(j-3),etn(j-2),etn(j-1),etn(j)
&         ,etn(j+1),etn(j+2),etn(j+3),etn(j+4),etn(j+5)
&         ,etn(j-4),etn(j-5),etn(j-6),etn(j-7),etn(j-8),etn(j-10)
&         ,etn(j+6),etn(j+7),etn(j+8),etn(j+9),etn(j+10)
&         )
c
        if(etn(j).eq.etalocalmax) then
c
            if(etn(j).lt.0.0) goto 759

            do itrough=j,jpre
                if(etn(itrough).lt.etalocalmin) then
                    etalocalmin=etn(itrough)
                    i=itrough
                endif
            enddo

            if(i.eq.j) goto 759

c
            ursell=(etn(j)-etn(i))*((jpre-j)*dx)**2/
&             (max(h(i),ddx)**3)
c

```

```

if(abs(etn(i)).lt.1.0e-6) then
  dp=max(ddx,h(j))
  celerityt=sqrt(ga*dp)
  wsize=(ipre-i)*dx
elseif(ursell.gt.60.) then
  dp=max(ddx,(h(i)+etn(i)))
  celerityt=sqrt(ga*dp)
else
  wsize=(ipre-i)*dx
  call celeritycalc(i,celerityt,wsize)
  if(ursell.gt.30.) then
    omega1=((ursell-30.)/30.)**0.5
    dp=max(ddx,(h(i)+etn(i)))
    celerityt=(1.-omega1)*celerityt+omega1*sqrt(ga*dp)
  endif
endif
c
wsizec=(jpre-j)*dx
call celeritycalc(j,celerityc,wsizec)
cc
ipre=i
jpre=j
c
if (celerityt.eq.0.0) then
  dp=max(ddx,h(i))
  celerityt=sqrt(ga*dp)
endif
c
froude=(celerityc-un(i))/celerityt
if(it.ge.itg(1).and.it.le.itg(6)) then
  write(*,*) it,i,celerityt,j,celerityc,un(i),froude
endif
if(froude.gt.frccritical) then
  cbr=1.0
  itbrk=1
  do k=j,i
    dp=max(ddx,h(k))
    edvis(k)=cbr*(cbrk*0.7)**2*dp*abs(e(1,k))
  enddo
endif
endif
759 continue

```

```

        enddo
c
        iprev=it
c
        endif
c-----
        call fltr(edvis)

do i=2,m1
    fb(i)=+rdx*(edvis(i+1)*heu_x(i+1)-edvis(i-1)*heu_x(i-1))
    dp=etn(i)+h0
    if(dp.LT.1.0e-3)then
        print*,'Negative total-water-depth at i= ',i
        print*,'eta=',etn(i),'cbr= ',cbr,'it=',it
        ite=31
        call printing
        stop
    endif
enddo

do i=2,m1
    tdp=max(0.001,he(i))
    f(1,i)=f(1,i)+fb(i)/tdp
enddo

if(idslot.NE.1)then
    do i=1,mx
        dp=max(hs(i)+etn(i),dmin)
        f(1,i)=f(1,i)-ga*abs(un(i))*un(i)/dp*fcbt(i)
    enddo
else
    delta2=delta/2.0
    do i=1,mx
        dp=max(delta2,he(i)+delta2)
        f(1,i)=f(1,i)-ga*fcbt(i)*abs(un(i))*un(i)/dp
    enddo
endif

if(ibe.EQ.2)then
    call eval_f2
    do i=1,mx
        f(1,i)=f(1,i)+f2(i)
    enddo
endif

```

```
    enddo
    call eval_ut
endif
return
end
```

```
C* :21 *****
```

```

C* :29 *****
c
c   Subroutine for calculating wave celerity by the least square
c     estimation method
c
c     subroutine celeritycalc(i,celerity,wsize)
C*****
  include 'param.h'
  implicit real(a-h,o-z)
  implicit integer(i-n)
  common/input1/ibe,imch,ianm,a0,h0,tpd,dx,dt,mx,nt,itbgn,itend,itde
&l,itscr,itftr,cbkv,ck_bt,delta,slmda,isltb,islte
  common/input2/isrc,swidth,cspg,cspg2,cspg3,isp(2),ngage,ixg(20),i
&tg(6)
  common/input3/f1n,f2n,f3n,f4n,f5n,f6n,f7n
  common/input4/itide,tideco(3)
  common/const1/rdx,rdt,rx2,a1,a2,b1,b2,ga,pi,alpha,alpha1,clnr
  common/const2/m1,m2,m3,m4,idpc,it,ite,iwd,t,twrp,cph,omg
  common/const3/et_xc,cbreak,dmin,cbt,etem,uem,beta
  common/const4/p(7),q(7),ta(7),cb(4),td3(8),td4(8)
  common/const5/cf1(5),cf2(5),cf3(5),cf4(5)
  common/array1/etn(iq),un(iq),ete(iq),ue(iq),eto(iq),uo(iq)
  common/array2/et(4,iq),u(4,iq),e(4,iq),f(4,iq),f2(iq),e2(iq)
  common/array3/hu(iq),he(iq),p_x(iq),hpx(iq),heu_x(iq),epx(iq)
  common/array4/h(iq),za(iq),eta_x(iq),u_x(iq),u_xx(iq)
  common/array5/ft(4,iq),fgt(iq),fg(iq),u_t(4,iq)
  common/breaks/edvis(iq),fb(iq),fbt(iq),w1(iq),w2(iq),w3(iq)
  common/ludecs/a(2,iq),b(2,iq),c(2,iq),d(2,iq),adx(iq),bdx(iq)
  common/etaout1/ettg(6,iq),etxg(20,nq),s(nq)
  common/etastorage/ets1(iq),ets2(iq),ets3(iq),ets4(iq)
  common/celerity/celerityc,celerityt

  common/plotvar/xoff,hoff,eoff,fboff,amfh,amfx,amfet,amffb,etnum(12
&,iq),hreff

  common/runup/hs(iq),hcr(iq),fcbt(iq),corb(iq),ih0,nspg,irp,dlmda,
&dltts,cospg(iq),z0,idslot,pxtmp(iq)

  common/brkn/et1,et2,cbrk,coeft,ddx,itbrk,itb(iq),ctb(iq)
  character f1n*30,f2n*30,f3n*30,f4n*30,f5n*30,f6n*30,f7n*30
c

```

```

wsize=wsize*0.5
dxc=0.001

c
cmax=sqrt(ga*(h(i)+etn(i)))*(dt*4.)
cmax=max(cmax,0.04)
epsilonmin=1000000.
do xi=0.,cmax,dxc
  ixi=int(xi/dx)
  dxc1=(wsize-xi)/400.
  iwxi=int((wsize-xi)/dx)
  gx0=etn(i+ixi)+(etn(i+ixi+1)-etn(i+ixi))*(xi-ixi*dx)/dx
&      +(etn(i+ixi+2)-2.*etn(i+ixi+1)+etn(i+ixi))
&      *(xi-ixi*dx)/dx*((xi-ixi*dx)/dx-1.)/2.
  fxn=ets4(i+iwxi)+(ets4(i+iwxi+1)-ets4(i+iwxi))
&      *((wsize-xi)-iwxi*dx)/dx
&      +(ets4(i+iwxi+2)-2.*ets4(i+iwxi+1)+ets4(i+iwxi))
&      *((wsize-xi)-iwxi*dx)/dx*((wsize-xi)-iwxi*dx)/dx-1.)/2.
  gxn=etn(i+ixi+iwxi)+(etn(i+ixi+iwxi+1)-etn(i+ixi+iwxi))
&      *((wsize-xi)-iwxi*dx+xi-ixi*dx)/dx
&      +(etn(i+ixi+iwxi+2)-2.*etn(i+ixi+iwxi+1)+
&      etn(i+ixi+iwxi))
&      *((wsize-xi)-iwxi*dx+xi-ixi*dx)/dx*
&      (((wsize-xi)-iwxi*dx+xi-ixi*dx)/dx-1.)/2.
  epsilon2=((ets4(i)-gx0)**2+(fxn-gxn)**2)/3.*dxc1

do x=dxc1,wsize-xi-dxc1,dxc1*2.
  ix=int(x/dx)
  fx1=ets4(i+ix)+(ets4(i+ix+1)-ets4(i+ix))*(x-ix*dx)/dx
&      +(ets4(i+ix+2)-2.*ets4(i+ix+1)+ets4(i+ix))
&      *(x-ix*dx)/dx*((x-ix*dx)/dx-1.)/2.
  fx2=ets4(i+ix)+(ets4(i+ix+1)-ets4(i+ix))*(x-ix*dx+dxc1)/dx
&      +(ets4(i+ix+2)-2.*ets4(i+ix+1)+ets4(i+ix))
&      *(x-ix*dx+dxc1)/dx*((x-ix*dx+dxc1)/dx-1.)/2.
  gx1=etn(i+ixi+ix)+(etn(i+ixi+ix+1)-etn(i+ixi+ix))
&      *(x-ix*dx+xi-ixi*dx)/dx
&      +(etn(i+ixi+ix+2)-2.*etn(i+ixi+ix+1)+etn(i+ixi+ix))
&      *(x-ix*dx+xi-ixi*dx)/dx*((x-ix*dx+xi-ixi*dx)/dx
&      -1.)/2.
  gx2=etn(i+ixi+ix)+(etn(i+ixi+ix+1)-etn(i+ixi+ix))
&      *(x-ix*dx+xi-ixi*dx+dxc1)/dx
&      +(etn(i+ixi+ix+2)-2.*etn(i+ixi+ix+1)+etn(i+ixi+ix))
&      *(x-ix*dx+xi-ixi*dx+dxc1)/dx*((x-ix*dx+xi-ixi*dx

```

```

&      +dxc1)/dx-1.)/2.
c
      epsilon2=epsilon2+(fx1-gx1)*(fx1-gx1)*4./3.*dxc1
&      +(fx2-gx2)*(fx2-gx2)*2./3.*dxc1
      enddo
      fx1=ets4(i+ix)+(ets4(i+ix+1)-ets4(i+ix))*(x-ix*dx)/dx
&      +(ets4(i+ix+2)-2.*ets4(i+ix+1)+ets4(i+ix))
&      *(x-ix*dx)/dx*((x-ix*dx)/dx-1.)/2.
      gx1=etn(i+ixi+ix)+(etn(i+ixi+ix+1)-etn(i+ixi+ix))
&      *(x-ix*dx+xi-ixi*dx)/dx
&      +(etn(i+ixi+ix+2)-2.*etn(i+ixi+ix+1)+etn(i+ixi+ix))
&      *(x-ix*dx+xi-ixi*dx)/dx*((x-ix*dx+xi-ixi*dx)/dx
&      -1.)/2.
      epsilon2=epsilon2+(fx1-gx1)*(fx1-gx1)*4./3.*dxc1
      epsilonmin=min(epsilonmin,epsilon2)
      if(epsilonmin.eq.epsilon2) then
        cx=xi
      endif
      epsilon2=0.0
    enddo
c
195  continue
c
      celerity=cx/(dt*4.)
c
      return
      end

```

## APPENDIX B : RESULT (SLOPE EFFECT)

Table B.1: T=0.75sec, H=0.016m (RTFN)

	Location (m)				Depth (m)				Wave Breaking Height(m)
	Initiation		Termination		Initiation		Termination		
	Crest	Trough	Crest	Trough	Crest	Trough	Crest	Trough	
1:10	3.500	3.700	cont.	cont.	0.0500	0.0300	cont.	cont.	0.0104
1:15	5.450	5.575	cont.	cont.	0.0367	0.0283	cont.	cont.	0.0132
1:20	7.350	7.475	cont.	cont.	0.0313	0.0250	cont.	cont.	0.0151
1:25	9.275	9.375	cont.	cont.	0.0290	0.0250	cont.	cont.	0.0148
1:30	11.200	11.300	cont.	cont.	0.0267	0.0233	cont.	cont.	0.0157
1:35	13.050	13.175	cont.	cont.	0.0271	0.0236	cont.	cont.	0.0170
1:40	N/A	N/A	N/A	N/A	N/A	N/A	N/A	N/A	N/A

Table B.2: T=0.75sec, H=0.016m (FUNWAVE)

	Location (m)				Depth (m)				Wave Breaking Height(m)
	Initiation		Termination		Initiation		Termination		
	Crest	Trough	Crest	Trough	Crest	Trough	Crest	Trough	
1:10	N/A	N/A	N/A	N/A	N/A	N/A	N/A	N/A	N/A
1:15	N/A	N/A	N/A	N/A	N/A	N/A	N/A	N/A	N/A
1:20	N/A	N/A	N/A	N/A	N/A	N/A	N/A	N/A	N/A
1:25	9.350	9.425	9.425	9.450	0.0260	0.0230	0.0230	0.0220	0.0158
1:30	11.250	11.350	11.425	11.525	0.0250	0.0217	0.0192	0.0158	0.0165
1:35	13.025	13.125	13.450	13.550	0.0279	0.0250	0.0157	0.0129	0.0172
1:40	N/A	N/A	N/A	N/A	N/A	N/A	N/A	N/A	N/A

Table B.3: T=0.75sec, H=0.052m (RTFN)

	Location (m)				Depth (m)				Wave
	Initiation		Termination		Initiation		Termination		Breaking
	Crest	Trough	Crest	Trough	Crest	Trough	Crest	Trough	Height(m)
1:10	3.000	3.250	cont.	cont.	0.1000	0.0750	cont.	cont.	N/A
1:15	4.950	5.175	cont.	cont.	0.0700	0.0550	cont.	cont.	N/A
1:20	6.775	6.975	cont.	cont.	0.0600	0.0500	cont.	cont.	N/A
1:25	8.575	8.850	cont.	cont.	0.0570	0.0460	cont.	cont.	N/A
1:30	10.325	10.535	cont.	cont.	0.0558	0.0492	cont.	cont.	N/A
1:35	12.000	12.275	cont.	cont.	0.0571	0.0493	cont.	cont.	N/A
1:40	N/A	N/A	N/A	N/A	N/A	N/A	N/A	N/A	N/A

Table B.4: T=0.75sec, H=0.052m, (FUNWAVE)

	Location (m)				Depth (m)				Wave
	Initiation		Termination		Initiation		Termination		Breaking
	Crest	Trough	Crest	Trough	Crest	Trough	Crest	Trough	Height(m)
1:10	3.175	3.375	cont.	cont.	0.0825	0.0625	cont.	cont.	N/A
1:15	4.875	5.100	cont.	cont.	0.0750	0.0600	cont.	cont.	N/A
1:20	6.525	6.750	7.475	7.600	0.0725	0.0612	0.0250	0.0187	N/A
1:25	8.225	8.425	9.450	9.575	0.0710	0.0630	0.0220	0.0170	N/A
1:30	9.800	10.050	11.475	11.575	0.0733	0.0650	0.0175	0.0147	N/A
1:35	11.325	11.600	13.450	13.550	0.0764	0.0686	0.0157	0.0129	N/A
1:40	12.000	12.275	12.475	12.625	0.0719	0.0650	0.0131	0.0100	N/A

Table B.5: T=1.0sec, H=0.016m (RTFN)

	Location (m)				Depth (m)				Wave Breaking Height(m)
	Initiation		Termination		Initiation		Termination		
	Crest	Trough	Crest	Trough	Crest	Trough	Crest	Trough	
1:10	3.375	3.600	cont.	cont.	0.0625	0.0400	cont.	cont.	0.0188
1:15	5.275	5.450	cont.	cont.	0.0483	0.0367	cont.	cont.	0.0212
1:20	7.100	7.275	cont.	cont.	0.0438	0.0350	cont.	cont.	0.0228
1:25	9.075	9.225	cont.	cont.	0.0370	0.0310	cont.	cont.	0.0249
1:30	10.900	11.075	cont.	cont.	0.0367	0.0317	cont.	cont.	0.0243
1:35	12.750	12.900	cont.	cont.	0.0357	0.0314	cont.	cont.	0.0252
1:40	14.625	14.775	cont.	cont.	0.0344	0.0306	cont.	cont.	0.0253

Table B.6: T=1.0sec, H=0.016m, (FUNWAVE)

	Location (m)				Depth (m)				Wave Breaking Height(m)
	Initiation		Termination		Initiation		Termination		
	Crest	Trough	Crest	Trough	Crest	Trough	Crest	Trough	
1:10	N/A	N/A	N/A	N/A	N/A	N/A	N/A	N/A	N/A
1:15	5.375	5.525	5.500	5.650	0.0417	0.0317	0.3333	0.2333	0.0244
1:20	7.125	7.275	7.475	7.600	0.0425	0.0350	0.0250	0.0187	0.0248
1:25	8.975	9.125	9.475	9.600	0.0410	0.0350	0.0210	0.0160	0.0248
1:30	10.775	10.925	11.475	11.600	0.0408	0.0358	0.0175	0.0133	0.0238
1:35	12.575	12.725	13.475	13.575	0.0407	0.0364	0.0150	0.0121	0.0244
1:40	14.350	14.500	15.450	15.575	0.0413	0.0375	0.0138	0.0106	0.0247

Table B.7: T=1.0sec, H=0.052m (RTFN)

	Location (m)				Depth (m)				Wave Breaking
	Initiation		Termination		Initiation		Termination		
	Crest	Trough	Crest	Trough	Crest	Trough	Crest	Trough	Height(m)
1:10	2.450	2.875	cont.	cont.	0.1550	0.1125	cont.	cont.	N/A
1:15	4.375	4.700	cont.	cont.	0.1083	0.0867	cont.	cont.	N/A
1:20	6.100	6.375	cont.	cont.	0.0938	0.0800	cont.	cont.	N/A
1:25	7.700	7.975	cont.	cont.	0.0920	0.0810	cont.	cont.	N/A
1:30	9.500	9.825	cont.	cont.	0.0833	0.0725	cont.	cont.	N/A
1:35	10.925	11.300	cont.	cont.	0.0878	0.0771	cont.	cont.	N/A
1:40	12.750	13.100	cont.	cont.	0.0813	0.0725	cont.	cont.	N/A

Table B.8: T=1.0sec, H=0.052m, (FUNWAVE)

	Location (m)				Depth (m)				Wave Breaking
	Initiation		Termination		Initiation		Termination		
	Crest	Trough	Crest	Trough	Crest	Trough	Crest	Trough	Height(m)
1:10	2.825	3.150	cont.	cont.	0.1175	0.0850	cont.	cont.	N/A
1:15	4.275	4.600	5.625	5.800	0.1150	0.0933	0.0250	0.0133	N/A
1:20	5.675	6.000	7.525	7.650	0.1150	0.0988	0.0225	0.0163	N/A
1:25	7.125	7.500	9.500	9.650	0.1150	0.1000	0.0200	0.0140	N/A
1:30	8.575	8.975	9.675	11.525	0.1142	0.1008	0.0192	0.0158	N/A
1:35	10.050	10.450	13.475	13.600	0.1129	0.1014	0.0150	0.0114	N/A
1:40	11.600	12.025	15.475	15.600	0.1100	0.0994	0.0131	0.0100	N/A

Table B.9: T=1.5sec, H=0.016m (RTFN)

	Location (m)				Depth (m)				Wave Breaking
	Initiation		Termination		Initiation		Termination		
	Crest	Trough	Crest	Trough	Crest	Trough	Crest	Trough	Height(m)
1:10	3.275	3.625	cont.	cont.	0.0725	0.0375	cont.	cont.	0.0210
1:15	5.050	5.325	cont.	cont.	0.0633	0.0450	cont.	cont.	0.0215
1:20	6.925	7.125	cont.	cont.	0.0525	0.0425	cont.	cont.	0.0236
1:25	8.850	9.025	cont.	cont.	0.0460	0.0390	cont.	cont.	0.0272
1:30	10.700	10.875	cont.	cont.	0.0433	0.0375	cont.	cont.	0.0279
1:35	12.550	12.725	cont.	cont.	0.0410	0.0364	cont.	cont.	0.0308
1:40	14.425	14.600	cont.	cont.	0.0394	0.0350	cont.	cont.	0.0309

Table B.10: T=1.5sec, H=0.016m, (FUNWAVE)

	Location (m)				Depth (m)				Wave Breaking
	Initiation		Termination		Initiation		Termination		
	Crest	Trough	Crest	Trough	Crest	Trough	Crest	Trough	Height(m)
1:10	N/A	N/A	N/A	N/A	N/A	N/A	N/A	N/A	N/A
1:15	5.325	5.475	5.550	5.700	0.0450	0.0350	0.0300	0.0200	0.0268
1:20	7.050	7.225	7.500	7.625	0.0462	0.0375	0.0238	0.0175	0.0288
1:25	8.825	9.000	9.500	9.625	0.0470	0.0400	0.0200	0.0150	0.0275
1:30	10.600	10.775	11.500	11.600	0.0467	0.0408	0.0167	0.0133	0.0289
1:35	12.325	12.525	13.475	13.600	0.0479	0.0421	0.0150	0.0114	0.0294
1:40	14.100	14.275	15.475	15.600	0.0475	0.0431	0.0131	0.0100	0.0289

Table B.11: T=1.5sec, H=0.052m (RTFN)

	Location (m)				Depth (m)				Wave Breaking Height(m)
	Initiation		Termination		Initiation		Termination		
	Crest	Trough	Crest	Trough	Crest	Trough	Crest	Trough	
1:10	N/A	N/A	N/A	N/A	N/A	N/A	N/A	N/A	N/A
1:15	4.200	4.575	cont.	cont.	0.1200	0.0950	cont.	cont.	N/A
1:20	5.750	6.125	cont.	cont.	0.1125	0.0925	cont.	cont.	N/A
1:25	7.425	7.750	cont.	cont.	0.1030	0.0900	cont.	cont.	N/A
1:30	9.200	9.500	cont.	cont.	0.0933	0.0833	cont.	cont.	N/A
1:35	10.575	10.950	cont.	cont.	0.0979	0.0864	cont.	cont.	N/A
1:40	12.450	12.800	cont.	cont.	0.0887	0.0800	cont.	cont.	N/A

Table B.12: T=1.5sec, H=0.052m, (FUNWAVE)

	Location (m)				Depth (m)				Wave Breaking Height(m)
	Initiation		Termination		Initiation		Termination		
	Crest	Trough	Crest	Trough	Crest	Trough	Crest	Trough	
1:10	N/A	N/A	N/A	N/A	N/A	N/A	N/A	N/A	N/A
1:15	4.200	4.575	N/A	N/A	0.1200	0.0950	N/A	N/A	N/A
1:20	5.675	5.975	N/A	N/A	0.1150	0.1000	N/A	N/A	N/A
1:25	7.075	7.475	N/A	N/A	0.1170	0.1010	N/A	N/A	N/A
1:30	8.350	8.725	N/A	N/A	0.1217	0.1092	N/A	N/A	N/A
1:35	9.925	10.375	N/A	N/A	0.1164	0.1036	N/A	N/A	N/A
1:40	11.225	11.625	N/A	N/A	0.1194	0.1094	N/A	N/A	N/A

Table B.13: T=2.0sec, H=0.016m (RTFN)

	Location (m)				Depth (m)				Wave
	Initiation		Termination		Initiation		Termination		Breaking
	Crest	Trough	Crest	Trough	Crest	Trough	Crest	Trough	Height(m)
1:10	N/A	N/A	N/A	N/A	N/A	N/A	N/A	N/A	N/A
1:15	4.625	5.100	cont.	cont.	0.0917	0.0600	cont.	cont.	0.0240
1:20	6.525	6.875	cont.	cont.	0.0725	0.0550	cont.	cont.	0.0270
1:25	8.500	8.750	cont.	cont.	0.0600	0.0500	cont.	cont.	0.0320
1:30	10.225	10.475	cont.	cont.	0.0592	0.0508	cont.	cont.	0.0325
1:35	12.025	12.275	cont.	cont.	0.0564	0.0493	cont.	cont.	0.0360
1:40	13.875	14.100	cont.	cont.	0.0531	0.0475	cont.	cont.	0.0415

Table B.14: T=2.0sec, H=0.016m, (FUNWAVE)

	Location (m)				Depth (m)				Wave
	Initiation		Termination		Initiation		Termination		Breaking
	Crest	Trough	Crest	Trough	Crest	Trough	Crest	Trough	Height(m)
1:10	N/A	N/A	N/A	N/A	N/A	N/A	N/A	N/A	N/A
1:15	5.200	5.375	5.575	5.750	0.0533	0.0417	0.0283	0.0167	0.0330
1:20	6.850	7.100	7.525	7.675	0.0563	0.0437	0.0225	0.0150	0.0330
1:25	8.575	8.800	9.500	9.650	0.0570	0.0480	0.0200	0.0140	0.0360
1:30	10.225	10.475	11.500	11.600	0.0592	0.0508	0.0167	0.0133	0.0363
1:35	11.850	12.100	13.450	13.600	0.0614	0.0543	0.0157	0.0114	0.0368
1:40	13.500	13.775	15.475	15.600	0.0625	0.0556	0.0131	0.0100	0.0372

Table B.15: T=2.0sec, H=0.052m (RTFN)

	Location (m)				Depth (m)				Wave Breaking Height(m)
	Initiation		Termination		Initiation		Termination		
	Crest	Trough	Crest	Trough	Crest	Trough	Crest	Trough	
1:10	N/A	N/A	N/A	N/A	N/A	N/A	N/A	N/A	N/A
1:15	N/A	N/A	N/A	N/A	N/A	N/A	N/A	N/A	N/A
1:20	5.100	5.550	cont.	cont.	0.1432	0.1212	cont.	cont.	N/A
1:25	6.625	7.175	cont.	cont.	0.1350	0.1130	cont.	cont.	0.0810
1:30	8.025	8.625	cont.	cont.	0.1325	0.1125	cont.	cont.	0.0810
1:35	9.725	10.150	cont.	cont.	0.1221	0.1100	cont.	cont.	0.0910
1:40	11.250	12.050	cont.	cont.	0.1187	0.0998	cont.	cont.	0.1140

Table B.16: T=2.0sec, H=0.052m, (FUNWAVE)

	Location (m)				Depth (m)				Wave Breaking Height(m)
	Initiation		Termination		Initiation		Termination		
	Crest	Trough	Crest	Trough	Crest	Trough	Crest	Trough	
1:10	N/A	N/A	N/A	N/A	N/A	N/A	N/A	N/A	N/A
1:15	N/A	N/A	N/A	N/A	N/A	N/A	N/A	N/A	N/A
1:20	4.875	5.375	7.725	7.900	0.1550	0.1300	0.0125	0.0037	0.0840
1:25	6.425	7.000	9.675	9.825	0.1430	0.1200	0.0130	0.0070	0.0820
1:30	7.750	8.325	11.600	11.775	0.1417	0.1225	0.0133	0.0075	0.0795
1:35	8.975	9.475	13.550	13.700	0.1436	0.1293	0.0129	0.0086	0.0822
1:40	9.975	10.575	15.525	15.650	0.1506	0.1356	0.0119	0.0088	0.0820

## VITA

Biographical sketch

Takashi Okamoto

### Professional Preparation

B.S.	Aggricultural Engineering	Kyoto University (Japan)	March 1995
M.S.	Aggricultural Engineering	Kyoto University (Japan)	March 1997
Ph.D.	Civil Engineering	Old Dominion University	December 2003

### Appointments

Research Assistant, Old Dominion University	1999–2002
---	-----------

### Publication

N/A

### Other significant Publications

- Basco, D. R. and T. Okamoto, 2000, "Criteria to Assess the Impact of Sand Volume Removed on the Nearshore Wave Climate", Proceedings of 27<sup>th</sup> ICCE (Sydney), ASCE, New York, 3243–3253
- Basco, D. R. and T. Okamoto, 2002, "A New Wave Breaking Trigger Criteria for Phase-Resolving Numerical Models", Proceedings of 28<sup>th</sup> ICCE (Cardiff), ASCE, New York, 319–331